Isothermal Amplification Techniques for the Detection of Nucleic Acids and Proteins

by

Ashley Meagan Newbigging

A thesis submitted in partial fulfillment of the requirements for the degree of

Doctor of Philosophy

in

Analytical and Environmental Toxicology

Department of Laboratory Medicine and Pathology
University of Alberta

Abstract

The early detection of disease is beneficial for improved patient prognoses. One major challenge in early disease detection is the small, undetectable amounts of biomarkers. Detection strategies that confer amplification of the biomarker itself or of the detection signal are therefore desirable. Furthermore, emerging strategies conferring amplification at isothermal temperatures offer improvements in technical procedures by circumventing the requirement for multiple different reaction temperatures as is required in polymerase chain reaction. Despite the advances in isothermal amplification strategies using nucleic acids, there are still some drawbacks such as the technical difficulty of protocols and number of reagents required. The primary objective of my research was to develop novel techniques to improve and simplify the detection of nucleic acid and protein targets. In order to address this objective, I developed three new techniques for the isothermal and amplified detection of nucleic acid and protein targets with improved features.

To improve isothermal and exponential amplified detection, I developed a new technique called Beacon-mediated Exponential Amplification Reaction (**BEAR**) to detect nucleic acid targets. **BEAR** only required a single enzyme and a single primer. I applied **BEAR** to detect Myoclonus Epilepsy with Ragged Red Fibres (MERRF). I achieved a limit of detection of 10 fM in 80 min and a recovery of ~91% in cell lysate for the MERRF sequence using **BEAR**.

To improve isothermal and amplified detection without using enzymes, I developed a new turn-on fluorescence technique inspired by hybridization chain reaction (HCR) enabling the generation of turn-on fluorescence signals from label-free hairpins. This HCR technique uses four hairpins which overcomes the background that could arise when using two label-free hairpins. Using this new technique, I achieved a limit of detection of 660 pM of a nucleic acid target in solution when using 50 nM of hairpins in 30 min at room temperature.

To improve the protocols of localized protein imaging, I adapted the concept of binding-induced DNA assembly (BINDA) to the developed HCR technique. I used BINDA to convert protein binding into the generation of a DNA strand. The formation of the DNA strand initiated the HCR that produced fluorescence signals. I applied this technique to detect a HER2+ breast cancer cell line where membrane fluorescence indicating the HER2 status of the cells was achieved in as soon as 5 min with strong fluorescence signals at about 45 min to 60 min. This technique did not require any enzymes or washing steps and was performed at room temperature.

These developed techniques feature isothermal reaction temperatures, low reaction volumes, and technically simple protocols because they are all in mix-and-read formats. These features allow potential applications of my techniques for improved clinical laboratory testing, point-of-care assays, and testing in resource-limited settings. Furthermore, the modularity of these developed DNA designs allows for the adaptation to other targets as well.

Preface

This thesis is an original work by Ashley M. Newbigging. The research project, of which this thesis is a part, received research ethics approval from the University of Alberta Research Ethics Board, Project Name "Detection of mitochondrial DNA mutations by isothermal DNA polymerization and exponential amplification" No. RES0028904, 2016/05.

Parts of Chapter 1 of this thesis have been published as Hanyong Peng, Ashley M. Newbigging, Michael S. Reid, Jagdeesh S. Uppal, Jingyang Xu, Hongquan Zhang, X. Chris Le. Anal. Chem. 2020, 92(1): 292-308. DOI: 10.1021/acs.analchem.9b04752. Accessed 7 Jan 2020 from: https://pubs.acs.org/doi/abs/10.1021/acs.analchem.9b04752
 I composed and wrote sections pertaining to using the technique, Hybridization Chain Reaction. I also revised all parts of the manuscript. Reprinted with permission. Copyright 2020 American Chemical Society (ACS). Further copyright permissions requests are to be directed to ACS.

Chapter 2 of this thesis has been published as Ashley M. Newbigging, Hongquan Zhang, X. Chris Le. Beacon-mediated amplification reaction (BEAR) using a single enzyme and protein. Chem. Comm. 2019, 55, 10677-80. DOI: 10.1039/c9cc04226a. I conceptualized experimental design, data collection and analysis, text and schematic composition, and revisions of the overall manuscript. Published by the Royal Society of Chemistry.

Chapters 3, 4, and 5 have not been published.

Acknowledgements

I would like to express my sincere gratitude to my co-supervisors, Dr. X. Chris Le and Dr. Hongquan Zhang. Dr. Le, thank you for your guidance and your faith in me. Dr. Zhang, thank you for your patience and invaluable technical advice. It has been a great privilege to work with you both.

Thank you to Dr. Michael Weinfeld of my supervisory committee. Thank you for providing helpful suggestions, encouragement, and enthusiasm for my work. I am also grateful to Dr. Xing-fang Li also for her encouragement and for her confidence in me and my work.

I would like to thank Ms. Katerina Carastathis, for too much to list - for personal advice, for keeping me organized, for ordering countless DNA oligos, ... and so on. Thank you to Ms. Cheryl Titus and Dr. Monika Keelan for supporting my academic and professional development. Thank you to Ms. Dianne Sergy for her advice and support.

Dr. Birget Moe, Dr. Zhixin Wang, and Dr. Hanyong Peng, thank you all for training me in laboratory techniques and your patience in mentoring me.

To all AET, Chemistry, and LMP students who I have had the pleasure of meeting and sharing our time in graduate school together, thank you for making school fun. Thank you especially to Mike, Aleks, Rebecca, Lindsay, Yanwen, Ping, and Angela.

Lastly, thank you to my family and my husband, Steven, who have supported me throughout the years. Thank you to my beloved cockatiel, who has been and continues to be my constant companion for over twenty years.

Table of Contents

List of Abbreviations

List of Figures

List of Abbreviations

ΔTt	Change in threshold time
ATCC	American Type Culture Collection
BEAR	Beacon-mediated Exponential Amplification Reaction
BINDA	Binding induced DNA assembly
bp	Base pairs
BSA	Bovine serum albumin
Cy5	Cyanine 5
C_t	Cycle threshold
CV	Coefficient of variation
DAPI	4',6-diamidino-2-phenylindole
DIC	Differential Interference Contrast (microscopy)
DNA	Deoxyribonucleic acid
DPBS	Dulbecco's phosphate buffered saline
dsDNA	Double stranded DNA
EDTA	Ethylenediaminetetraacetic acid
ELISA	Enzyme-linked immunosorbent assay
FAM	6-carboxyfluorescein
FBS	Fetal bovine serum
FRET	Förster/fluorescence resonance energy transfer
HER2	Human epidermal growth factor receptor 2
HCR	Hybridization chain reaction
IaBkFQ	Iowa Black® FQ (Dark Quencher)
IaBkRQ	Iowa Black® RQ (Dark Quencher)
Ig	Immunoglobulin
IHC	Immunohistochemistry
MERRF	Myoclonus epilepsy with ragged red fibres
miRNA	MicroRNA
mRNA	Messenger RNA
mtDNA	Mitochondrial DNA

MW	Molecular weight
NC	Negative control
nt	Nucleotide
PAGE	Polyacrylamide gel electrophoresis
oligo(s)	oligonucleotide(s)
PCR	Polymerase chain reaction
PLA	Proximity ligation assay
RCA	Rolling circle amplification
RNA	Ribonucleic acid
SA	Streptavidin
Tt	Time threshold

<u>Chapter One: Introduction</u>[*]

1.1 Detection of biomarkers

The presence of certain biomarkers or perturbations in their amounts can be detected using analytical laboratory tests to screen, diagnose, or monitor patients for various health concerns. Ideal laboratory tests are sensitive, specific, and practical to perform in clinical laboratories[1]. Candidates for biomarkers are those substances that are present in human samples and detectable using available laboratory equipment. Many important biomarkers are nucleic acids and proteins.

Early disease detection is important for the prognosis of patients because it can result in prompt treatment for better patient outcomes[2–6]. However, early detection of disease can be challenging due to the low concentration of biomarkers which cannot be detected directly. A common strategy to overcome this limitation is to amplify undetectable amounts of biomarkers to detectable amounts. For example, polymerase chain reaction (PCR) directly amplifies nucleic acid targets from small, undetectable amounts to large, detectable amounts[7,8]. Proteins cannot be directly amplified; however, assays linked with enzymes can amplify the detection signal instead. For example, in enzyme immunoassays, the enzyme label confers amplified signals by continuously catalyzing substrates for the indirect detection of protein targets[9]. Similarly, for localized protein detection, immunostaining is used where the label is often an enzyme[10]. Many advances have been made in developing novel strategies for amplifying the target or the detection signal for biomarkers. In this chapter, I discussed PCR as an exponential amplification technique and prominent isothermal amplification strategies.

---

[*] A portion of this chapter is adapted from Peng H., Newbigging A., Reid M., Uppal J., Xu J., Zhang H., Le X.C. *Anal Chem*. 2020, 92(1): 292-308. Accessed on 7 Jan 2020 from: **https://pubs.acs.org/doi/abs/10.1021/acs.analchem.9b04752**[30]
Further requests for copyright permissions are to be directed to ACS.

1.2 Polymerase chain reaction (PCR)

Nucleic acid amplification strategies, like PCR, are increasingly being used for biosensing applications[7,8,11]. PCR is commonly used in laboratories to exponentially amplify nucleic acid targets from small, undetectable amounts to large, detectable amounts. Thus, nucleic acid targets can be directly amplified whereas proteins cannot. The amplification of nucleic acids can be used to amplify the detection signal for protein targets. For example, in immuno-PCR, a DNA oligonucleotide (oligo) is used to label the secondary antibody instead of an enzyme, then PCR is used to amplify the label for indirect amplified detection of the protein target[12]. PCR requires at least two specially designed primers complementary to the nucleic acid target, a heat stable polymerase, and an instrument capable of cycling through high and low temperatures. High temperatures (e.g. 95°C) are necessary to separate double stranded nucleic acids (dsDNA) to single strands (ssDNA) and lower temperatures allow the primers to anneal (e.g. 60°C). Another temperature change is required for extension (e.g. 70°C) via the polymerase. Additionally, the length of time required for PCR is prolonged because each cycle requires user-determined timed incubations at each temperature. Another disadvantage is the exponential increase of the amount of the target, which poses risks for contamination of subsequent PCR runs[13]. It may be necessary to separate prior and post PCR reaction handling of the samples to avoid contamination of samples with amplicons.

1.3 Isothermal amplification

Improvements to technical procedures for signal amplification have been achieved by emerging advances in isothermal amplification strategies[14–16]. Where PCR uses heat denaturation, isothermal amplification strategies use enzymes, the strand displacement activity of polymerases and/or toehold-mediated reactions to separate dsDNA to ssDNA, and therefore require only a

single reaction temperature. Isothermal amplification of nucleic acid targets is highly desired because it retains the extraordinary amplification power of PCR while obviating the need for thermal cycling that is essential to PCR. Eliminating thermal cycling allows the use of simpler devices, which is particularly useful for point-of-care testing and testing in resource limited settings[17]. Additionally, isothermal techniques can have improved reaction kinetics over PCR because the speed of the reaction is not limited by the time required for incubation at each temperature.

Isothermal signal amplification strategies that do not require enzymes at all are further desirable because the removal of the requirement for enzymes tends to result in simpler technical protocols and less strict reagent storage requirements. These strategies use toehold mediated strand displacement or toehold mediated strand exchange reactions that typically consists of using a portion of a ssDNA to bind to a toehold: an exposed, ssDNA region of a dsDNA duplex[18–20]. After binding of the incoming ssDNA to the toehold, the incoming ssDNA can bind to the rest of the DNA strand through random walk branch migration, displacing the already bound strand in the dsDNA duplex. The result is the new dsDNA duplex containing the incoming strand with a higher melting temperature than the previous dsDNA duplex to drive the reaction in this direction. Through using these strategies, the rational design of nucleic acids can facilitate amplified detection of nucleic acid and protein targets isothermally.

Isothermal amplification strategies that can be run at biological temperatures (e.g., ~37°C) have potential applications for biosensing within live cells or live cell detection. Those that are designed to run at room temperature are convenient and appropriate for resource-limited settings or point-of-care testing because no extra laboratory equipment is required to maintain reaction temperatures.

Here, I review isothermal nucleic acid amplification strategies that 1) confer exponential amplification, 2) do not require enzymes, or 3) enable localized protein detection.

1.3.1 Isothermal exponential amplification strategies

Many isothermal exponential amplification strategies require enzymes to separate dsDNA to ssDNA in addition to a polymerase for amplification. The following section is an overview on prominent strategies using the rational design of nucleic acids to enable exponential amplification under isothermal reaction conditions.

1.3.1.1 Helicase-Dependent Amplification (HDA) and Recombinase Polymerase Amplification (RPA)

Recombinase, used in recombinase polymerase amplification (RPA), and helicase, used in helicase dependent amplification (HDA), are both similar in that the named enzyme of each strategy disrupts the dsDNA to allow binding of primers. Single stranded binding proteins (SSB) are used in both strategies to prevent the renaturation of the DNA strands.

HDA, introduced by Kong's group in 2004[21], provided a novel method of exponentially amplifying nucleic acids isothermally as an alternative to using PCR. Kong's group aimed to develop a new technique for long targets with simple schemes. In HDA, the helicase enzyme is used to unwind dsDNA to ssDNA to allow the binding of primers for nucleic acid elongation using a polymerase. SSB are added to prevent ssDNA from renaturation with its complement. The authors found that omitting SSB yielded no amplification. The reaction took a total of 2 h to run at 37°C.

RPA introduced by Piepenburg et al.[22] RPA used recombinase complexed with primers to unravel dsDNA to ssDNA for the primers to bind. SSB are also used to stabilize the ssDNA

and prevent the strands from renaturation and displacing the primers. A polymerase extends the 3' end of the primer. Because the newly formed DNA is dsDNA, the recombinase-primer complex can act on it again for exponential amplification of the nucleic acid target. RPA takes 60 min at 37°C and reactions can be monitored using a dsDNA intercalating dye, such as SYBR green. As low as 10 genomic copies of MRSA were detected. RPA and HDA are both powerful strategies but both may be limited in applicability because an additional enzyme to the polymerase is required, the helicase or the recombinase, as well as the requirement for SSB.

1.3.1.2 Strand displacement amplification (SDA) and exponential amplification reaction (EXPAR)

Strand displacement amplification (SDA) was first introduced by Walker and co-workers in 1992 to isothermally amplify DNA targets[23]. The first iteration of SDA used restriction enzymes to cleave a DNA target into a smaller, manageable size. The additional restriction enzyme step in the protocol complicated the method and limited the choice in DNA targets because it required those targets that were 1) double stranded and 2) flanked by restriction endonuclease recognition sites. The next iteration of SDA used a hemiphosphorothiorate HincII site and circumvented the requirement for targets that were flanked by restriction endonuclease recognition sites by introducing the recognition sequence on primers. The hemiphosphorothioate modification of the DNA strand inhibited cleavage and so only one strand was cleaved or nicked. In SDA, two steps are involved, one to generate the target, and another to amplify the target. The target DNA is denatured from dsDNA to ssDNA using heat. Two inner primers contain the complementary sequence to the nucleic acid target but have an unbound portion containing the HincII cleavage sequence. Two outer primers are complementary to the nucleic acid target outside of the inner primers, such that when extended, the two inner primer

elongation products are displaced by the elongation of the outer primers. The end result is the dsDNA nucleic acid target sequence flanked by the HincII cleavage site. The nicking of the HincII and subsequent polymerase extension initiate the amplification cycle. The target is exponentially amplified because when target is elongated, the nicking site is reformed and can be nicked again. Subsequent polymerase extension displaces the previously synthesized strand. This strand can bind to the second primer, forming the same reaction but on the complement of the target, producing another molecule of the target for the continuation of the reaction. Walker et al. reported a detection limit of 10-50 copies of the target DNA. A limit of detection of 16 zmol was also reported when detecting miRNA[24].

Exponential amplification reaction (EXPAR) was introduced in 2003 by Van Ness et al[25]. EXPAR is particularly useful for detecting shorter nucleic acids of known sequences that are 8-16 nt in length rapidly and sensitively. EXPAR consists of two phases: one with linear amplification and the other enabling for exponential amplification of the target sequence. In the linear amplification phase, an EXPAR template is designed to contain two copies of the complementary sequence of the target DNA sequence separated by a nicking site in the middle. When the target binds to the first copy of the complement within a template, the DNA polymerase extends it, creating a dsDNA structure containing two copies of the target separated by the nicking site. The completion of the nicking site from ssDNA to dsDNA site allows the nicking endonuclease to nick the synthesized strand. The polymerase can extend the nicking site, displacing the synthesized copy of the target. The displaced targets can further bind to additional EXPAR templates for the same reaction, exponentially amplifying the amount of target. Although the amplification efficiency of EXPAR is high with large amounts of the target being amplified in a short amount of time, EXPAR has limitations. EXPAR is subject to high background and the exponentially amplified amplicons pose risks for contamination of

subsequent runs. Reid et al[26]. recently addressed these issues in a review with further discussion on the various applications, scheme variations, and continuing challenges of EXPAR.

1.3.1.3 Transcription mediated amplification (TMA)

Transcription mediated amplification (TMA) uses the biological machinery used in transcription to enable exponential amplification at isothermal temperatures. Generally, TMA uses primers to create cDNA from an RNA template using RNA polymerases. Because the product is an RNA-DNA hybrid, RNase is used to digest the RNA strand, leaving the cDNA single-stranded. The primer has an unbound region, which carries the sequence of a promoter for transcription. Another primer binds to the cDNA sequence and extends it, making the promoter region dsDNA. The RNA polymerase can then continuously create more of the RNA target which can undergo the same reaction, thereby exponentially amplifying the original target sequence. Self-sustained sequence replication (3SR), introduced by Guatelli et al.[27], and nucleic acid sequence based amplification (NASBA), introduced by J. Compton[28], are both similar techniques using transcription machinery and their names have been used interchangeably. NASBA and 3SR differ from TMA because TMA uses a reverse transcriptase with RNase activity where NASBA and 3SR use an additional RNase enzyme[16]. However, the requirement for multiple enzymes and primers is a disadvantage of these transcription-based amplification strategies. TMA requires two enzymes, reverse transcriptase with RNAse activity and an RNA polymerase, while NASBA and 3SR requires three, reverse transcriptase, RNase H, and RNA polymerase. Furthermore, two primers are required in TMA, NASBA, and 3SR.

1.3.1.4 Loop-mediated isothermal amplification (LAMP)

Loop-mediated isothermal amplification (LAMP) is unique in that it only uses one enzyme to confer exponential amplification of large nucleic acid targets[29]. However, LAMP requires four primers: two pairs of inner and outer primers. Two reaction steps are required where the first produces a dumbbell DNA structure from the target nucleic acid sequence, which can then facilitate exponential amplification. In the first step to form the dumbbell structure, one inner primer binds to the target sequence. The inner primer contains an overhang sequence that creates a short hairpin loop when elongated via a polymerase using the target as a template. The outer primer displaces the elongated inner primers from the target DNA. After displacement, the elongated inner primer changes conformation to the hairpin shape. The second inner and outer primer pair performs the same reaction on the other end of this product, forming another hairpin. The product therefore consists of hairpins on both 5' and 3' ends with short stems to form the dumbbell structure required for the exponential amplification step. Exponential amplification is enabled because the two inner primers producing the dumbbell structure can bind to the ssDNA loops to further propagate the reaction. Furthermore, the 3' end of the stem acts as a primer that can be elongated by the polymerase. The end products are long, concatemers of the repeating target sequence that are described as cauliflower-like in shape. LAMP takes 1 h at 65°C. The authors were able to detect as low as 6 copies of the DNA target. LAMP is a powerful strategy to exponentially amplify long nucleic acid targets using only a single enzyme. However, LAMP's applicability is limited in its ability to detect long length targets (~100 bp or more), its requirement for at least four primers, and its complex design.

1.3.2 Isothermal amplification strategies without enzymes with a focus on hybridization chain reaction (HCR)

Isothermal strategies that do not use enzymes but enable signal amplification include catalytic hairpin assembly (CHA), entropy driven catalysis (EDC), and hybridization chain reaction (HCR)[30]. CHA consists of two specially designed DNA hairpins to store potential energy[31,32]. The hairpins are complementary to each other, but they cannot react due to the stable hairpin conformation. When the target nucleic acid is introduced, it binds to its complementary region on one hairpin, opening it, and allowing the second hairpin to hybridize to it, displacing the target. The target can go on to react with additional hairpins. The detection of the hairpin complex confers amplified detection of the target. CHA has been applied for the detection of microRNA[33–36], porphyrin-DNA complexes[37], proteins[38–41], and metal ions[42]. EDC uses toehold mediated exchange reactions. The reaction uses a three-stranded substrate complex consisting of a linker strand hybridized to an output strand and a signal strand. The target, called the catalyst strand, hybridizes to its toehold on the linker strand and displaces the signal strand. Another strand, called the fuel strand, then hybridizes to its toehold on the linker strand which was liberated by the displacement of the signal strand. The fuel strand displaces both the output strand and the target strand, recycling the target. One target can liberate multiple signal and output strands, leading to amplification of the detection signal. The reaction is driven by a gain in entropy from releasing molecules because the net number of base pairing keeps constant during the reaction. EDC has been applied for the detection of platelet-derived growth factor-BB[43], bacterial DNA[44], and miRNA[45].

HCR was introduced by Dirks and Pierce in 2004[46]. HCR uses two metastable DNA hairpins to store potential energy. Each of the DNA hairpins contains a short, single-stranded sticky end, and are designed to be complementary to one another. Although the reaction

between two hairpins is thermodynamically favorable, the reaction is kinetically trapped by the hairpin structure. Therefore, HCR does not begin until addition of a single-stranded initiator. The initiator reacts with and opens the first hairpin through a toehold-mediated strand displacement reaction, exposing a new single-stranded domain. This new domain acts as a second initiator to react with and open the second hairpin, which produces a single-stranded domain identical to the first initiator. This chain reaction continues, producing a long, nicked dsDNA polymer called a concatemer. However, a major disadvantage of the original HCR design is the requirement for 24 h of incubation to allow for substantial formation of the concatemer. Since 2004, there have been many developments that use HCR for the real time detection of various biomarkers with improvements in both incubation times and detection methods. A detailed review focusing on the applications of HCR was recently published[47]. Despite the advances in HCR, HCR protocols still require lengthy incubation times (e.g., ~6 h) for signal amplification.

Developments to HCR include different methods for the generation of signal, adaptions to detect different biomarkers, and overall improvements. Pierce's group demonstrated the application of HCR by detecting messenger RNA (mRNA) expression in situ[48–50]. Initiators were designed to contain a region complementary to H1, a region complementary to the mRNA target, and a region complementary to H2. These initiator probes were added to the samples and were allowed to hybridize to the mRNA targets for 16 h. Unbound probes were washed away for 2 h before adding fluorophore-labeled HCR hairpins specific to each probe, and again was incubated for another 16 h. H1 hybridized to its complementary region on the initiators bound to the mRNA targets, which opened the hairpin and thus initiated HCR. H2 also hybridizes to its complementary region downstream on the probe, and also initiates another round of HCR starting with H2. Unreacted hairpins were washed away for 2 h. Pierce's group further advanced

the technology to third generation HCR[51] to reduce the spurious initiation of HCR by splitting

the initiator sequences in half onto two separate oligos that were complementary to the mRNA

target. Only when both probes hybridized to adjacent locations on the mRNA target, the full

initiator sequence could initiate HCR by hybridizing to H1. However, the reaction time still

remained long, with two 2 h wash steps and two 16 h incubations.

To improve the signal output from HCR, Tan's group labeled their hairpins with pyrene

residues as a dye[52]. When the pyrenes of both hairpins were brought into close proximity in the

concatemer, an excimer was formed that produced a longer wavelength than the individual

moieties with a longer lifetime. The authors' rationale was to detect the fluorescence at a

reaction time where the autofluorescence of the biological matrix has decayed, but the

fluorescence of the pyrene-excimer remains strong.

Liu et al. developed a colorimetric technique for the detection of a nucleic acid target

using HCR by using the aggregation of gold nanoparticles (AuNP)[53]. Single stranded overhangs

of HCR hairpins allowed adsorption onto the surface of AuNP, preventing aggregation of the

AuNP, which resulted in a red solution. Initiation of HCR caused the hairpins to form a

concatemer that dissociated from the AuNP. As a result, the AuNP were allowed to aggregate

with each other, resulting in a colour change from red to purple. Limits of detection of 50 pM

and 100 pM were achieved using a spectrophotometer and by eye, respectively.

Förster resonance energy transfer (FRET) is widely used for generating detection signals[54].

A common strategy is to conjugate one hairpin with a donor, and the other hairpin with an acceptor.

No FRET occurs before HCR because of the large distance between the donor and acceptor. When

the HCR concatemer is formed, the donor and acceptor are brought into close proximity, enabling

FRET. When hairpins conjugated to fluorophores are quenched by adsorption onto nanomaterials,

the degradation of the hairpins results in release of the fluorophores and restoration of the

fluorescence, increasing background. However, when FRET is used to detect concatemers, background arising from degradation of hairpins is avoided. Li et al. conjugated a FAM molecule to the 5' end of one hairpin, and TMR to a nucleotide of the stem of the second hairpin, such that when organized into a concatemer, FAM and TMR are in close proximity of each other for FRET to occur[55]. The formation of the concatemer brought both donors into close proximity to the acceptor for FRET. Ou et al. conjugated one hairpin with two adjacent FAM molecules within the loop and the second hairpin with one TAMRA molecule at the 5'- end[56]. The authors found that two donors and one acceptor yielded significantly higher detection signal when compared to one donor molecule.

Alternatively, turn-on fluorescence is also a viable strategy for HCR. One hairpin can be conjugated with a fluorophore-quencher pair so that the fluorescence is quenched when in the hairpin conformation. The formation of the concatemer disrupts the hairpin structure and separates the fluorophore and quencher, restoring the fluorescence. Yang et al. conjugated two base-pairing nucleotides within the hairpin stem with FAM and a dark quencher, respectively, to detect pre-miRNA-155[57]. The interaction of pre-miRNA-155 with the hairpin opens the stem, initiating HCR and restoring fluorescence. The authors also designed a second HCR system for detection of matured miRNA-155 where one hairpin was dually labeled with Cy3 and another dark quencher for multiplex detection of both pre- and mature miRNA-155.

Additional amplification strategies can be coupled to HCR to further amplify the detection signal produced from HCR. The HCR hairpins can be designed to form a concatemer containing functional domains that could trigger a second signal amplification to achieve further signal amplification. For example, the sequence of DNAzymes can be split such that the DNAzymes are inactive when the hairpins are monomers but when brought together in the concatemer become active. Such designs are called multicomponent enzymes (MNAzymes)

where each inactive part of the DNAzyme are called partzymes[58]. Willner and co-workers included split MNAzymes onto the HCR hairpins so that the formation of the concatemer assembled an active MNAzyme that then cleaved substrates, achieving tandem signal amplification[59]. He et al. similarly used DNAzymes for intracellular mRNA detection to further amplify the detection signal that may be applicable to intracellular miRNA detection[60]. After the degradation of their ZnO@PDA-hpDNA delivery nanosystem, the hairpins were released into the cytoplasm of the cell. One hairpin contained the initiating sequence for HCR, where only upon binding to intracellular mRNA, the hairpin opened and initiated HCR. The sequence of a DNAzyme was split on the hairpins of HCR such that when organized adjacently in the concatemer, the sticky ends created the intact DNAzyme. As the DNAzymes cleaved molecular beacon substrates, the fluorescence signal was substantially amplified with a detection limit of 1 fM in 2-5 h. Similarly, Wu et al. also split the sequence of a G-quadruplex peroxidase-mimicking DNAzyme on HCR hairpins[61]. To enhance the detection of their protein target, thrombin, the DNAzyme further amplified detection signals by continuously oxidizing its substrate which produced an amplified signal.

The design of branched HCR concatemers have also provided further signal amplification. Liu et al. developed a HCR circuit to image mRNA within cells by coupling two reactions to create branched HCR[62]. The mRNA target was used as the initiator for the first circuit of HCR. The first hairpin, H1, contained a portion of the initiating sequence for the second circuit of HCR and the second hairpin, H2, contained the other portion of the initiating sequence within its loop. Thus, the initiating sequence for the second circuit was only formed when the first circuit forms the concatemer. Fluorescence was detected because one of the hairpins was labeled with a fluorophore and quencher pair. The fluorescence was quenched within the hairpin but was restored when in the concatemers. With the first circuit of HCR, a

limit of detection of 10 pM was achieved. However, with the two-circuit branched HCR, they achieved a limit of detection of 500 fM of mRNA in HeLa cells. The branched HCR took 3 h of incubation in 37°C. Similarly, Wei et al. developed a concatenated HCR (C-HCR) system consisting of 7 hairpins[63]. The miR-21 target hybridized to and opened a hairpin containing the initiating sequence for HCR. The concatemer created an initiating strand for a second HCR, using four hairpins. The second concatemer was detected by FRET because one hairpin was conjugated to TAMRA and the other was conjugated to FAM. The result was a branched C-HCR product with multiple FRET events. The authors achieved a detection limit of 3 pM in 2 h with C-HCR. Zhou et al. also developed multibranched HCR to detect cancer cells[64]. They used biotinylated branched arms to conjugate avidin-horseradish peroxidase to further amplify the detection signal. They achieved a limit of detection of 4 cancer cells.

Wu and co-workers demonstrated the first application of HCR in living cells[65]. They developed cationic peptide coated AuNP to deliver fluorescently labeled HCR hairpins into target cells. The intracellular survivin mRNA was used as an initiator for HCR. As the concatemer was forming, the hairpins dissociated from the AuNPs. The concatemer placed the fluorescence donor and acceptor, that were separately conjugated to each hairpin, in close proximity, generating a FRET signal for detection.

Aptamers can be combined with HCR to detect non-nucleic acid targets. For example, Chen et al. developed HCR to generate electrochemical signals for the detection of thrombin[66]. Their protocol used S, N co-doped reduced graphene oxide (SN-rGO) as an electrode substrate and AuNP conjugated with DNA oligos (T-DNA) deposited on a glassy carbon electrode. The T-DNA was immobilized on the AuNP on the surface of the SN-rGO electrode. To detect the thrombin target, a thrombin aptamer was used. The authors hybridized a DNA oligo to a portion of the aptamer. When the aptamer binds thrombin, this complementary DNA oligo was

displaced. The oligo was captured by the T-DNA on the surface of the electrode, and then acted as the initiator for HCR. The concatemer was therefore grown on the electrode surface. H1 and H2 were both biotinylated and so the formation of the concatemer was detected when avidin conjugated to horseradish peroxidase was added. When the avidin bound to the concatemer, a large electrochemical signal could be detected after the catalysis of H_2O_2 by the peroxidase. The HCR required 2 h of incubation with a low detection limit of 11.6 fM.

Polychlorinated biphenyl compounds (PCBs) were also detected using aptamers combined with HCR. Wang et al. developed HCR to detect PCBs which used nicking endonucleases to enhance fluorescence signals from upconversion nanoparticles (UCNPs)[67]. A complementary strand of DNA was hybridized to an aptamer of PCB72/106. The aptamers were conjugated to magnetic beads. When the aptamer bound to its target, the cDNA dissociated. The cDNA in the supernatant was purified from the sample using magnetic bead separation to remove the PCB-aptamer-magnetic bead complex. The cDNA was then used to initiate HCR. For signal output, the hairpins were conjugated with quenchers and the UCNPs, where the hairpin conformation brought the UCNP and quencher into close proximity, quenching the fluorescence. When the hairpins were in the concatemer formation, the fluorescence of the UCNPs were restored due to the increase in distance from the quenchers. However, the addition of nicking endonucleases caused release of the UCNPs from the concatemer for maximum fluorescence recovery. The procedure took about 6 h with incubations at 37°C and the authors achieved a discrimination factor of 3 (LOD of 0.0035 ng/mL).

To summarize, HCR has seen many advancements and adaptations while maintaining the overall general concept of using hairpins to store potential energy and their cross-opening after exposure to an initiating nucleic acid. However, many HCR strategies still face long

incubation times to create the concatemer (5 h to 24 h) as a result of slow amplification efficiency.

1.3.3 Localized protein detection

The localized detection of proteins on cell surfaces is routinely achieved through immunostaining with an enzymatic label[68]. Examples of immunostaining include immunohistochemistry (IHC) or immunocytochemistry (ICC). IHC methods detect protein targets in tissue samples and ICC methods detect protein targets in cell samples. Immunostaining procedures involve using a primary antibody to recognize the protein target of interest followed by the production of amplified detection which is usually conferred by conjugating the secondary antibody to an enzyme. The enzyme continuously converts its substrate and another molecule, such as a chromogen, in redox reactions to produce a colour change. However, immunostaining technical procedures are long and can be time consuming and laborious. Additionally, the use of enzymes may require strict reagent storage requirements. For IHC and ICC specifically, many laborious steps can be involved, such as epitope retrieval if using fixed samples, blocking of endogenous peroxidase if using horseradish peroxidase as the enzyme label, and multiple time-consuming wash and incubation steps. The end result may show a diffuse staining pattern that is somewhat localized to the cell surfaces. In some cases, this localization may be sufficient for acceptable pathological analyses. However, in other cases, specific localization to cell surfaces may be favourable, such as in flow cell cytometry or immunocytostaining, for individual cell identification. Fluorophore tags instead of enzymatic tags can be conjugated to the secondary antibody in immunofluorescence staining strategies.

Advances in the field to improve the sensitivity of localized protein detection methods have been developed using the rational design of nucleic acids to amplify the detection signal.

16

However, a disadvantage common to all immunostaining strategies is the reliance on the availability, specificity, and sensitivity of antibodies. Also, all immunostaining strategies reviewed here require washing of unbound probes or unbound imaging molecules prior to imaging, which can increase turnaround times and is laborious to perform.

1.3.3.1 DuoLink® Proximity Ligation Assay (DuoLink® PLA)

Proximity ligation assay (PLA) confers increased sensitivity by accumulating multiple fluorophores localized to the protein or protein interaction being detected[69]. PLA used the simultaneous binding of probes to proteins in close proximity of each other to produce a signal. The proximity probes consisted of the sequence for the PDGF-BB aptamer and the complementary region to the other probe. When both probes were bound to both B units of a PDGF-BB complex, the probes are brought close together such that they both bind to a connector oligo and then could be ligated using a ligase. The ligated products were originally detected using PCR; however, DuoLink® PLA, trademarked by Sigma Aldrich, is an isothermal adaptation combining PLA and RCA for protein-protein interactions[70]. In DuoLink® PLA, the addition of the ligase and a connector oligo forms a circular template by hybridizing to the proximity probes. One of the oligos bound to the secondary antibodies acts as a primer to the circularized template and is elongated with a polymerase. The elongation of the circularized template is continued and the concatemer product contains multiple repeats of the same sequence as the polymerase has strand displacement activity. The concatemer is detected using hybridization probes which are short oligos that are fluorescently labeled and complementary to each repeat of the sequence. Multiple fluorophores accumulate on the product due to the repeats which results in signal amplification. Although this is a successful and established method, multiple incubation steps are required, such as incubations for primary and secondary antibody

binding, ligation, amplification, and detection. Additionally, wash steps are required after each of the above listed steps. Lastly, two enzymes are required: the polymerase and the ligase[70].

1.3.3.2 Immuno-rolling circle amplification (immuno-RCA)

Ward's group used an immunometric rolling circle amplification (RCA) to detect proteins[71]. In immuno-RCA, a short DNA oligo was conjugated to an antibody. After the antibody bound to an immobilized protein target, a circular template was added. The DNA oligo tag on the antibody served as a primer using the circular template for polymerase extension. When the polymerase traveled around the circular template and met the start of the template that was dsDNA due to elongation, the displacement activity allowed the continuation of elongation. The product was a long, ssDNA, whose sequence was multiple, consecutive repeats of the complement of the circularized probe. The product was detected using the hybridization of labeled oligos to the product sequence. However, the protocol of immuno-RCA was time consuming: antibodies conjugated to the primer were added to the sample for 30 min followed by washing, then circular DNA templates were added to the primer-conjugated antibodies prior to analysis for 30 min. Another 30 min incubation was required for the polymerase to produce the concatemer. The samples were washed multiple times before fluorescently labeled oligos were added and incubated for another 30 min for imaging of the products. Not including the wash steps, a total of 2 h of incubation periods were required[71]. RCA originally used Vent DNA polymerase with a reaction temperature of 62-66.5°C, and was complete within 60-90 min[72]. Ali et al. published a comprehensive review on the improvements and advances of RCA[73].

1.3.3.3 Immunostaining with signal amplification by exchange reaction (immuno-SABER)

Immunostaining with signal amplification by exchange reaction (immuno-SABER)[74] used the strategy of primer exchange reaction (PER)[75] to enable amplified detection signals in tissues. Immuno-SABER used antibodies conjugated with DNA oligos that were complementary to a PER primer. Immuno-SABER involved two steps: the first, to bind primary antibodies conjugated with DNA to the target of interest and the second, to hybridize the conjugated DNA to concatemers. The concatemers must be produced separately by PER prior to imaging analysis. PER required one primer, one hairpin, and a polymerase with strand displacement activity. The hairpin had a long overhang that was complementary to the primer, and another repeat of the same sequence to make up the stem. When the primer bound to the overhang, it was elongated by the polymerase and the stem opened. The stem contained a stop sequence near the loop and when the polymerase encountered it, elongation was halted, and the polymerase dissociated. Through random walk branch migration, the primer was displaced from the hairpin as the stem was reformed. The displaced primer, now elongated with two repeats of the same sequence, could bind to the hairpin overhang for the same reaction. The concatemer was produced from elongated primers with multiple repeats of the same sequence. The concatemer was exposed to target samples with the antibody pre-hybridized, and the elongated primer bound to its complementary DNA sequence on the antibody. After washing the imaging oligos, short oligos conjugated to fluorophores that were complementary to one repeat of the elongated primer, were added so that the elongated primer could accumulate multiple fluorophores. The authors further amplified the signal by using multiple oligo branching. However, long incubation times were required to allow the imaging oligos to bind to the elongated primer. For example, 75 min to overnight incubations were required for producing fluorescence signals for

imaging. Another disadvantage were the sequence effects when extending the primers. The authors found that efficiency of the polymerase was affected by different sequences which lead to possible signal intensity bias when performing multiplex detection that required multiple primer sets. Thus, the authors were required to optimize reaction conditions for each different sequence of primer used.

1.3.3.4 Immuno-hybridization chain reaction (immuno-HCR)

Choi et al. first reported immuno-HCR[76]. Immuno-HCR improved the technical procedures of localized protein imaging by removing the requirement for enzymes while still enabling for signal amplification. Similar to other immunostaining methods, a primary antibody was added to bind to the protein target of interest prior to the secondary antibody. The secondary antibody was labeled with the initiator of HCR. Each incubation step required washing steps. After washing, the HCR hairpins were added to the solution to produce concatemers. Both of the HCR hairpins were conjugated to fluorophores. The formation of the concatemer on the initiator strand produced localized fluorescence. Signal amplification was achieved because multiple hairpins, and thus multiple fluorophores, made up one concatemer. Because both hairpins were conjugated to fluorophores, thorough washing after the formation of the concatemer was required to remove the background fluorescence. Although immuno-HCR simplified immunostaining methods by removing the requirement for the enzyme, the protocol still required many time-consuming wash steps. Another example of immuno-HCR, for the ultrasensitive detection of proteins, was developed by Knopp's group using AuNP probes conjugated to a capture antibody and the initiator for HCR[77]. Dai et al. used a similarly designed probe for the detection of IgG[78].

Lin et al. developed isHCR, referring to the use of HCR for immunosignal amplification[79]. After primary antibodies bound to the protein target of interest, secondary antibodies were added. For signal amplification, the secondary antibodies were conjugated to biotin. Streptavidin was added and bound to the biotinylated secondary antibodies, followed by the addition of biotinylated initiators for HCR. Signal amplification was achieved because one molecule of streptavidin can bind four biotin molecules. Therefore, three biotinylated initiators could then bind to the remaining sites in streptavidin. The hairpins were conjugated with fluorophores which allowed detection of the formation of concatemers. The authors achieved an increase in signal when compared to conventional IHC methods. However, the protocol was long and laborious because HCR required an overnight to two days incubation at 37°C, followed by three washing steps. Furthermore, the authors showed an increase in the background when compared with IHC in some samples, such as brain tissue sections, and thus required a prior step using graphene oxide to adsorb and quench unbound hairpins.

Proximity HCR (prox-HCR), an alternative protein detection method using HCR, was developed by Koos et al[80]. Four hairpins are used: two hairpins for HCR and two additional hairpins were conjugated to secondary antibodies and used as proximity probes. After the primary antibodies bound to protein targets, the proximity probes were added. The secondary antibodies of the proximity probes bound to the primary antibodies and brought the hairpins of the proximity probes into close proximity. A third ssDNA oligo, called an invading strand, hybridized to one of the hairpins of one proximity probe to open it. When opened, the hairpin could invade the hairpin of the other proximity probe, opening it. When the second hairpin was opened, it revealed the initiator strand for HCR that was previously locked within the stem. The two hairpins for HCR were labeled with fluorophores for fluorescence signal production. The authors reported that distinctive fluorescence was achieved after only 30 min of incubation, with

fluorescence seen after only 5 min. However, the protocol for prox-HCR requires overnight incubation of the samples with primary antibodies at 4°C, followed by washing twice, incubation of proximity probes for 1 h at 37°C, and again washing twice more. The activator oligo was added and incubated for 30 min, followed by another washing step. Finally, the hairpins for HCR were added and incubated for 1 h at 37°C, followed by two washing steps, nuclei staining, and coverslipping for fluorescence detection.

Tan's group, using aptamer-tethered nanodevcies (apt-ND), also achieved localized cell surface detection using HCR[81]. Pre-formed HCR concatemers in solution were initiated by an aptamer sequence. After the formation of the aptamer-concatemer complex, the apt-ND, it was exposed to cell surfaces. The aptamer would bind to the cell surface and the concatemer provided amplified detection signals using conjugated fluorophores, dsDNA intercalating fluorescence dyes, or FRET mechanisms. However, the formation of the concatemer took 24 h at room temperature. Furthermore, washing is required to remove the unbound concatemer-aptamer oligos.

A proximity-induced initiation of HCR was used by Li et al. to detect protein-specific glycosylation in living cells and zebrafish larvae[82]. The authors developed two probes, one to detect glycans, called Glycan Conversion Probes (GCP), and one to detect protein, called protein recognition probes. The glycans on cell surface were modified with GCP, a nucleic acid oligo. The protein recognition probes were DNA hairpins that consisted of an aptamer sequence, a GCP complement, and the initiator sequence. When the protein recognition probes bound to the specific protein and to GCP, the hairpin was opened, and the initiator was free to initiate HCR. The reaction time for HCR within cells was 2 h. To modify the glycans, cells were incubated with GCP probes for 30 min and washed twice. Protein recognition probes were added and incubated for 30 min again, followed by three washing steps. Lastly, the two hairpins

were added and incubated for 3 h. Therefore, again, the protocol required multiple washing steps and incubation steps.

Although the principle of HCR is advantageous in many applications because it offers signal amplification without the requirement for enzymes, there are still some limitations: each of the above discussed strategies using HCR requires multiple incubations and washing steps. Additionally, the generation of the concatemer is time consuming and when combined with each antibody incubation and washing steps, the protocol can be long and laborious.

1.4 Rationale and scope of the thesis

To summarize, currently used techniques for protein and nucleic acid detection have laborious and time-consuming protocols. Currently available isothermal strategies for exponential amplification require multiple enzymes and/or multiple primers. LAMP is an exception because it only requires one enzyme; however, LAMP requires at least four primers, the design is complex, and it is not appropriate for short length targets. Isothermal nucleic acid amplification techniques for localized protein detection require multiple washing steps and incubation steps. Therefore, the objective of this thesis was to develop isothermal techniques using rational DNA design for the detection of nucleic acids and proteins that are simpler and easier to perform in terms of technical protocols, such as the number of required reagents and washing steps, than those currently available. In this thesis work, I introduce three novel isothermal amplification techniques.

This thesis consists of five chapters. Chapter 1 reviewed various prominent isothermal strategies for the amplified detection of nucleic acids and proteins. Chapter 2 introduces a technique for the isothermal and exponential amplified detection of a DNA target. Chapter 3 discusses the development of a HCR technique that enables turn-on fluorescence generated from

label-free hairpins. Chapter 4 focuses on the development of a protein-initiated HCR technique

for localized detection of a cell surface protein. Chapter 5 discusses the conclusions and

significance of this research and possible future research directions.

1.5 References

(1)   Holland, R. L. What Makes a Good Biomarker? *Adv. Precis. Med.* **2016**, *1*, 66.

(2)   Etzoni, R.; Urban, N.; Ramsey, S.; McIntosh, M.; Schwartz, S.; Reid, B.; Radich, J.; Anderson, G.; Hartwell, L. The Case for Early Detection. *Nat. Rev. Cancer* **2003**, *3*, 243–252.

(3)   Wulfkuhle, J. D.; Liotta, L. A.; Petricoin, E. F. Proteomic Applications for the Early Detection of Cancer. *Nat. Rev. Cancer* **2003**, *3*, 267–275.

(4)   Swarup, V.; Rajeswari, M. R. Circulating (Cell-Free) Nucleic Acids - A Promising, Non-Invasive Tool for Early Detection of Several Human Diseases. *FEBS Lett.* **2007**, *581*, 795–799.

(5)   Martin, K. J.; Fournier, M. V.; Veer Reddy, G. P.; Pardee, A. B. A Need for Basic Research on Fluid-Based Early Detection Biomarkers. *Cancer Res.* **2010**, *70*, 5203–5206.

(6)   Schwarzenbach, H.; Hoon, D. S. B.; Pantel, K. Cell-Free Nucleic Acids as Biomarkers in Cancer Patients. *Nat. Rev. Cancer* **2011**, *11*, 426–437.

(7)   Mullis, K. B.; Faloona, F. A. Specific Synthesis of DNA in Vitro via a Polymerase-Catalyzed Chain Reaction. *Methods Enzymol.* **1987**, *155*, 335–350.

(8)   Saiki, R.; Scharf, S.; Faloona, F.; Mullis, K.; Horn, G.; Erlich, H.; Arnheim, N. Enzymatic Amplification of Beta-Globin Genomic Sequences and Restriction Site Analysis for Diagnosis of Sickle Cell Anemia. *Science*, 1985, *230*, 1350–1354.

(9)   Lequin, R. M. Enzyme Immunoassay (EIA)/Enzyme-Linked Immunosorbent Assay (ELISA). *Clin. Chem.* **2005**, *51*, 2415–2418.

(10)   Maity, B.; Sheff, D.; Fisher, R. A. *Immunostaining. Detection of Signaling Protein Location in Tissues, Cells and Subcellular Compartments.*; Elsevier, 2013; Vol. 113.

(11)   Kubista, M.; Andrade, J. M.; Bengtsson, M.; Forootan, A.; Jonák, J.; Lind, K.; Sindelka,

R.; Sjöback, R.; Sjögreen, B.; Strömbom, L.; *et al.* The Real-Time Polymerase Chain Reaction. *Mol. Aspects Med.* **2006**, *27*, 95–125.

(12) Sano, T.; Smith, C. L.; Cantor, C. R. Immuno-PCR: Very Sensitive Antigen Detection by Means of Specific Antibody-DNA Conjugates. *Science* **1992**, *258*, 120–122.

(13) Persing, D. H. Polymerase Chain Reaction: Trenches to Benches. *J. Clin. Microbiol.* **1991**, *29*, 1281–1285.

(14) Yan, L.; Zhou, J.; Zheng, Y.; Gamson, A. S.; Roembke, B. T.; Nakayama, S.; Sintim, H. O. Isothermal Amplified Detection of DNA and RNA. *Mol. Biosyst.* **2014**, *10*, 970–1003.

(15) Li, J.; Macdonald, J. Advances in Isothermal Amplification: Novel Strategies Inspired by Biological Processes. *Biosens. Bioelectron.* **2014**, *64*, 196–211.

(16) Zhao, Y.; Chen, F.; Li, Q.; Wang, L.; Fan, C. Isothermal Amplification of Nucleic Acids. *Chem. Rev.* **2015**, *115*, 12491–12545.

(17) Peeling, R. W.; Holmes, K. K.; Mabey, D.; Ronald, A. Rapid Tests for Sexually Transmitted Infections (STIs): The Way Forward. *Sex. Transm. Infect.* **2006**, *82*, v1–v6.

(18) Srinivas, N.; Ouldridge, T. E.; Šulc, P.; Schaeffer, J. M.; Yurke, B.; Louis, A. A.; Doye, J. P. K.; Winfree, E. On the Biophysics and Kinetics of Toehold-Mediated DNA Strand Displacement. *Nucleic Acids Res.* **2013**, *41*, 10641–10658.

(19) Yang, X.; Tang, Y.; Traynor, S. M.; Li, F. Regulation of DNA Strand Displacement Using an Allosteric DNA Toehold. *J. Am. Chem. Soc.* **2016**, *138*, 14076–14082.

(20) Zhang, D. Y.; Chen, S. X.; Yin, P. Optimizing the Specificity of Nucleic Acid Hybridization. *Nat. Chem.* **2012**, *4*, 208–214.

(21) Vincent, M.; Xu, Y.; Kong, H. Helicase-Dependent Isothermal DNA Amplification. *EMBO Rep.* **2004**, *5*, 795–800.

(22) Piepenburg, O.; Williams, C. H.; Stemple, D. L.; Armes, N. A. DNA Detection Using

Recombination Proteins. *PLoS Biol.* **2006**, *4*, 1115–1121.

(23) Walker, G. T.; Fraiser, M. S.; Schram, J. L.; Little, M. C.; Nadeau, J. G.; Malinowski, D. P. Strand Displacement Amplification--an Isothermal, in Vitro DNA Amplification Technique. *Nucleic Acids Res.* **1992**, *20*, 1691–1696.

(24) Shi, C.; Liu, Q.; Ma, C.; Zhong, W. Exponential Strand-Displacement Amplification for Detection of Micrornas. *Anal. Chem.* **2014**, *86*, 336–339.

(25) Van Ness, J.; Van Ness, L. K.; Galas, D. J. Isothermal Reactions for the Amplification of Oligonucleotides. *Proc. Natl. Acad. Sci. U. S. A.* **2003**, *100*, 4504–4509.

(26) Reid, M. S.; Le, X. C.; Zhang, H. Exponential Isothermal Amplification of Nucleic Acids and Assays for Proteins, Cells, Small Molecules, and Enzyme Activities: An EXPAR Example. *Angew. Chem. Int. Ed. Engl.* **2018**, *57*, 11856–11866.

(27) Guatelli, J. C.; Whitfield, K. M.; Kwoh, D. Y.; Barringer, K. J.; Richman, D. D.; Gingeras, T. R. Isothermal, in Vitro Amplification of Nucleic Acids by a Multienzyme Reaction Modeled after Retroviral Replication. *Proc. Natl. Acad. Sci. U. S. A.* **1990**, *87*, 1874–1878.

(28) Compton, J. Nucleic Acid Sequence-Based Amplification. *Nature* **1991**, *350*, 273–291.

(29) Notomi, T.; Okayama, H.; Masubuchi, H.; Yonekawa, T.; Watanabe, K.; Amino, N.; Hase, T. Loop-Mediated Isothermal Amplification of DNA. *Nucleic Acids Res.* **2000**, *28*, E63.

(30) Peng, H.; Newbigging, A. M.; Reid, M. S.; Uppal, J. S.; Xu, J.; Zhang, H.; Le, X. C. Signal Amplification in Living Cells: A Review of MicroRNA Detection and Imaging. *Anal. Chem.* **2020**, *92*, 292–308.

(31) Yin, P.; Choi, H. M. T.; Calvert, C. R.; Pierce, N. A. Programming Biomolecular Self-Assembly Pathways. *Nature* **2008**, *451*, 318–322.

(32) Jiang, Y.; Li, B.; Milligan, J. N.; Bhadra, S.; Ellington, A. D. Real-Time Detection of Isothermal Amplification Reactions with Thermostable Catalytic Hairpin Assembly. *J. Am. Chem. Soc.* **2013**, *135*, 7430–7433.

(33) Zhuang, J.; Lai, W.; Chen, G.; Tang, D. A Rolling Circle Amplification-Based DNA Machine for MiRNA Screening Coupling Catalytic Hairpin Assembly with DNAzyme Formation. *Chem. Commun.* **2014**, *50*, 2935–2938.

(34) Zhang, Y.; Yan, Y.; Chen, W.; Cheng, W.; Li, S.; Ding, X.; Li, D.; Wang, H.; Ju, H.; Ding, S. A Simple Electrochemical Biosensor for Highly Sensitive and Specific Detection of MicroRNA Based on Mismatched Catalytic Hairpin Assembly. *Biosens. Bioelectron.* **2015**, *68*, 343–349.

(35) Li, J.; Lei, P.; Ding, S.; Zhang, Y.; Yang, J.; Cheng, Q.; Yan, Y. An Enzyme-Free Surface Plasmon Resonance Biosensor for Real-Time Detecting MicroRNA Based on Allosteric Effect of Mismatched Catalytic Hairpin Assembly. *Biosens. Bioelectron.* **2016**, *77*, 435–441.

(36) Hao, N.; Dai, P. P.; Yu, T.; Xu, J. J.; Chen, H. Y. A Dual Target-Recycling Amplification Strategy for Sensitive Detection of MicroRNAs Based on Duplex-Specific Nuclease and Catalytic Hairpin Assembly. *Chem. Commun.* **2015**, *51*, 13504–13507.

(37) Zang, Y.; Lei, J.; Ling, P.; Ju, H. Catalytic Hairpin Assembly-Programmed Porphyrin-DNA Complex as Photoelectrochemical Initiator for DNA Biosensing. *Anal. Chem.* **2015**, *87*, 5430–5436.

(38) Zheng, A. X.; Wang, J. R.; Li, J.; Song, X. R.; Chen, G. N.; Yang, H. H. Enzyme-Free Fluorescence Aptasensor for Amplification Detection of Human Thrombin via Target-Catalyzed Hairpin Assembly. *Biosens. Bioelectron.* **2012**, *36*, 217–221.

(39) Tang, Y.; Lin, Y.; Yang, X.; Wang, Z.; Le, X. C.; Li, F. Universal Strategy To Engineer

Catalytic DNA Hairpin Assemblies for Protein Analysis. *Anal. Chem.* **2015**, 150806081532007.

(40)   Liu, S.; Cheng, C.; Gong, H.; Wang, L. Programmable Mg(2+)-Dependent DNAzyme Switch by the Catalytic Hairpin DNA Assembly for Dual-Signal Amplification toward Homogeneous Analysis of Protein and DNA. *Chem. Commun. (Camb).* **2015**, *51*, 7364–7367.

(41)   Chang, C. C.; Chen, C. P.; Chen, C. Y.; Lin, C. W. DNA Base-Stacking Assay Utilizing Catalytic Hairpin Assembly-Induced Gold Nanoparticle Aggregation for Colorimetric Protein Sensing. *Chem. Commun.* **2016**, *52*, 4167–4170.

(42)   Wu, Z.; Fan, H.; Satyavolu, N. S. R.; Wang, W. J.; Lake, R.; Jiang, J. H.; Lu, Y. Imaging Endogenous Metal Ions in Living Cells Using a DNAzyme–Catalytic Hairpin Assembly Probe. *Angew. Chem. Int. Ed. Engl.* **2017**, *56*, 8721–8725.

(43)   Li, D.; Li, X.; Shen, B.; Li, P.; Chen, Y.; Ding, S.; Chen, W. Aptamer Recognition and Proximity-Induced Entropy-Driven Circuit for Enzyme-Free and Rapid Amplified Detection of Platelet-Derived Growth Factor-BB. *Anal. Chim. Acta* **2019**, *1092*, 102–107.

(44)   Zong, Y.; Liu, F.; Zhang, Y.; Zhan, T.; He, Y.; Hun, X. Signal Amplification Technology Based on Entropy-Driven Molecular Switch for Ultrasensitive Electrochemical Determination of DNA and Salmonella Typhimurium. *Sensors Actuators, B Chem.* **2016**, *225*, 420–427.

(45)   Zhang, N.; Shi, X. M.; Guo, H. Q.; Zhao, X. Z.; Zhao, W. W.; Xu, J. J.; Chen, H. Y. Gold Nanoparticle Couples with Entropy-Driven Toehold-Mediated DNA Strand Displacement Reaction on Magnetic Beads: Toward Ultrasensitive Energy-Transfer-Based Photoelectrochemical Detection of MiRNA-141 in Real Blood Sample. *Anal. Chem.* **2018**, *90*, 11892–11898.

(46)   Dirks, R. M.; Pierce, N. A. Triggered Amplification by Hybridization Chain Reaction. *Proc. Natl. Acad. Sci. U. S. A.* **2004**, *101*, 15275–15278.

(47)   Bi, S.; Yue, S.; Zhang, S. Hybridization Chain Reaction: A Versatile Molecular Tool for Biosensing, Bioimaging, and Biomedicine. *Chem. Soc. Rev.* **2017**, *46*, 4281–4298.

(48)   Choi, H. M. T.; Chang, J. Y.; Trinh, L. A.; Padilla, J. E.; Fraser, S. E.; Pierce, N. A. Programmable in Situ Amplification for Multiplexed Imaging of MRNA Expression. *Nat. Biotechnol.* **2010**, *28*, 1208–1212.

(49)   Choi, H. M. T.; Beck, V. A.; Pierce, N. A. Next-Generation in Situ Hybridization Chain Reaction: Higher Gain, Lower Cost, Greater Durability. *ACS Nano* **2014**, *8*, 4284–4294.

(50)   Choi, H. M. T.; Calvert, C. R.; Husain, N.; Huss, D.; Barsi, J. C.; Deverman, B. E.; Hunter, R. C.; Kato, M.; Lee, S. M.; Abelin, A. C. T.; *et al.* Mapping a Multiplexed Zoo of MRNA Expression. *Development* **2016**, *143*, 3632–3637.

(51)   Choi, H. M. T.; Schwarzkopf, M.; Fornace, M. E.; Acharya, A.; Artavanis, G.; Stegmaier, J.; Cunha, A.; Pierce, N. A. Third-Generation in Situ Hybridization Chain Reaction: Multiplexed, Quantitative, Sensitive, Versatile, Robust. *Development* **2018**, *145*, 1–10.

(52)   Huang, J.; Wu, Y.; Chen, Y.; Zhu, Z.; Yang, X.; Yang, C. J.; Wang, K.; Tan, W. Pyrene-Excimer Probes Based on the Hybridization Chain Reaction for the Detection of Nucleic Acids in Complex Biological Fluids. *Angew. Chem. Int. Ed. Engl.* **2011**, *50*, 401–404.

(53)   Liu, P.; Yang, X.; Sun, S.; Wang, Q.; Wang, K.; Huang, J.; Liu, J.; He, L. Enzyme-Free Colorimetric Detection of DNA by Using Gold Nanoparticles and Hybridization Chain Reaction Amplification. *Anal. Chem.* **2013**, *85*, 7689–7695.

(54)   Stryer, L. Fluorescence Energy Transfer as a Spectroscopic Ruler. *Annu. Rev. Biochem.* **1978**, *47*, 819–846.

(55)   Li, J.; Li, D.; Yuan, R.; Xiang, Y. Biodegradable MnO2 Nanosheet-Mediated Signal

Amplification in Living Cells Enables Sensitive Detection of Down-Regulated Intracellular MicroRNA. *ACS Appl. Mater. Interfaces* **2017**, *9*, 5717–5724.

(56)   Ou, M.; Huang, J.; Yang, X.; He, X.; Quan, K.; Yang, Y.; Xie, N.; Li, J.; Wang, K. Live-Cell MicroRNA Imaging through MnO2 Nanosheet-Mediated DD-A Hybridization Chain Reaction. *ChemBioChem* **2018**, *19*, 147–152.

(57)   Yang, F.; Cheng, Y.; Cao, Y.; Dong, H.; Lu, H.; Zhang, K.; Meng, X.; Liu, C.; Zhang, X. Sensitively Distinguishing Intracellular Precursor and Mature MicroRNA Abundance. *Chem. Sci.* **2019**, *10*, 1709–1715.

(58)   Mokany, E.; Bone, S. M.; Young, P. E.; Doan, T. B.; Todd, A. V. MNAzymes, a Versatile New Class of Nucleic Acid Enzymes That Can Function as Biosensors and Molecular Switches. **2015**, 1051–1059.

(59)   Wang, F.; Elbaz, J.; Orbach, R.; Magen, N.; Willner, I. Amplified Analysis of DNA by the Autonomous Assembly of Polymers Consisting of DNAzyme Wires. *J. Am. Chem. Soc.* **2011**, *133*, 17149–17151.

(60)   He, D.; He, X.; Yang, X.; Li, H.-W. A Smart ZnO@polydopamine-Nucleic Acid Nanosystem for Ultrasensitive Live Cell MRNA Imaging by the Target-Triggered Intracellular Self-Assembly of Active DNAzyme Nanostructures. *Chem. Sci.* **2017**, *31*, 748.

(61)   Wu, H.; Zhang, K.; Liu, Y.; Wang, H.; Wu, J.; Zhu, F.; Zou, P. Binding-Induced and Label-Free Colorimetric Method for Protein Detection Based on Autonomous Assembly of Hemin/G-Quadruplex DNAzyme Amplification Strategy. *Biosens. Bioelectron.* **2015**, *64*, 572–578.

(62)   Liu, L.; Liu, J. W.; Wu, H.; Wang, X. N.; Yu, R. Q.; Jiang, J. H. Branched Hybridization Chain Reaction Circuit for Ultrasensitive Localizable Imaging of MRNA in Living Cells.

Anal. Chem. **2018**, *90*, 1502–1505.

(63) Wei, J.; Gong, X.; Wang, Q.; Pan, M.; Liu, X.; Liu, J.; Xia, F.; Wang, F. Construction of an Autonomously Concatenated Hybridization Chain Reaction for Signal Amplification and Intracellular Imaging. *Chem. Sci.* **2017**, *9*, 52–61.

(64) Zhou, G.; Lin, M.; Song, P.; Chen, X.; Chao, J.; Wang, L.; Huang, Q.; Huang, W.; Fan, C.; Zuo, X. Multivalent Capture and Detection of Cancer Cells with DNA Nanostructured Biosensors and Multibranched Hybridization Chain Reaction Amplification. *Anal. Chem.* **2014**, *86*, 7843–7848.

(65) Wu, Z.; Liu, G. Q.; Yang, X. L.; Jiang, J. H. Electrostatic Nucleic Acid Nanoassembly Enables Hybridization Chain Reaction in Living Cells for Ultrasensitive MRNA Imaging. *J. Am. Chem. Soc.* **2015**, *137*, 6829–6836.

(66) Chen, Y. X.; Huang, K. J.; He, L. L.; Wang, Y. H. Tetrahedral DNA Probe Coupling with Hybridization Chain Reaction for Competitive Thrombin Aptasensor. *Biosens. Bioelectron.* **2018**, *100*, 274–281.

(67) Wang, Y.; Bai, J.; Huo, B.; Yuan, S.; Zhang, M.; Sun, X.; Peng, Y.; Li, S.; Wang, J.; Ning, B.; *et al.* Upconversion Fluorescent Aptasensor for Polychlorinated Biphenyls Detection Based on Nicking Endonuclease and Hybridization Chain Reaction Dual-Amplification Strategy. *Anal. Chem.* **2018**, *90*, 9936–9942.

(68) Sandhaus, L. M.; Gajl-Peczalska, K. J.; Brunning, R. D. Immunophenotyping of Leukaemia: An Immunoperoxidase Method Using Air-dried Smears. *Br. J. Haematol.* **1984**, *56*, 131–138.

(69) Fredriksson, S.; Gullberg, M.; Jarvius, J. Protein Detection Using Proximity-Dependent DNA Ligation Assays. *Nat. Biotechnol.* **2002**, *20*, 473–477.

(70) Duolink® PLA Fluorescence Protocol | Sigma-Aldrich

https://www.sigmaaldrich.com/technical-documents/protocols/biology/duolink-fluorescence-user-manual.html#fluorescence (accessed Oct 3, 2019).

(71)   Schweitzer, B.; Wiltshire, S.; Lambert, J.; O'Malley, S.; Kukanskis, K.; Zhu, Z.; Kingsmore, S. F.; Lizardi, P.; Ward, D. C. Immunoassays with Rolling Circle DNA Amplification: A Versatile Platform for Ultrasensitive Antigen Detection. *Proc. Natl. Acad. Sci.* **2000**, *97*, 10113–10119.

(72)   Lizardi, P. M.; Huang, X.; Zhu, Z.; Bray-Ward, P.; Thomas, D. C.; Ward, D. C. Mutation Detection and Single-Molecule Counting Using Isothermal Rolling-Circle Amplification. *Nat Genet* **1998**, *19*, 225–232.

(73)   Ali, M. M.; Li, F.; Zhang, Z.; Zhang, K.; Kang, D.-K.; Ankrum, J. a; Le, X. C.; Zhao, W. Rolling Circle Amplification: A Versatile Tool for Chemical Biology, Materials Science and Medicine. *Chem. Soc. Rev.* **2014**, *43*, 3324–3341.

(74)   Saka, S. K.; Wang, Y.; Kishi, J. Y.; Zhu, A.; Zeng, Y.; Xie, W.; Kirli, K.; Yapp, C.; Cicconet, M.; Beliveau, B. J.; *et al.* Immuno-SABER Enables Highly Multiplexed and Amplified Protein Imaging in Tissues. *Nat. Biotechnol.* **2019**, *37*, 1080–1090.

(75)   Kishi, J. Y.; Schaus, T. E.; Gopalkrishnan, N.; Xuan, F.; Yin, P. Programmable Autonomous Synthesis of Single-Stranded DNA. *Nat. Chem.* **2018**, *10*, 155–164.

(76)   Choi, J.; Routenberg Love, K.; Gong, Y.; Gierahn, T. M.; Love, J. C. Immuno-Hybridization Chain Reaction for Enhancing Detection of Individual Cytokine-Secreting Human Peripheral Mononuclear Cells. *Anal. Chem.* **2011**, *83*, 6890–6895.

(77)   Zhang, B.; Liu, B.; Tang, D.; Niessner, R.; Chen, G.; Knopp, D. DNA-Based Hybridization Chain Reaction for Amplified Bioelectronic Signal and Ultrasensitive Detection of Proteins. *Anal. Chem.* **2012**, *84*, 5392–5399.

(78)   Dai, S.; Xue, Q.; Zhu, J.; Ding, Y.; Jiang, W.; Wang, L. An Ultrasensitive Fluorescence

Assay for Protein Detection by Hybridization Chain Reaction-Based DNA Nanotags. *Biosens. Bioelectron.* **2014**, *51*, 421–425.

(79)   Lin, R.; Feng, Q.; Li, P.; Zhou, P.; Wang, R.; Liu, Z.; Wang, Z.; Qi, X.; Tang, N.; Shao, F.; *et al.* A Hybridization-Chain-Reaction-Based Method for Amplifying Immunosignals. *Nat. Methods* **2018**, *15*, 275–278.

(80)   Koos, B.; Cane, G.; Grannas, K.; Löf, L.; Arngården, L.; Heldin, J.; Clausson, C.-M.; Klaesson, A.; Hirvonen, M. K.; de Oliveira, F. M. S.; *et al.* Proximity-Dependent Initiation of Hybridization Chain Reaction. *Nat. Commun.* **2015**, *6*, 1–10.

(81)   Zhu, G.; Zhang, S.; Song, E.; Zheng, J.; Hu, R.; Fang, X.; Tan, W. Building Fluorescent DNA Nanodevices on Target Living Cell Surfaces. *Angew. Chem. Int. Ed. Engl.* **2013**, *52*, 5490–5496.

(82)   Li, J.; Liu, S.; Sun, L.; Li, W.; Zhang, S. Y.; Yang, S.; Li, J.; Yang, H. H. Amplified Visualization of Protein-Specific Glycosylation in Zebrafish via Proximity-Induced Hybridization Chain Reaction. *J. Am. Chem. Soc.* **2018**, *140*, 16589–16595.

Chapter Two: Development of an isothermal and exponential amplification technique using a single enzyme and primer[*]

2.1 Introduction

PCR is powerful for the amplification of nucleic acids. Each cycle of PCR requires changes in temperatures between lower temperatures for annealing (*e.g.*, 60°C) and extension (*e.g.*, 70°C), and a higher temperature for denaturation (*e.g.*, 95°C) of double stranded DNA (dsDNA) to single stranded DNA (ssDNA). Eliminating thermal cycling would allow the use of simpler devices and facilitate the potential for point-of-care testing particularly in resource limited settings. Several isothermal and exponential amplification techniques have been developed,[1,2] such as exponential strand displacement amplification (E-SDA),[3,4] exponential rolling circle amplification (E-RCA),[5–10] exponential amplification reaction (EXPAR),[11–16] nucleic acid sequence based amplification (NASBA),[17–20] helicase-dependent amplification (HDA),[21,22] and recombinase polymerase amplification (RPA).[23] Although there is no need for these techniques to use a high temperature for denaturation, they require enzymes in addition to the polymerase, to help generate ssDNA from dsDNA. EXPAR and SDA[24,25] use the cooperation of an endonuclease and a polymerase to generate ssDNA. HDA and RPA use helicase and recombinase, respectively, to convert dsDNA to ssDNA. One exception is loop-mediated isothermal amplification (LAMP),[26–28] which uses only a polymerase. However, LAMP requires four to six primers, which complicates the design.

Limiting the number of required enzymes and primers would simplify technical procedures and reduce the restrictions on reagent storage requirements, both of which can extend the applicability of amplification techniques for use in point-of-care testing. Despite many recent

---

[*] This chapter has been published as Newbigging A. M., Zhang H., Le X.C. Beacon-mediated exponential amplification reaction (BEAR) using a single enzyme and primer. *Chem. Comm.* **2019**, 55, 10677-10680[40].

advances in isothermal methods with exponential amplification,[29–36] there is no technique that uses a single enzyme and a single primer for isothermal and exponential amplification.

I introduced a new technique, Beacon-mediated Exponential Amplification Reaction (**BEAR**), for the detection of nucleic acid targets using isothermal and exponential signal amplification with a single enzyme and a single primer (Figure 2.1). Key to the **BEAR** technique was a specially designed DNA beacon, the amplifiable beacon, that caged a primer-binding region. The target nucleic acid interacted with the amplifiable beacon and opened the stem, uncaging this region for the primer to bind and initiate polymerase extension. The target strand and an additional fluorophore-conjugated strand (**FS**) were displaced from the beacon and the displaced **FS** produced a fluorescence signal. The target was recycled and interacted with other amplifiable beacons to initiate additional reactions, which would result in linear amplification. To enable exponential amplification of the detection signal, I designed the displaced **FS** to also interact with amplifiable beacons to initiate the amplification reaction. Thus, after being displaced, the **FS** served as a reporter and also initiated more reactions.
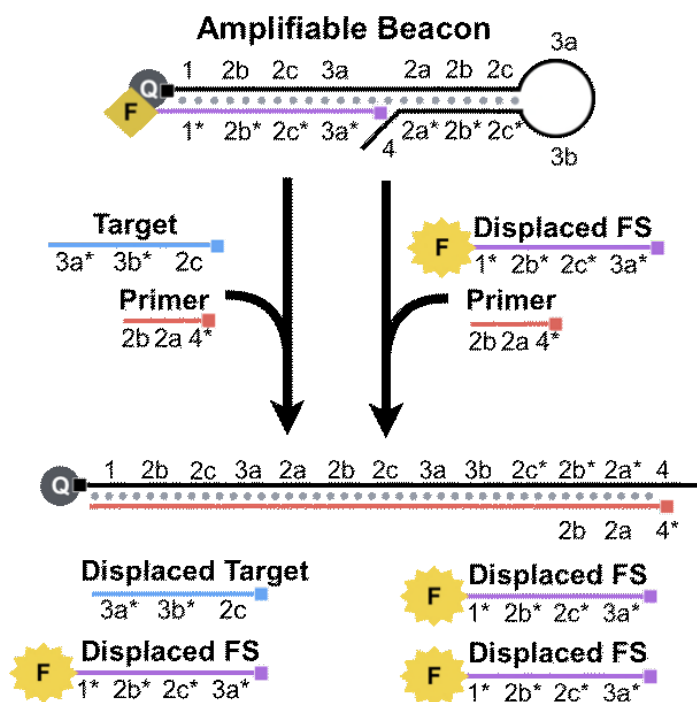
Figure 2.1 BEAR used an amplifiable beacon, a single enzyme, and a single primer to produce amplified fluorescence signals in response to a nucleic acid target. The target and an additional fluorescent strand, **FS**, were displaced. Exponential amplification was achieved because both the displaced target and displaced **FS** cycle back to react with the amplifiable beacon. The small square at the end of the DNA sequences indicates the 5'-end.

For the ease of explanation of the design, complementary domains are denoted with an asterisk (*e.g.* domain **1*** is complementary to domain **1**) (Figure 2.2). The amplifiable beacon was created by annealing the **FS** to the long overhang of a DNA hairpin, **HP**. A fluorescence quencher was conjugated to the 5′ end of **HP** and a fluorophore was conjugated to the 3′ end of the **FS**. When **HP** and **FS** were annealed together to form the beacon, the fluorescence was quenched. The sequence of **HP** contains functional loop (**3a** and **3b**), stem (**2a/2a***, **2b/2b***,

and **2c/2c***), primer-binding (**4**, **2a***, and **2b***), and long 5′ overhang (**1**, **2b**, **2c**, and **3a**) domains. I designed the 14-bp stem to cage a portion of the primer-binding region, **2a** and **2b***, and thus this region was unavailable for the primer to bind.

While **4** is complementary to part of the primer, the main intention of designing this short overhang was to prevent extension *via* the polymerase which would result in target-independent displacement of the **FS**.
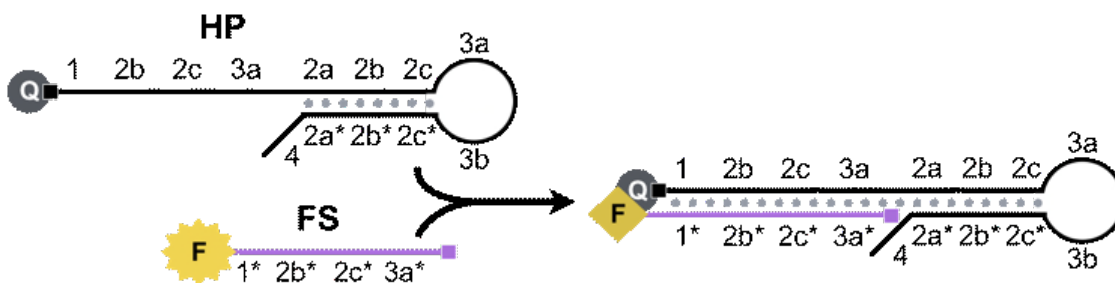
Figure 2.2 The amplifiable beacon was formed by annealing **HP** and **FS** together. **HP** folds into a hairpin with a long single-stranded overhang and is conjugated on its 5' end to a quencher. **FS** was complementary to the **HP** overhang and was conjugated to a fluorophore on its 3' end. The proximity of the quencher to the fluorophore in the amplifiable beacon resulted in quenched fluorescence. The small square at the end of the DNA sequences indicates the 5'-end.

2.2 Experimental

2.2.1 Preparation of DNA oligonucleotides

Sequences of the hairpin probe (**HP**) and fluorophore-conjugated stand (**FS**) are listed in Table 2.1. All DNA oligonucleotides (oligos) were synthesized and purified by Integrated DNA Technologies (IDT, Coralville, IA). Oligos **HP** and **FS** were resuspended to 30 µM using 20 mM TrisHCl pH 7.4. Target oligos (MERRF target, negative control, and mismatches) and primers were resuspended to 100 µM using 20 mM TrisHCl (pH 7.4), and Milli-Q ultrapure water. The stock oligonucleotides were stored at -18°C.

2.2.2 Preparation of the amplifiable beacon

Solutions of **HP** and **FS** mixtures to anneal the amplifiable beacon were prepared at room temperature. The solutions contained 5 µM **HP**, varying concentrations of **FS** depending on the desired **HP**:**FS** ratio, 250 mM $MgCl_2$, 20 mM TrisHCl (pH 7.4), and Milli-Q ultrapure water. Solutions were slowly cooled in a benchtop thermocycler (Biorad, USA) from 90 °C to 20 °C in 2 hr. Annealed amplifiable beacon solutions were stored at 4 °C for up to two weeks.

2.2.3 Procedures of BEAR and fluorescence detection

Reaction solutions were prepared at room temperature in a master mix and typically contained 100 nM of annealed amplifiable beacon solution, 0.1 U/µL Bst 2.0 DNA Polymerase (New England Biolabs, Whitby, ON, Canada), 500 nM primer, 200 µM Deoxynucleotide Solution Mix (dNTP) (New England Biolabs, Whitby, ON, Canada), 1X ROX Reference Dye (Thermofisher Scientific, Canada), 1X Isothermal Buffer that contained 20 mM Tris-HCl, 10 mM $(NH_4)_2SO_4$, and 50 mM KCl, 2 mM $MgSO_4$, 0.1% Tween® 20 (pH 8.8) (New England

Biolabs, Whitby, ON, Canada), and Milli-Q ultrapure water. Reaction solutions were added to 2 μL of either MERRF target sequence, negative control, mismatch target or Milli-Q ultrapure water for a total volume of 20 μL per reaction and incubated at 40°C in StepOnePlus Real-Time PCR System (Thermofisher Scientific, Canada) for isothermal fluorescence detection every 2 min for a total reaction run time of 80 min. Fluorescence intensity was normalized against a reference dye (Normalized Fluorescence), ROX. Normalized fluorescence was calculated by dividing the fluorescence emission of the reporter probe, **FS**, by that of the reference dye, ROX Reference Dye. Time thresholds (Tt) were set by the determination of a baseline by measuring the initial fluorescence in all samples prior to detection of an increase in fluorescence and multiplying the average value by 10 standard deviations.

2.2.4 Conditions of MCF-7 cell cultures and preparation of cell lysate

MCF-7 breast adenocarcinoma cells were cultured in 50 mL T-25 vented flasks treated for cell cultures. The DMEM medium was supplemented with 10% FBS and 1% of penicillin/streptomycin. Cells were grown in 5% CO_2 at 37 °C with 90% humidity. Cells were sub-cultured passaging every 3-4 days at 85-90% confluency using 0.25% (w/v) trypsin-EDTA to detach the cells. Detached cells were centrifuged, resuspended and added into new flasks with fresh, pre-warmed media.

Cells were detached from flasks, counted, and diluted according to the protocols by Osborn et al[37]., where 80 μL of Tris-HCl (pH 7.4) was added for every 10^7 cells. The cell suspension was sonicated to lyse cells and checked for complete lysis visually under microscope. The suspension was centrifuged for 14 min at 13000 rpm (16200xg RCF) to remove cellular debris, and the supernatant was saved. The supernatant was heated to 65°C for 10 min to

inactivate DNAses. The resulting solution was stored in 4°C and used as cell lysate in
subsequent experiments.

2.2.5 Amplifiable beacon design parameters

Table 2.1 Sequences of the MERRF target used, the clinical negative control (wildtype), **HP**,
and **FS**.

Oligo	Sequence of oligo (5'-3')
MERRF Target	GTT AAA GAT TAA GAG A<u>G</u>C CAA CAC CAA A[2]
Negative Control	GTT AAA GAT TAA GAG A<u>A</u>C CAA CAC CAA A[2]
HP	Dark Quencher -TGT GTG TCG TGC GCG TTA AAG GGT GT TGG CTC TCG GAC GCG TTA AAG GGT GTT GGC TCT CTT AAT CTT TAA CGC GTC CGT GAC TTT T
FS	AGA GCC AAC ACC CTT TAA CGC GCA CGA CAC ACA - FAM

Careful design of the oligonucleotides was important for the correct formation of the
amplifiable beacon and the efficiency of the technique. This section outlines important
considerations for designing **FS** and **HP**. Figure 2.3 shows the sequences of **HP** and **FS** forming
the amplifiable beacon separated into domains, Figure 2.2 shows the annealing of **FS** to **HP** to
create the amplifiable beacon, and Table 2.1 shows the sequences of DNA used.

FS was responsible for enabling exponential amplification of the detection signal. In
BEAR, one amplifiable beacon released two reaction initiators, the displaced target and the
displaced **FS**. Therefore, **FS** must be designed to bind to both the overhang of **HP** to form the

amplifiable beacon and the loop and stem domains to initiate **BEAR**. As a result, **FS** contained complementary regions to both the overhang of **HP** and the loop and stem region of **HP**.

To drive **FS** to preferentially bind to the overhang instead of the loop and stem for the correct formation of the amplifiable beacon, domain **1** was added on the overhang (and **1*** on **FS**) to increase the melting temperature of the duplex forming the stable amplifiable beacon. Because domain **1** was not dependent on target sequence, the sequence and length could be adjusted to tune the desired melting temperature of the duplex formed between **FS** and the overhang of **HP**. The complementary domains of **1/1*** were designed to increase the melting temperature of the **FS**:**HP** duplex by about 25°C versus the loop toehold, **3a/3a***.

The stem of **HP** must also be designed to balance the speed of the reaction while ensuring amplifiable beacons do not open in the absence of the target. Increasing the length of the stem and increasing GC content would increase the likelihood that the stem does not open in the absence of any reaction initiators. However, too long of a stem and too high of GC content may inhibit or slow the reaction. The stem was designed to be 14 bp with 57% GC content.

HP has a 3' overhang of four T residues. The function of this overhang was to prevent polymerase extension of the stem using the 5' overhang as a template. The 3' overhang also provided additional nucleotides upstream of the primer for polymerase binding.

Another important design consideration was the location of the 25 nt MERRF target when bound to the loop and stem of **HP**. I aimed to minimize the ability of the negative control sequence, the clinically healthy sequence, to open the stem. The complementary sequence to capture the MERRF target was oriented such that when bound to the amplifiable beacon, the location of the point mutation was placed in the centre of the loop with 8-nt and 9-nt flanking either side of the point mutation location. Additionally, the target had a 3-nt long 3' unhybridized

region when bound to its complementary domains on the loop and stem of the amplifiable

beacon. The function of this unhybridized region on the target was to inhibit the polymerase

from extending the target as if it were a primer.
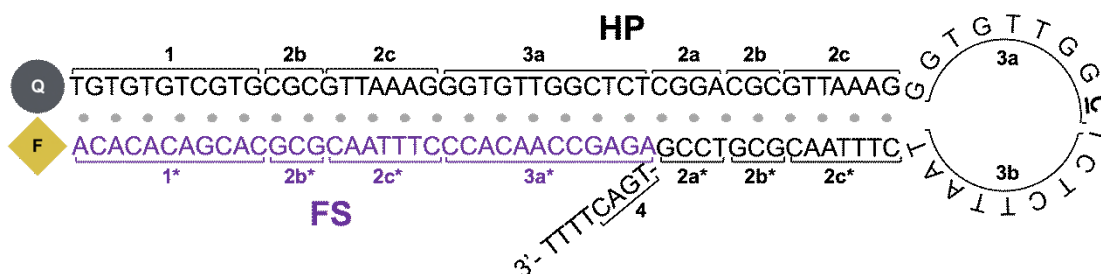
Figure 2.3 The sequence and domains of the amplifiable beacon. The amplifiable beacon
consisted of **HP** in a hairpin conformation with **FS** bound to its overhang. The 5' end of **HP** was
conjugated to a quencher and the 3' end of **FS** was conjugated to a fluorophore. The close
proximity of the fluorophore to the quencher quenched its fluorescence. The complementary
base of the MERRF target point mutation in the loop is bolded and underlined.

2.3 Results and Discussion

2.3.1 Reaction principle

BEAR began when a nucleic acid target binds to **3a**, **3b**, and **2c*** of the loop and stem

of **HP** within an amplifiable beacon (Figure 2.4A). The stem opened and exposed **2a*** and **2b*** to

the primer. The subsequent binding of the primer to **4**, **2a***, and **2b*** initiated 5′ to 3′

extension *via* a DNA polymerase, using **HP** as the template. The polymerase, Bst 2.0, was

selected for its strong strand displacement activity, lack of 3' to 5' exonuclease, and tolerance of a

large range of reaction temperatures. The polymerase displaced the target and the **FS** that

comprised the amplifiable beacon. When the **FS** was displaced from **HP**, the fluorophore and

quencher were separated, and the fluorescence was restored. After complete polymerase extension, **HP** had no further purpose in the reaction and was waste. The displaced target was cycled back to initiate new reactions by binding to other amplifiable beacons.

I achieved exponential amplification of the detection signal by allowing the displaced **FS** strands to also initiate additional reactions (Figure 2.4B). This is because I designed the **FS** to complement both the overhang of **HP** and the loop and stem of **HP**. Although the fluorescence of the **FS** bound to the overhang of **HP** was quenched, the **FS** bound to the loop and stem of **HP** retained its fluorescence. Similar to the reaction initiated by the target, binding of the **FS** to the loop and stem domains (**3a**, **2c**, and **2b**) of **HP** exposed **2a*** and **2b*** to the primer. The polymerase extended the primer and displaced both the initiating **FS** and the previously bound **FS**, restoring the fluorescence of the **FS**. Both displaced **FS** strands could further bind to other beacons to initiate additional reactions. The cyclic reactions initiated by the target and then by the displaced **FS** resulted in exponential amplification.

As a proof-of-concept, I applied my technique to detect the point mutation, 8344A > G, in mitochondrial DNA (mtDNA), as a 25-nt target[38]. This point mutation is associated with Myoclonus Epilepsy with Ragged Red Fibres (MERRF). The Seitz group has shown that the conformational constraint of the beacon can discriminate mismatches[39].
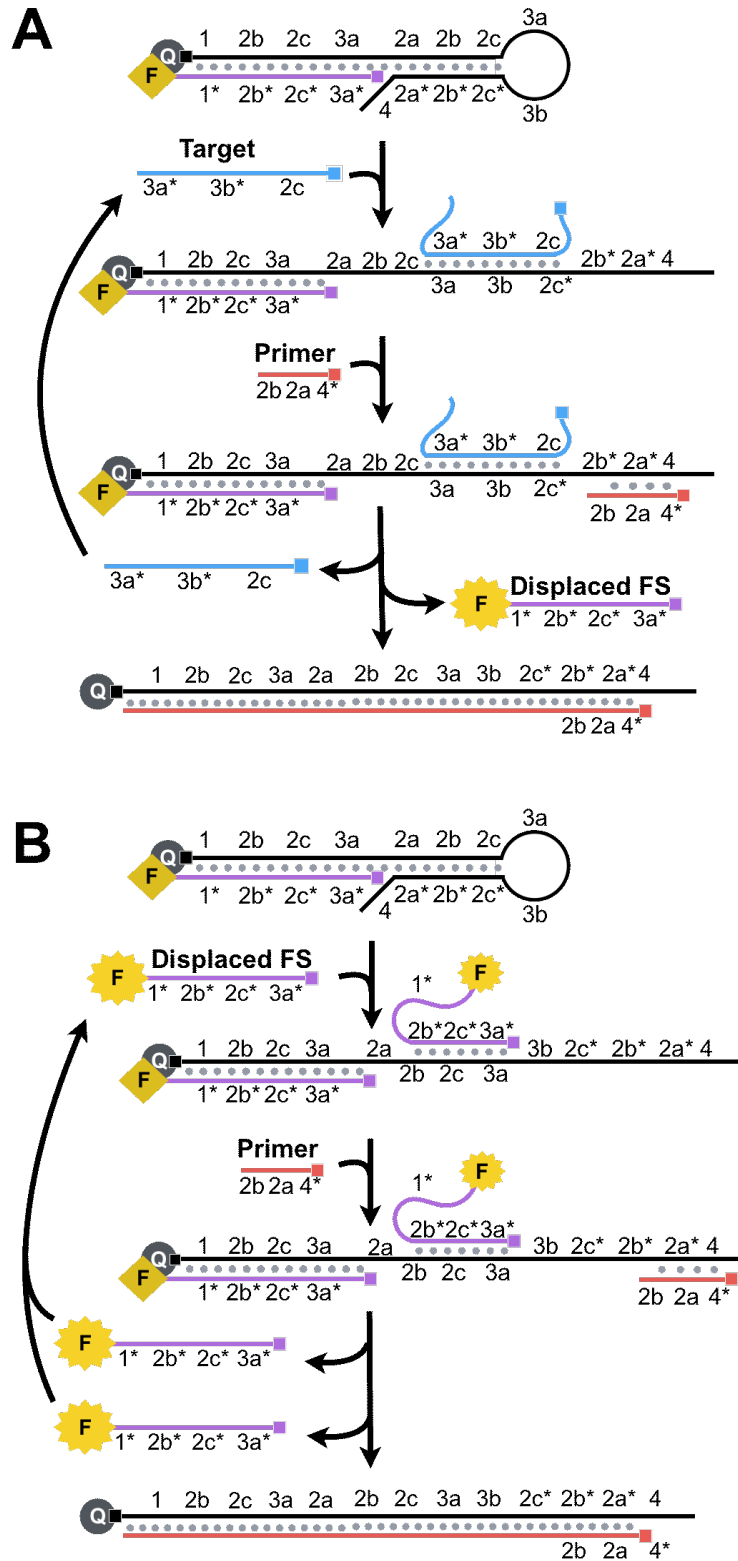
Figure 2.4 (A) Binding of the target to the loop and stem of **HP** (**3a**, **3b**, and **2c***) opened the stem to uncage the primer-binding domains (**2a*** and **2b***). Primer binding and subsequent

extension *via* the polymerase displaced the target and the previously annealed **FS**. The fluorescence of the **FS** was restored as it became separated from the quencher. The target was recycled and thus amplification was achieved. (B) The displaced **FS** also could bind to the loop and stem of **HP** (**3a**, **2c**, and **2b**) to open the stem and initiate the primer extension. Primer binding and subsequent extension *via* the polymerase displaced both copies of the **FS**. The displaced **FS** was fluorescent and was also recycled for the amplification reactions. Thus, the cyclic reactions involving both the target and the displaced **FS** resulted in the exponential amplification.

2.3.2 Typical amplification curves

Figure 2.5 shows the typical amplification curves of the **BEAR**. The sigmoidal shape of the curves generated by 100 pM of the synthetic MERRF target sequence and blank demonstrates characteristic exponential amplification. Similar to other techniques with exponential amplification, three phases were observed: lag, exponential, and plateau. The reaction at 0 min contained primarily amplifiable beacons, characterizing the lag phase. In the lag phase, there was a small number of initiating molecules (target or displaced **FS**), which resulted in the slow propagation of the reaction and fluorescence output below the detection limit of the fluorometer. The exponential phase, at ~26–54 min, generated substantial fluorescence because of the increased amount of displaced **FS** that are continually reacting with other amplifiable beacons to produce detectable fluorescence signals and more displaced **FS**. Both the lag phase and exponential phase consisted of amplifiable beacons that were readily available in abundance for the target or displaced **FS** to bind to for the propagation of the reaction. The plateau phase was a result of the exhaustion of available amplifiable beacons. In the plateau, all amplifiable beacons

were converted to waste. Because there were no available amplifiable beacons for **FS** to react

with, **FS** was free in solution.

The background signal may have arisen from the leakage of DNA structures as a result of

incomplete chemical synthesis. Leakage may have caused improper formation of amplifiable

beacons and may have resulted in target-independent displacement of the **FS** that was then

exponentially amplified.
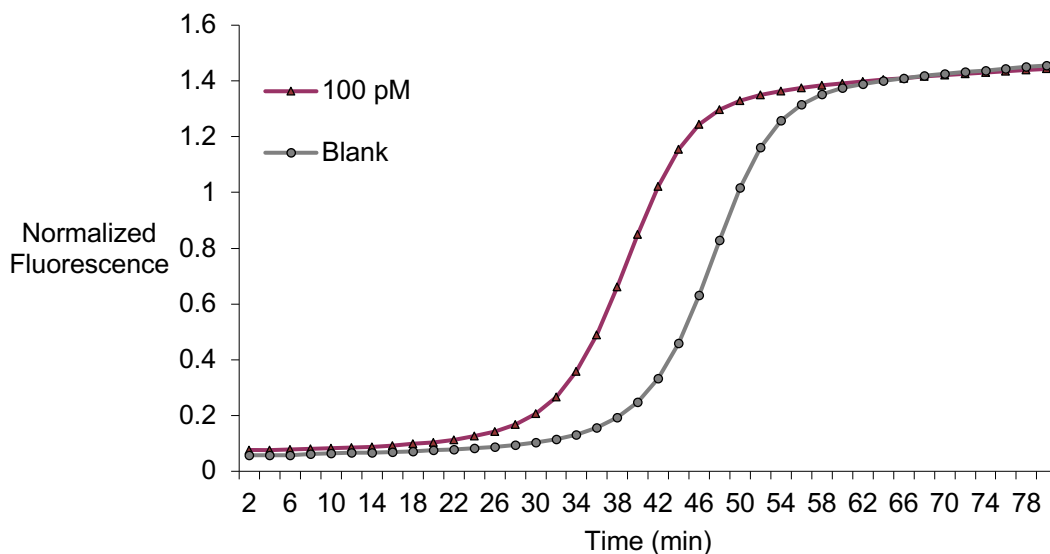
Figure 2.5 Typical signal amplification curves of **BEAR**, showing the progression of
fluorescence from reactions with either 100 pM of MERRF target or water as blank. The
sigmoidal shape of the curve is characteristic of exponential amplification. Fluorescence was
normalized against a reporter dye and monitored over time in minutes.

The amplification products were detected at various amplification time points by

sampling the reaction mixture and separating the components using PAGE (Figure 2.6). The

amplifiable beacon and reaction products, including the displaced **FS**, transient complexes, and

waste, were detected. The predicted products were detected in each phase: lag (0–28 min),
exponential (~32–46 min), and plateau (after 48 min). At 0 min, the only apparent band
corresponded to the annealed amplifiable beacon structure (iii). This band disappeared as the
reaction proceeded and yielded no fluorescence. Waste (ii), a higher molecular weight than the
amplifiable beacon, increased throughout the reaction and did not fluoresce. Both displaced **FS**
and **FS** bound to the loop/stem of **HP** within amplifiable beacons retained fluorescence. Thus,
the fluorescing product at 46-48 min corresponded to the high molecular weight complex of
amplifiable beacons bound to **FS**. Amplifiable beacons bound to **FS** appeared in the exponential
phase but disappeared as the reaction proceeded. The appearance and disappearance of this
transient structure was consistent with the **BEAR** reaction principle. Low molecular weight, free
FS (iv), could be seen fluorescing from 36-48 min when there the amount of waste was greater
than that of amplifiable beacons.
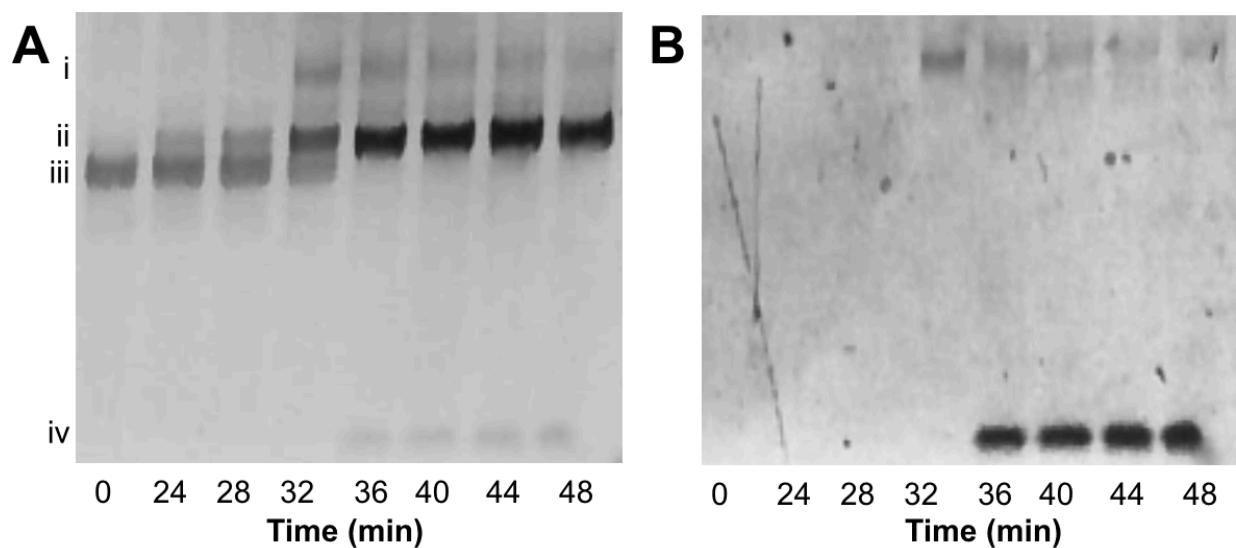
Figure 2.6 BEAR was stopped at various time points with chilled EDTA. The reaction
components at each time point were separated on a 10% Native PAGE and imaged after (A)
SYBR gold staining and using the detection of (B) FAM fluorescein.

2.3.3 Effect of amplifiable beacon concentrations

The effect of changing the concentration of amplifiable beacon in the reaction is shown in Figures 2.7 to 2.9. Decreasing the concentration of the amplifiable beacon decreased the maximum amount of fluorescence and vice versa. I expected this result because the total amount of fluorophores, conjugated to **FS**, was decreased since the amplifiable beacon was comprised of **FS** and **HP**. In changing the amount of amplifiable beacon, the amount of fluorescence output also changed.

The speed of the reaction was also changed when varying the concentration of the amplifiable beacon. The speed of the reaction was slower with 150 nM and 200 nM of amplifiable beacon as compared to using 100 nM of amplifiable beacon. This can be explained by a longer lag time where the absolute amount of empty **HP** in using 150 nM and 200 nM of amplifiable beacon was increased, when using the same **HP**:**FS** ratio. **HP** with no **FS** bound to it may have sequestered the target strand or displaced **FS**, which did not contribute to exponential amplification.
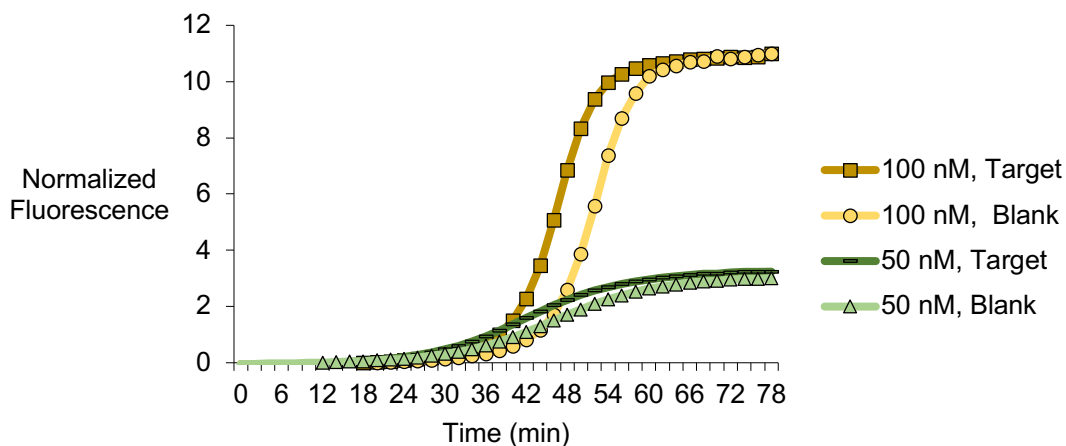
Figure 2.7 The effect of reducing the concentration of the amplifiable beacon from 100 nM to 50 nM with 100 pM of MERRF target.
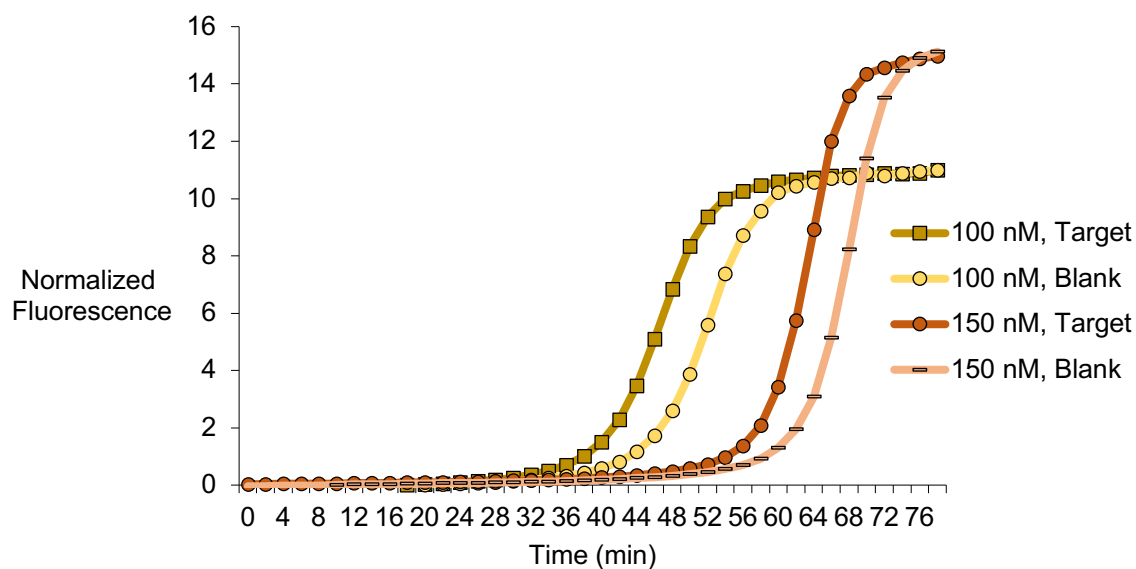
Figure 2.8 The effect of increasing the concentration of the amplifiable beacon from 100 nM to 150 nM with 100 pM of MERRF target.
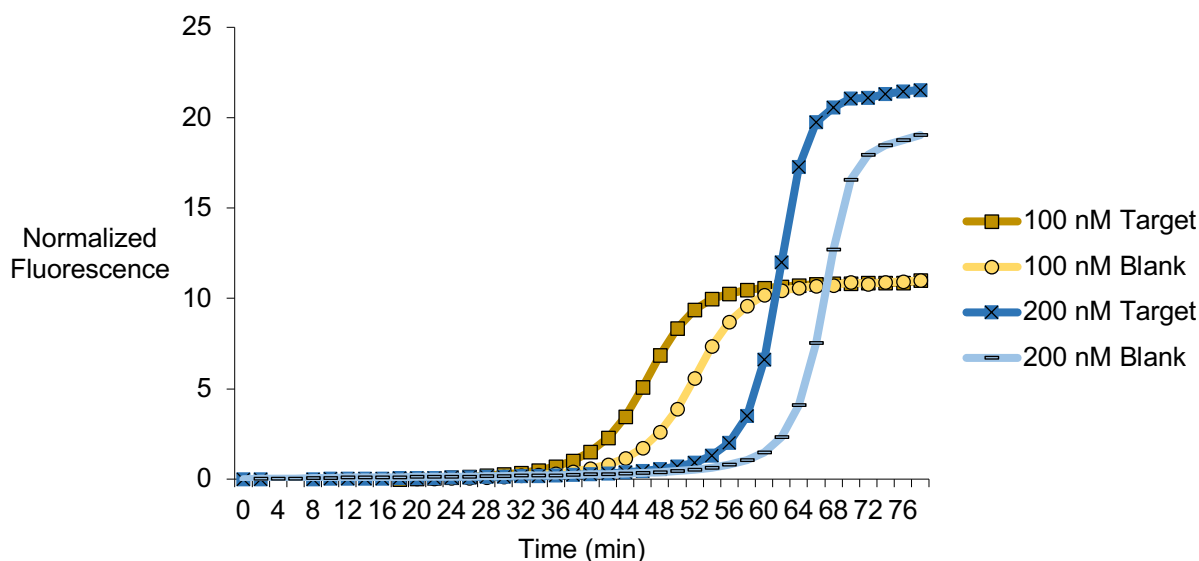
Figure 2.9 The effect of increasing the concentration of the amplifiable beacon from 100 nM to 200 nM with 100 pM of MERRF target.

2.3.4 Effect of the ratio of FS to HP

For the formation of the amplifiable beacon, the **FS** must be bound to the 5′ overhang

of **HP** instead of the loop and stem, as the **FS** is complementary to both. If the **FS** binds the loop

and stem in the absence of the target, the resulting reaction would produce background. To drive

the binding of the **FS** to the overhang, I increased the complementarity of the **FS** to the overhang

relative to that of the loop and stem by extending the length of **1** on the overhang.

I tested the annealing of the **FS** to **HP** using various ratios of [**HP**] to [**FS**]. I separated the

annealing products from each of these reaction mixtures using polyacrylamide gel

electrophoresis (PAGE) (Figure 2.10). Product (iii) corresponded to **HP**, and the increasing band

intensity corresponded to increasing amounts of **HP** relative to the **FS**. Product (ii) was the

correctly formed amplifiable beacon whose fluorescence was completely quenched. When the

amount of **FS** was in excess of **HP** in a ratio of 1.5:1, product (i) was detectable, representing the

annealed amplifiable beacon with an additional **FS** bound to the loop and stem. The addition of

51

the **FS** in excess of **HP** in a ratio of 1.5:1 to force the **FS** to bind the loop and stem of the beacon supported the fact that domain **1** was sufficient to drive the binding of the **FS** to the overhang of **HP**. I further optimized the ratios of [**HP**] to [**FS**] to maximize amplification of the target while minimizing the background (Figure 2.11).
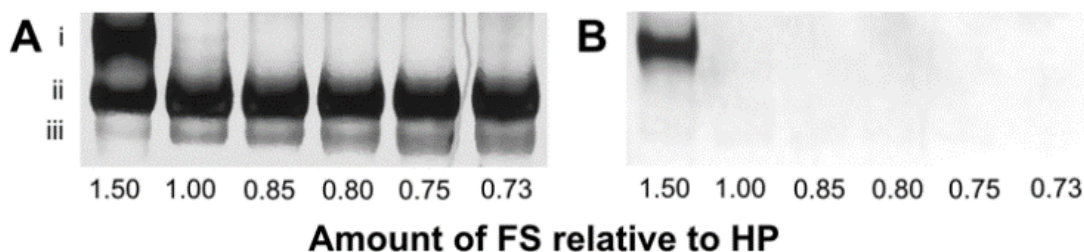
Figure 2.10 Native PAGE (10%) analyses of amplifiable beacon solutions containing various ratios of [**HP**] to [**FS**] (1:1.5, 1:1.0, 1:0.85, 1:0.80, 1:0.75, and 1:0.73). The gel was imaged for FAM fluorescence (B), then stained with SYBR Gold (A) and imaged again. All products are therefore visualized in image A, and only products that have unquenched fluorescence are visualized in image B. The bands correspond to: (i) amplifiable beacon bound to the **FS**, (ii) amplifiable beacon, and (iii) **HP**.

I prepared the amplifiable beacon by mixing 5 μM of **HP** and various amounts of **FS** in a single tube with annealing solution and I heat denatured the solution by heating at 95°C for 5 min, followed by slow cooling to room temperature over 2 h. Denaturation of **HP** and **FS** converted any dsDNA secondary structures into ssDNA. Slow cooling the solution to room temperature resulted in **HP** folding into a hairpin first, followed by **FS** annealing to the 5'

overhang of **HP**. **FS** preferentially bound to the overhang of **HP** instead of the loop and stem of

HP due to the greater duplex stability attributed to the additional **1/1*** domain interaction.

Although it was possible that **HP** could dimerize because of the nature of the hairpin stem, the

domains that make up the stem were too short (14-bp) to withstand the initial denaturation and

the formation of the more favourable intrastrand hairpin conformation preceded over **HP**

interstrand dimerization.

The ratio of **HP** to **FS** was important to consider when annealing the amplifiable beacon.

In ratios with an excess of **HP** to **FS**, the resulting solution contained amplifiable beacon and **HP**

in a hairpin conformation. In ratios with an excess of **FS** to **HP**, the resulting solution contained

amplifiable beacons bound to **FS**. High amounts of **FS** in annealing mixes may lead to the

formation of amplifiable beacons with an additional **FS** bound to the loop and/or stem. This was

undesirable because the additional **FS** bound to amplifiable beacons could initiate **BEAR** in the

absence of the target, thereby increasing the background signal. My strategy to prevent

background due to **FS** binding to amplifiable beacons in the annealing process was to use

annealing solutions where **HP** was always in excess of **FS**. Adjusting the ratios of [**HP**] to [**FS**]

could control the correct formation of the amplifiable beacon and could be further analyzed by

reaction with the target and blank in **BEAR**.

Figure 2.11 shows the effect on **BEAR** when using amplifiable beacon annealed from

various ratios of [**HP**] to [**FS**]. Nominal ratios 1:0.85 and 1:0.83 were presumed to have *de facto*

excess **FS** relative to **HP**, as both of these ratios showed an increase in both the reaction and

blank signal, where the target-initiated reaction and blank signal become indistinguishable. On

the other hand, if **HP** was in excess, there would be some free **HP** with its overhang not

hybridized to **FS**. Because the complementarity of **FS** to the 5' overhang was more favourable

than that of the loop and stem of **HP**, it was likely that the displaced **FS** from the target-initiated

reaction would preferentially bind to the free 5' overhang on **HP** instead of the loop, which

would halt the propagation of the reaction. I suspected that the lag time prior to the exponential

amplification for each of the curves may partially be due to displaced **FS** binding to the overhang

of free **HP** in solution, rather than the loops and stems of **HP** within amplifiable beacons,

resulting in linear amplification. This prediction was supported by the results obtained with

excess of **HP** over **FS**. With an **HP:FS** ratio of 1:0.75, the high **HP** concentration relative to **FS**

did not produce detectable exponential amplification for the duration of the 80 min. The

annealing solution corresponding to a nominal ratio of 1:0.80 of **HP** to **FS** maximized the

amount of the correctly formed amplifiable beacon without increasing the blank signal

substantially and was used for subsequent reactions.
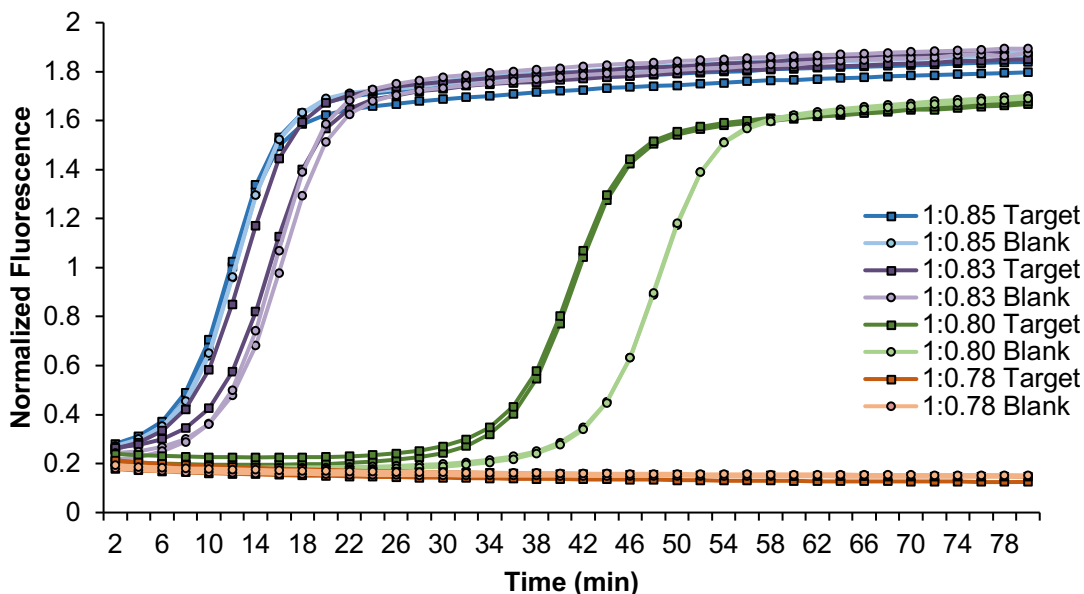
Figure 2.11 Amplification curves showing the effect of varying the nominal amount of **FS** (0.85, 0.83, 0.80, 0.78) relative to **HP** in amplifiable beacon annealing solutions. Target refers to 100 pM MERRF target sequence, and blank refers to all reagents in the **BEAR** mixture without the MERRF target.

2.3.5 Effect of primer length and position

The primer binding location on **HP** was partially caged within the stem, **2b*** and **2a***, and partially exposed, **4**. I designed two sets of primers to determine the optimal primer length. In one set, I fixed the sequence of the primer on the 5′ end (Primer 5-n) and changed the length of the domain complementary to the stem of **HP** (**2b*** and **2a***). In the second set, I fixed the sequence of the primer on the 3′ end (Primer 3-n) and changed the length of **4***. I also tested a full-length primer of 11-nt (Primer 11). The names and sequences of each primer used are shown in Table 2.2, and the binding positions of each primer are shown in Figure 2.12. Primer 11 refers to the full-length primer.

Figure 2.13 shows that the full-length primer, Primer 11, produced a fast reaction in both the target and the blank, resulting in a small ΔTt (difference between Tt_{blank} and Tt_{target}). As expected, both primer sets resulted in slower reactions with decreasing primer lengths, which implied that the duplex stability of the bound primer contributed to the rate of the reaction. The shortest primer in each set produced the largest ΔTt. Primers 5–8 and 3–8 showed no substantial difference in ΔTt, indicating that the binding position of the primer did not substantially affect ΔTt. For subsequent experiments, I used Primer 5–8. To determine the optimal concentration of Primer 5-8, I tested various concentrations of Primer 5-8, shown in Figure 2.14. Because 500 nM of Primer 5-8 produced the greatest ΔTt, I used a concentration of 500 nM for subsequent reactions.

Table 2.2 Primer sequences with the original, 9 nt primer, and variations in length and position.

Name of Oligonucleotide	Sequence of Oligonucleotide (5'-3')
Primer 11	GTCACGGACGC
Primer 5-10	TCACGGACGC
Primer 5-9	CACGGACGC
Primer 5-8	ACGGACGC
Primer 5-7	CGGACGC
Primer 3-10	GTCACGGACG
Primer 3-9	GTCACGGAC
Primer 3-8	GTCACGGA
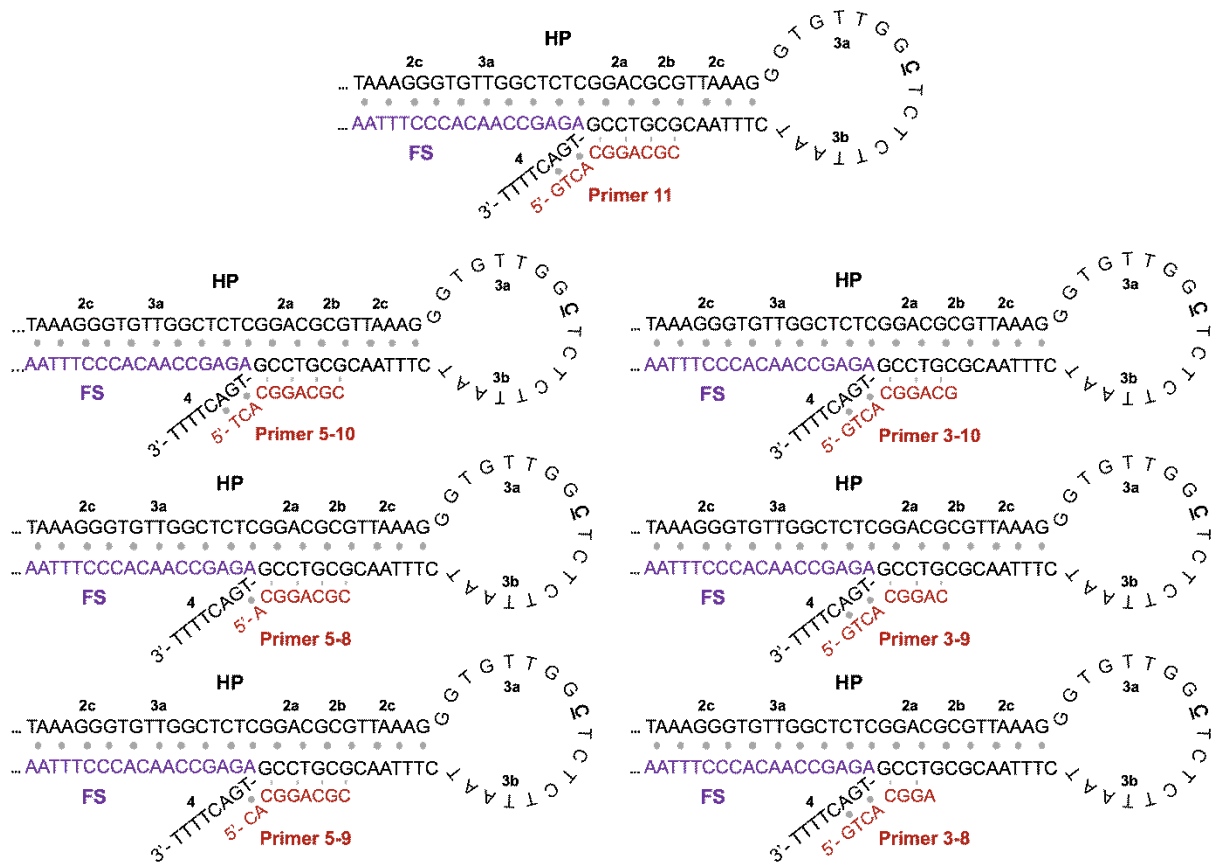
Figure 2.12 The binding locations of the 11-nt primer (Primer 11) and each truncated primer (Primer 5-n and Primer 3-n) to **HP** within amplifiable beacons. Stem opening via either the target or **FS** is not shown. The location of the base in the loop of **HP** that is complementary to the point mutation in the MERRF target is bolded and underlined.
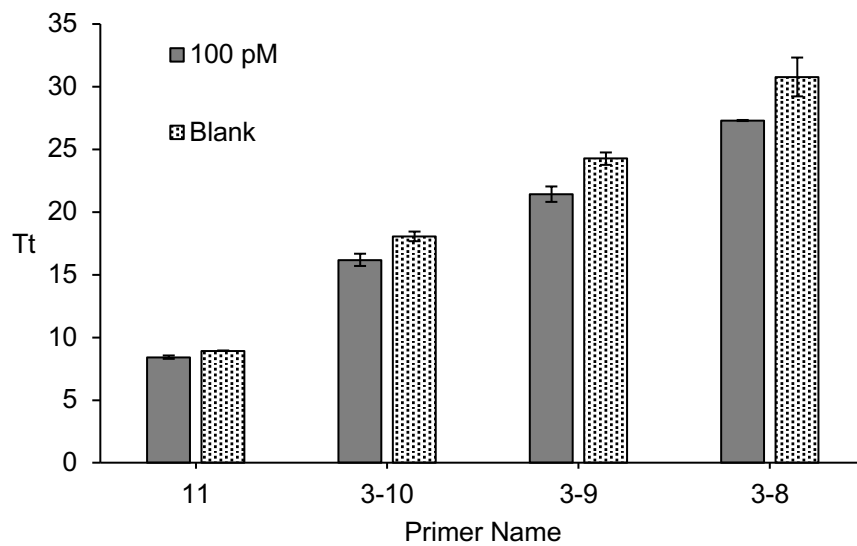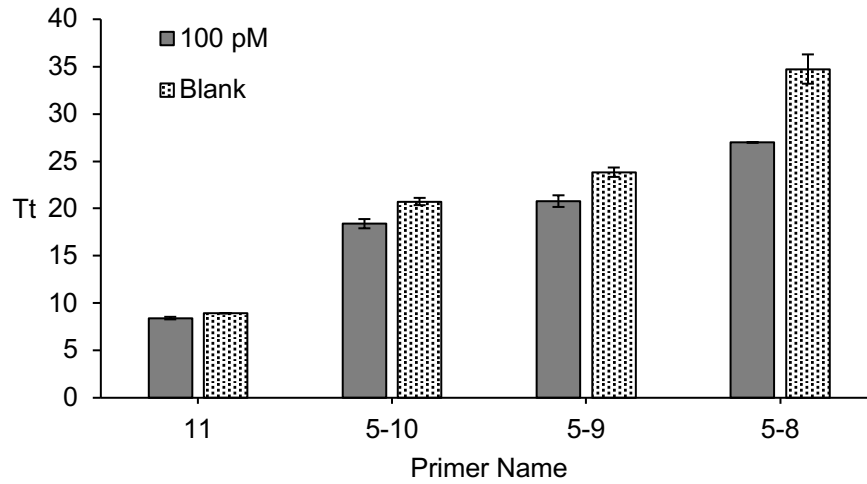
Figure 2.13 The effect on **BEAR** when using 100 pM of MERRF target (100 pM) or water (Blank) when truncating the primer from 11 nt to 10 nt, 9 nt, 8 nt from the (**A**) 5' end (Primer 5-n) or (**B**) 3' end (Primer 3-n). Primer 5-7 yielded no detectable signal in the experimental timeframe.
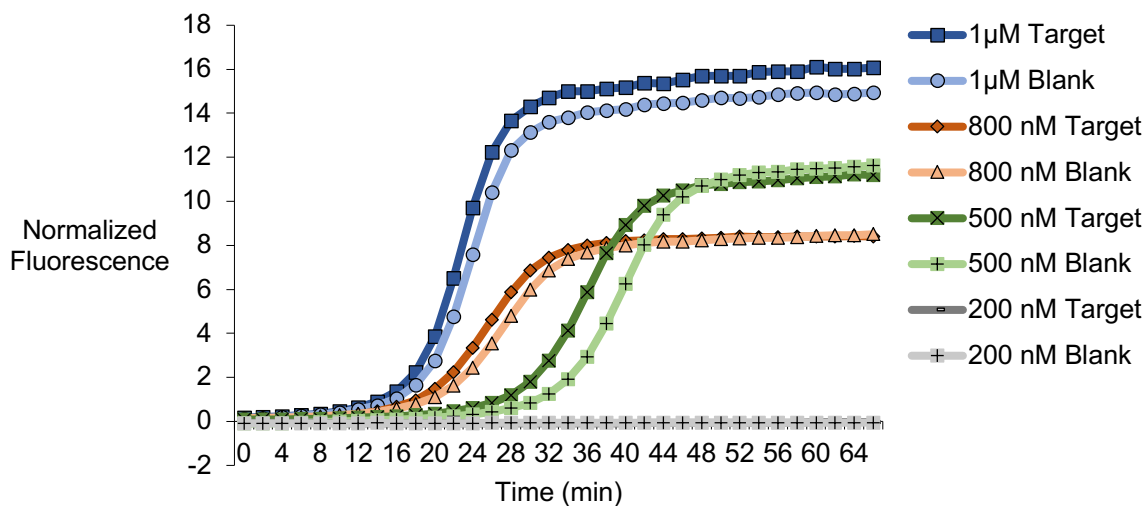
Figure 2.14 Various concentrations of Primer 5-n tested with 100 nM of MERRF target.

2.3.6 Effect of varying reaction conditions

The rate of the **BEAR** can be increased or decreased by varying the temperature and

concentration of polymerase used. Figures 2.15 and 2.16 show that although the reaction is

increased at higher temperatures or increased concentrations of polymerase, respectively, the

background is also increased. Reaction conditions of a temperature of 40 °C with 0.1 U/L of Bst

2.0 polymerase resulted in the most optimal target to blank signal ratio in <1 hr.
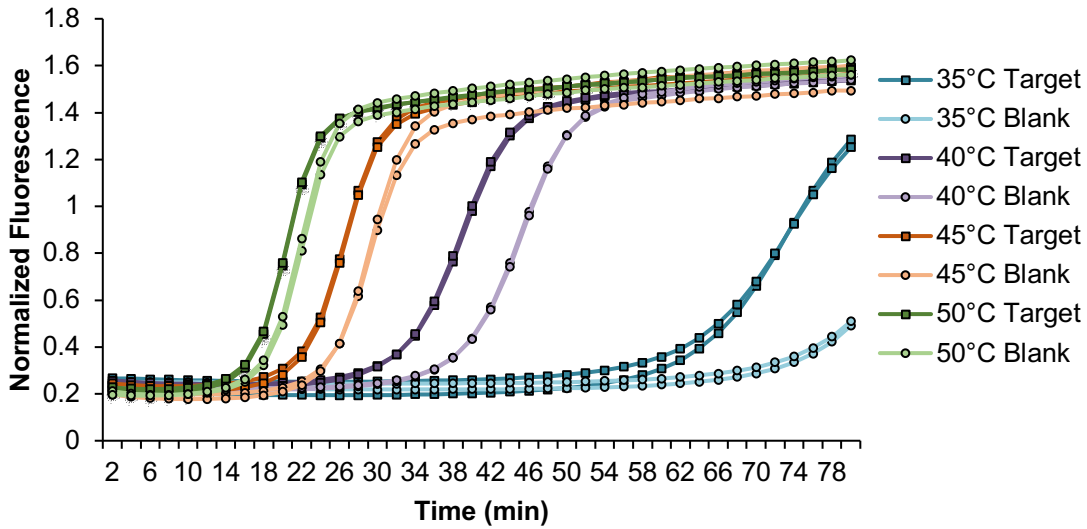
Figure 2.15 Amplification curves showing the effect of temperature (35, 40, 45, 50°C) on **BEAR** with 100 pM of MERRF target and blank.
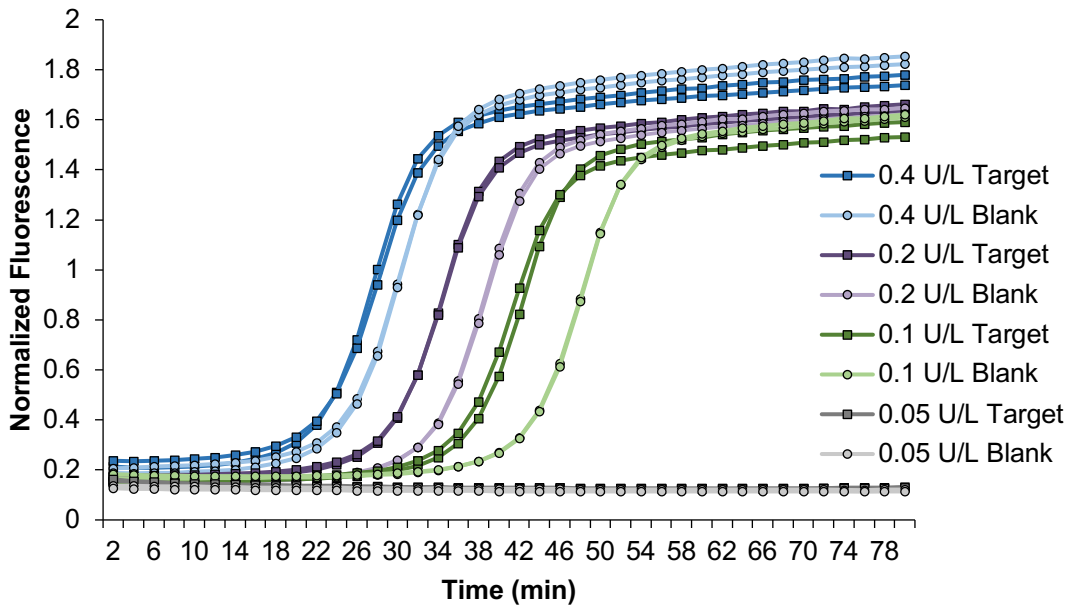
Figure 2.16 Amplification curves showing the effect of varying Bst 2.0 polymerase concentrations (0.4, 0.2, 0.1, 0.05 U/L) on **BEAR** with 100 pM of MERRF target and blank.

2.3.7 Effect of the mismatch placement on the loop of HP

The **BEAR** technique for the detection of the 25-nt nucleic acid sequence corresponding to the

8344A>G point mutation resulting in MERRF situated the location of the point mutation in the

centre of the loop of **HP** when the target was bound and therefore, the clinical negative control

(Negative Control) contained a mismatch at this location. The location of the mismatch could

affect the specificity of the reaction by its ability to open the stem after binding to the loop. To

determine the optimal location of the point mutation, I tested the MERRF target, Negative

Control and three mismatches located on either side of the loop, and on the stem nearest to the 3'

end of **HP**. To do this, I designed three arbitrary mismatches (Mismatch 1, 2, and 3) in the

MERRF target sequence. The sequences for the MERRF target, negative control, and arbitrary

mismatches are listed in Table 2.3 and the locations when bound to the amplifiable beacon are

shown in Figure 2.17.

Table 2.3 Sequences of the MERRF target A8344G mutation in comparison to the clinical negative control (wildtype) and other mismatches tested to determine the optimal complementary region on **HP** for the position of the point mutation. Location of MERRF point mutation is underlined. Arbitrary mismatches created are bolded.

Name of Oligonucleotide	Mismatch Position Relative to HP	Sequence of Oligonucleotide (5'-3')
MERRF Target	Centre of loop	GTTAAAGATTAAGAGAGCCAACACCAAA
Negative Control	Centre of loop	GTTAAAGATTAAGAGA<u>A</u>CCAACACCAAA
Mismatch 1	On loop near **HP** 3' end	GTTAAAGAT**G**AAGAGAGCCAACACCAAA
Mismatch 2	On stem near **HP** 3' end	GTT**G**AAGATTAAGAGAGCCAACACCAAA
Mismatch 3	On loop near **HP** 5' end	GTTAAAGATTAAGAGAGCCAA**G**ACCAAA
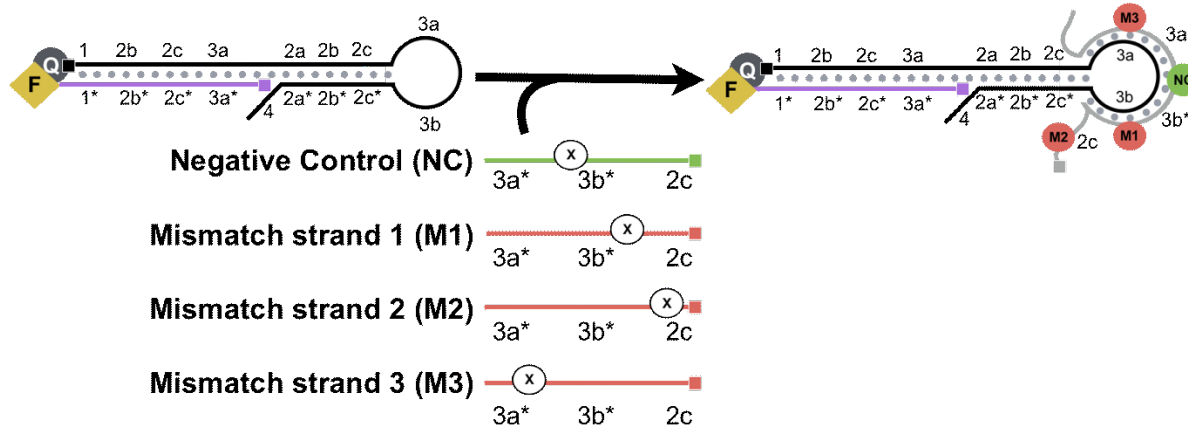
Figure 2.17 Locations of each mismatch when the clinical negative control (NC) and arbitrary mismatch strands to simulate the effect of mismatches at each location, Mismatch 1 (M1), Mismatch 2 (M2), and Mismatch 3 (M3), are bound to **HP**. The (x) positioned on each sequence indicates the general location of the mismatch within the strand.

The ΔTt resulting from 100 pM of MERRF target, Negative Control, and the three mismatches (Mismatch 1-3) are shown in Figure 2.18. A large ΔTt for the MERRF target, and low ΔTt for the Negative Control is desirable for specificity. Aside from the Negative Control, Mismatch 1 produced the largest ΔTt. This mismatch was placed on the loop adjacent to the stem binding domain, **2c**. Mismatch 2, which places the mismatch within **2c**, yielded a similar ΔTt to the MERRF target. Because this mismatch had the complete loop toehold complementary sequence, it was able to bind to the loop as did the MERRF target, yielding poor specificity. Mismatch 3 also produced ΔTt similar to that of the MERRF target. When comparing Mismatch 1 and 3, Mismatch 1 was more effective in producing better specificity than that of Mismatch 3, indicating that the position of the mismatch on the loop relative to the stem was an important

factor in opening the stem. Mismatch 1 was located adjacent to the stem complementary domain **2c**, which may have inhibited stem opening. Thus, as Mismatch 3 was placed further away from **2c**, it allowed complete binding to the loop adjacent to the stem domain and as a result, stem opening for the initiation of the reaction. The Negative Control yielded the most optimal specificity as the point mutation was placed in the centre of the loop. This location reduced the ability for the Negative Control to effectively bind the loop toehold to initiate the reaction.
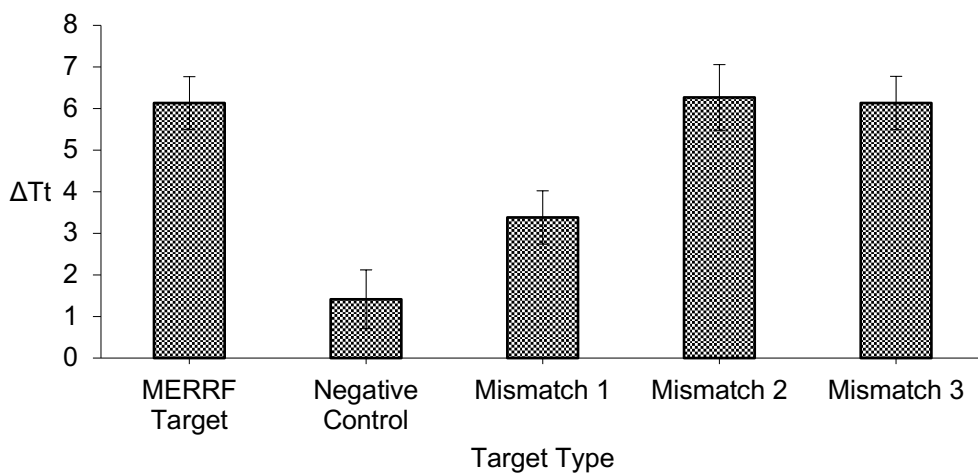
Figure 2.18 The ΔTt (difference between target and blank time at threshold) of Mismatch locations, the MERRF clinical negative control, and the MERRF target. Reactions initiated with 100 pM of each respective oligonucleotide and performed in triplicates. Error bars represent the standard deviation.

2.3.8 Sensitivity and selectivity

I assessed the dynamic range of **BEAR** using various concentrations of the MERRF target sequence, from 1 nM to 10 fM (Figure 2.19). I also obtained the limit of detection (LOD) by testing seven replicate blanks and comparing it to our calibration. The LOD, calculated as the concentration equivalent to three times the standard deviation of blanks plus the background signal ($3SD_{blank} + Tt_{blank}$), was about 10 fM (0.2 amol). The curves of the low concentrations (10 pM to 1 fM) are shown in Figure 2.20 from 32 to 56 min.
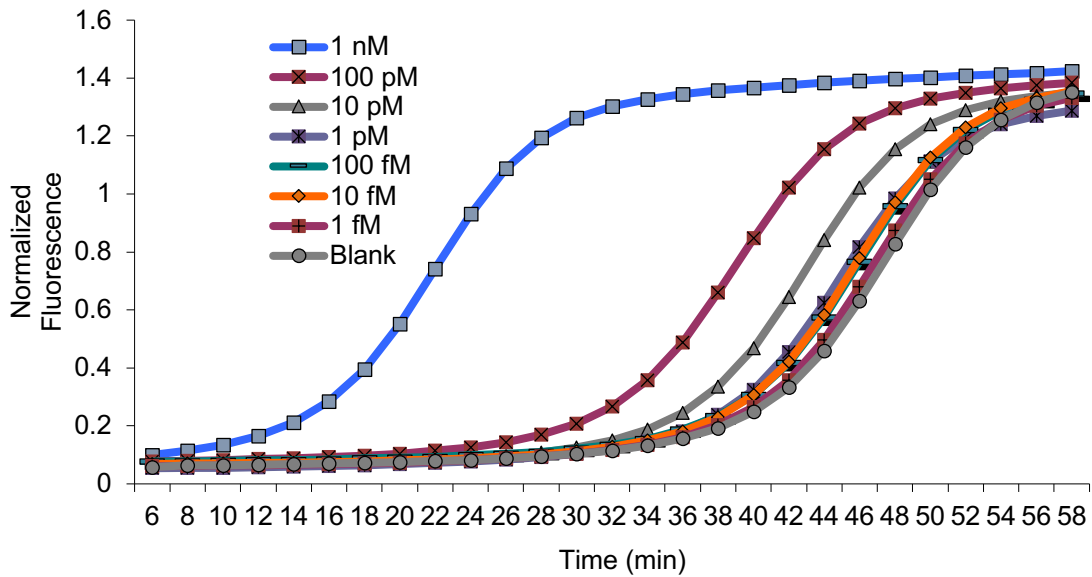
Figure 2.19 Amplification curves using various concentrations of the MERRF target.
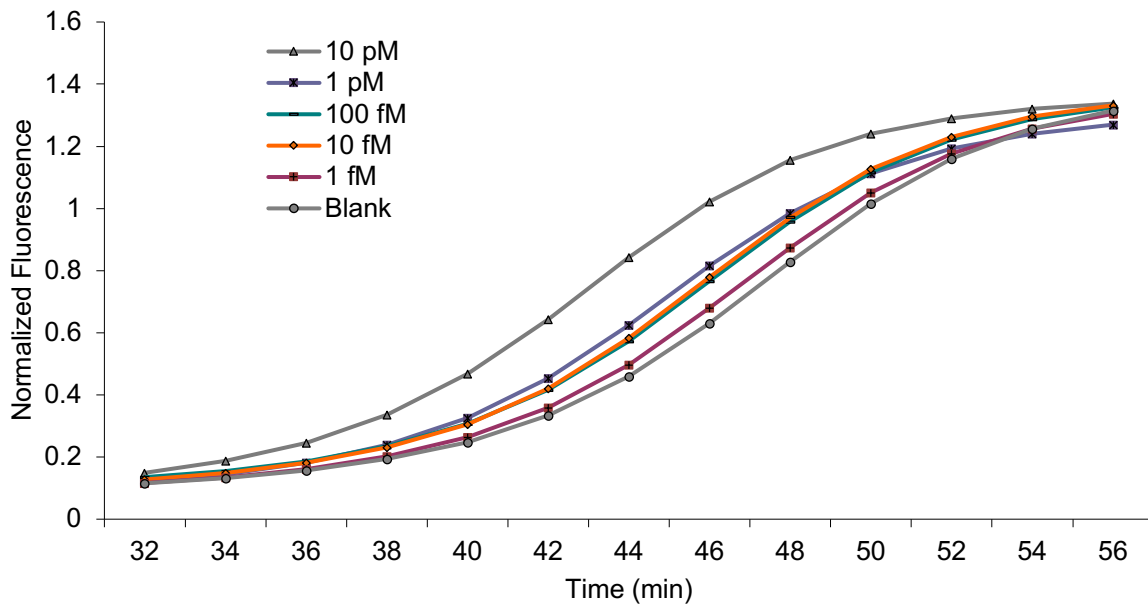
Figure 2.20 Amplification curves of concentrations from reactions containing low concentrations MERRF target, ranging from 10 pM to 1 fM. Reactions times from 32 min to 56 min were shown.

I also investigated the specificity of **BEAR** by assessing the detection of the MERRF target sequence and the clinical negative control (NC), the normal mtDNA sequence. I compared the reaction of 100 pM of the MERRF target with 100 pM of the clinical negative control (Figure 2.21). The **BEAR** achieved a discrimination factor of 16.
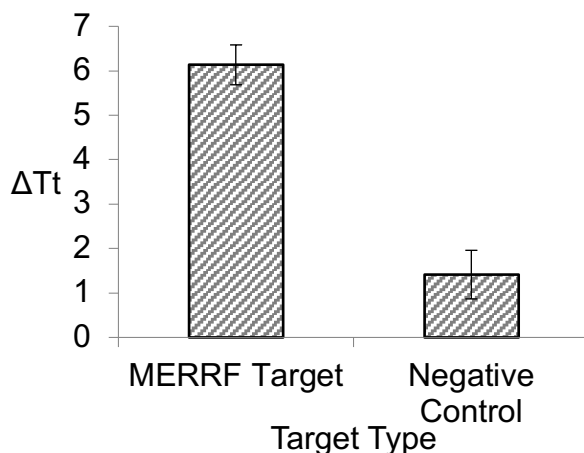
Figure 2.21 Comparison between 100 pM of the MERRF target and 100 pM of the negative control against the difference of time at threshold between target and blank (ΔTt). Error bars represent standard deviation from triplicate analyses.

2.3.9 Detection of MERRF target in cell lysate

I tested detection of the MERRF target DNA spiked in the lysate of MCF-7 human breast adenocarcinoma cells. I added a measured amount of MERRF target DNA to the lysate of 10^7 MCF-7 human adenocarcinoma cells so that the concentration of the MERRF target DNA was 10 pM. Representative amplification curves from the detection of 10 pM MERRF target DNA in the lysate of MCF-7 human adenocarcinoma cells and from the reagent blank are shown in

Figure 2.22. Using triplicate analyses of the cell lysate, using a calibration of the MERRF target DNA in buffer solutions, I determined that the concentration of the MERRF DNA was 9.1 ± 0.8 pM. These results, representing an average recovery of 91%, were consistent with the expected concentration of 10 pM. No MERRF DNA was detectable in the cell lysate without the addition of the MERRF DNA.
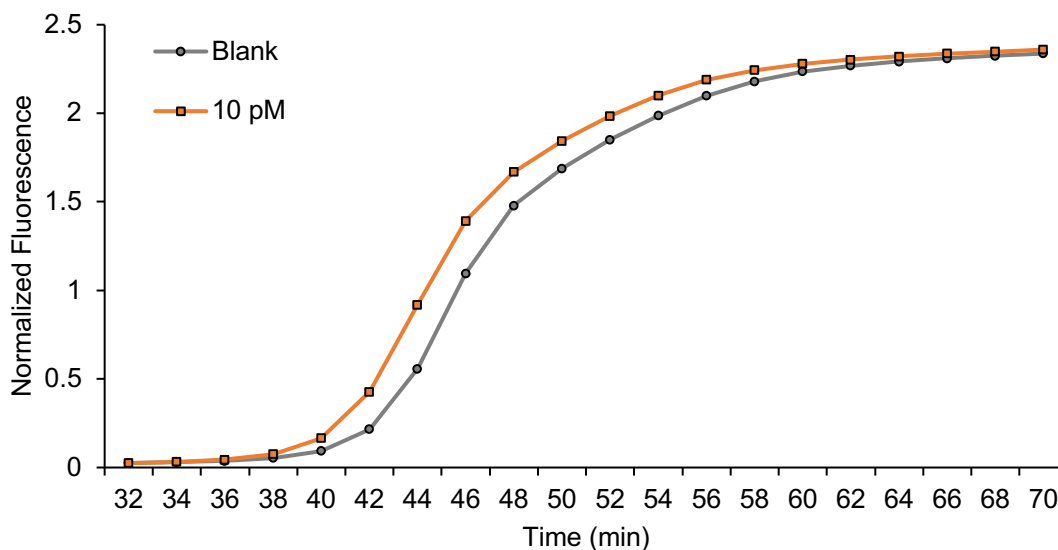
Figure 2.22 Representative amplification curves of 10 pM of MERRF target in MCF-7 cell lysate and reagent blank from 32 min to 70 min.

2.3.10 Sources of background

Similar to other strategies with exponential amplification, any small background could be exponentially amplified as well. I considered the various sources of background and attempted to minimize them in the optimization processes. The background may come from two main sources: (1) malformation of the **HP** stem and (2) **FS** bound to the loop of amplifiable beacons.

Malformation of the **HP** stem may arise in events such as base mismatch or DNA synthesis errors. I attempted to reduce the contribution of background from stem malformation through careful design of the stem sequence and through denaturation followed by the 2 h slow cooling process to create the amplifiable beacon. I also chose the primer length and position combination that produced the best signal to background ratio.

Secondly, **FS** bound to the loop of amplifiable beacons can increase background. In the design of **HP**, the inclusion of Domain 1 helps to drive the binding of **FS** to the overhang of **HP** to form the amplifiable beacon. When forming the amplifiable beacon, **FS** is mixed with an excess amount of **HP**. However, it is possible that even if **HP** is in excess, some **FS** may bind the loop and stem of **HP** in amplifiable beacons, which initiates the reaction and increases the background. I minimized the contribution to background from this source by optimizing the ratio of **HP** to **FS** when annealing the amplifiable beacon prior to target analysis.

2.4 Conclusions

These results demonstrated that with a single enzyme and a single primer the **BEAR** technique is able to achieve isothermal and exponential amplification of the detection signal for a clinically relevant mutation target. Using a single polymerase and a single primer simplifies the technical procedure, which is valuable for point-of-care testing and on-site analysis. **BEAR** is particularly appropriate for the detection of short nucleic acid targets, as I have demonstrated the detection of a 25-nt MERRF target. Future applications could also include the detection of microRNA (miRNA). The short length of miRNAs poses challenges in accommodating more than one primer as is often required in other techniques.

2.5 References

(1)   Yan, L.; Zhou, J.; Zheng, Y.; Gamson, A. S.; Roembke, B. T.; Nakayama, S.; Sintim, H. O. Isothermal Amplified Detection of DNA and RNA. *Mol. Biosyst.* **2014**, *10*, 970–1003.

(2)   Kim, J.; Easley, C. J. Isothermal DNA Amplification in Bioanalysis: Strategies and Applications. *Bioanalysis* **2011**, *3*, 227–239.

(3)   Zhang, Z.; Zhang, C. Highly Sensitive Detection of Protein with Aptamer-Based Target-Triggering Two-Stage Amplification. *Anal. Chem.* **2012**, *84*, 1623–1629.

(4)   Shi, C.; Liu, Q.; Ma, C.; Zhong, W. Exponential Strand-Displacement Amplification for Detection of Micrornas. *Anal. Chem.* **2014**, *86*, 336–339.

(5)   Zhang, L. R.; Zhu, G.; Zhang, C. Y. Homogeneous and Label-Free Detection of Micrornas Using Bifunctional Strand Displacement Amplification-Mediated Hyperbranched Rolling Circle Amplification. *Anal. Chem.* **2014**, *86*, 6703–6709.

(6)   Jiang, H.; Xu, Y.; Dai, L.; Liu, X.; Kong, D. Ultrasensitive, Label-Free Detection of T4 Ligase and T4 Polynucleotide Kinase Based on Target-Triggered Hyper-Branched Rolling Circle Amplification. *Sensors Actuators, B Chem.* **2018**, *260*, 70–77.

(7)   Zhao, W.; Ali, M. M.; Brook, M. A.; Li, Y. Rolling Circle Amplification: Applications in Nanotechnology and Biodetection with Functional Nucleic Acids. *Angew. Chem. Int. Ed. Engl.* **2008**, *47*, 6330–6337.

(8)   He, D.; He, X.; Yang, X.; Li, H.-W. A Smart ZnO@polydopamine-Nucleic Acid Nanosystem for Ultrasensitive Live Cell MRNA Imaging by the Target-Triggered Intracellular Self-Assembly of Active DNAzyme Nanostructures. *Chem. Sci.* **2017**, *31*, 748.

(9)   Ali, M. M.; Li, F.; Zhang, Z.; Zhang, K.; Kang, D. K.; Ankrum, J. A.; Le, X. C.; Zhao, W. Rolling Circle Amplification: A Versatile Tool for Chemical Biology, Materials Science

and Medicine. *Chem. Soc. Rev.* **2014**, *43*, 3324–3341.

(10) Wang, Q.; Zheng, H.; Gao, X.; Lin, Z.; Chen, G. A Label-Free Ultrasensitive

Electrochemical Aptameric Recognition System for Protein Assay Based on

Hyperbranched Rolling Circle Amplification. *Chem. Commun.* **2013**, *49*, 11418–11420.

(11) Van Ness, J.; Van Ness, L. K.; Galas, D. J. Isothermal Reactions for the Amplification of

Oligonucleotides. *Proc. Natl. Acad. Sci. U. S. A.* **2003**, *100*, 4504–4509.

(12) Tan, E.; Erwin, B.; Dames, S.; Voelkerding, K.; Niemz, A. Isothermal DNA

Amplification with Gold Nanosphere-Based Visual Colorimetric Readout for Herpes

Simplex Virus Detection. *Clin. Chem.* **2007**, *53*, 2017–2020.

(13) Huang, M.; Zhou, X.; Wang, H.; Xing, D. Clustered Regularly Interspaced Short

Palindromic Repeats/Cas9 Triggered Isothermal Amplification for Site-Specific Nucleic

Acid Detection. *Anal. Chem.* **2018**, *90*, 2193–2200.

(14) Reid, M. S.; Le, X. C.; Zhang, H. Exponential Isothermal Amplification of Nucleic Acids

and Assays for Proteins, Cells, Small Molecules, and Enzyme Activities: An EXPAR

Example. *Angew. Chem. Int. Ed. Engl.* **2018**, *57*, 11856–11866.

(15) Nie, J.; Zhang, D. W.; Zhang, F. T.; Yuan, F.; Zhou, Y. L.; Zhang, X. X. Reporter-

Triggered Isothermal Exponential Amplification Strategy in Ultrasensitive Homogeneous

Label-Free Electrochemical Nucleic Acid Biosensing. *Chem. Commun.* **2014**, *50*, 6211–

6213.

(16) Wang, X.; Wang, H.; Liu, C.; Wang, H.; Li, Z. A Three-Way Junction Structure-Based

Isothermal Exponential Amplification Strategy for Sensitive Detection of 3′-Terminal 2′-

O-Methylated Plant MicroRNA. *Chem. Commun.* **2017**, *53*, 1124–1127.

(17) Compton, J. Nucleic Acid Sequence-Based Amplification. *Nature* **1991**, *350*, 273–291.

(18) Zhao, X.; Dong, T.; Yang, Z.; Pires, N.; Høivik, N. Compatible Immuno-NASBA LOC Device for Quantitative Detection of Waterborne Pathogens: Design and Validation. *Lab Chip* **2012**, *12*, 602–612.

(19) Mugasa, C. M.; Laurent, T.; Schoone, G. J.; Kager, P. A.; Lubega, G. W.; Schallig, H. D. F. H. Nucleic Acid Sequence-Based Amplification with Oligochromatography for Detection of Trypanosoma Brucei in Clinical Samples. *J. Clin. Microbiol.* **2009**, *47*, 630–635.

(20) Gootenberg, J. S.; Abudayyeh, O. O.; Lee, J. W.; Essletzbichler, P.; Dy, A. J.; Joung, J.; Verdine, V.; Donghia, N.; Daringer, N. M.; Freije, C. A.; *et al.* Nucleic Acid Detection with CRISPR-Cas13a/C2c2. *Science* **2017**, *356*, 438–442.

(21) Vincent, M.; Xu, Y.; Kong, H. Helicase-Dependent Isothermal DNA Amplification. *EMBO Rep.* **2004**, *5*, 795–800.

(22) Torres-Chavolla, E.; Alocilja, E. C. Nanoparticle Based DNA Biosensor for Tuberculosis Detection Using Thermophilic Helicase-Dependent Isothermal Amplification. *Biosens. Bioelectron.* **2011**, *26*, 4614–4618.

(23) Piepenburg, O.; Williams, C. H.; Stemple, D. L.; Armes, N. A. DNA Detection Using Recombination Proteins. *PLoS Biol.* **2006**, *4*, 1115–1121.

(24) Walker, G. T.; Little, M. C.; Nadeau, J. G.; Shank, D. D. Isothermal in Vitro Amplification of DNA by a Restriction Enzyme/DNA Polymerase System. *Proc. Natl. Acad. Sci. U. S. A.* **1992**, *89*, 392–396.

(25) Toley, B. J.; Covelli, I.; Belousov, Y.; Ramachandran, S.; Kline, E.; Scarr, N.; Vermeulen, N.; Mahoney, W.; Lutz, B. R.; Yager, P. Isothermal Strand Displacement Amplification (ISDA): A Rapid and Sensitive Method of Nucleic Acid Amplification for Point-of-Care

Diagnosis. *Analyst* **2015**, *140*, 7540–7549.

(26)   Notomi, T.; Okayama, H.; Masubuchi, H.; Yonekawa, T.; Watanabe, K.; Amino, N.; Hase, T. Loop-Mediated Isothermal Amplification of DNA. *Nucleic Acids Res.* **2000**, *28*, E63.

(27)   Dong, J.; Xu, Q.; Li, C. C.; Zhang, C. Y. Single-Color Multiplexing by the Integration of High-Resolution Melting Pattern Recognition with Loop-Mediated Isothermal Amplification. *Chem. Commun.* **2019**, *55*, 2457–2460.

(28)   Ma, C.; Wang, F.; Wang, X.; Han, L.; Jing, H.; Zhang, H.; Shi, C. A Novel Method to Control Carryover Contamination in Isothermal Nucleic Acid Amplification. *Chem. Commun.* **2017**, *53*, 10696–10699.

(29)   Connolly, A. R.; Trau, M. Isothermal Detection of DNA by Beacon-Assisted Detection Amplification. *Angew. Chem. Int. Ed. Engl.* **2010**, *49*, 2720–2723.

(30)   Zhang, Y.; Zhang, C. Y. Sensitive Detection of MicroRNA with Isothermal Amplification and a Single-Quantum-Dot-Based Nanosensor. *Anal. Chem.* **2012**, *84*, 224–231.

(31)   Tian, L.; Weizmann, Y. Real-Time Detection of Telomerase Activity Using the Exponential Isothermal Amplification of Telomere Repeat Assay. *J. Am. Chem. Soc.* **2013**, *135*, 1661–1664.

(32)   Huang, J. F.; Zhao, N.; Xu, H. Q.; Xia, H.; Wei, K.; Fu, W. L.; Huang, Q. Sensitive and Specific Detection of MiRNA Using an Isothermal Exponential Amplification Method Using Fluorescence-Labeled LNA/DNA Chimera Primers. *Anal. Bioanal. Chem.* **2016**, *408*, 7437–7446.

(33)   Sun, X.; Wang, L.; Zhao, M.; Zhao, C.; Liu, S.; Zhang, X. X.; Sun, D.; Fan, C.; Xia, F. An Autocatalytic DNA Machine with Autonomous Target Recycling and Cascade Circular

Exponential Amplification for One-Pot, Isothermal and Ultrasensitive Nucleic Acid Detection. *Chem. Commun.* **2016**, *52*, 11108–11111.

(34)   Shi, C.; Liu, Q.; Zhou, M.; Zhao, H.; Yang, T.; Ma, C. Nicking Endonuclease-Mediated Isothermal Exponential Amplification for Double-Stranded DNA Detection. *Sensors Actuators, B Chem.* **2016**, *222*, 221–225.

(35)   Qian, Y.; Fan, T.; Wang, P.; Zhang, X.; Luo, J.; Zhou, F.; Yao, Y.; Liao, X.; Li, Y.; Gao, F. A Novel Label-Free Homogeneous Electrochemical Immunosensor Based on Proximity Hybridization-Triggered Isothermal Exponential Amplification Induced G-Quadruplex Formation. *Sensors Actuators, B Chem.* **2017**, *248*, 187–194.

(36)   Gootenberg, J. S.; Abudayyeh, O. O.; Kellner, M. J.; Joung, J.; Collins, J. J.; Zhang, F. Multiplexed and Portable Nucleic Acid Detection Platform with Cas13, Cas12a, and Csm6. *Science* **2018**, *360*, 439–444.

(37)   Osborn, L.; Kunkel, S.; Nabel, G. J. Tumor Necrosis Factor Alpha and Interleukin 1 Stimulate the Human Immunodeficiency Virus Enhancer by Activation of the Nuclear Factor Kappa B. *Proc. Natl. Acad. Sci.* **2006**, *86*, 2336–2340.

(38)   Finsterer, J.; Harbo, H. F.; Baets, J.; Van Broeckhoven, C.; Di Donato, S.; Fontaine, B.; De Jonghe, P.; Lossos, a.; Lynch, T.; Mariotti, C.; *et al.* EFNS Guidelines on the Molecular Diagnosis of Mitochondrial Disorders. *Eur. J. Neurol.* **2009**, *16*, 1255–1264.

(39)   Grossmann, T. N.; Röglin, L.; Seitz, O. Triplex Molecular Beacons as Modular Probes for DNA Detection. *Angew. Chem. Int. Ed. Engl.* **2007**, *46*, 5223–5225.

(40)   Newbigging, A. M.; Zhang, H.; Le, X. C. Beacon-Mediated Exponential Amplification Reaction (BEAR) Using a Single Enzyme and Primer. *Chem. Commun.* **2019**, *55*, 10677–10680.

Chapter Three: Development of a hybridization chain reaction enabling turn-on fluorescence from label-free hairpins

3.1 Introduction

As discussed in the introduction, HCR consists of DNA hairpins that are complementary to each other, but do not bind to each other unless in the presence of an initiator. The first iterations of HCR in literature use an initiating strand of DNA that binds to its toehold on one hairpin and subsequently opens the hairpin stem. Opening of the first hairpin stem allows the second hairpin to bind to its toehold on the first hairpin. The process is repeated because when the second hairpin binds, its stem opens and another molecule of the first hairpin can bind for the same reaction. The product is a nicked polymer in which the "monomers" are each species of hairpin that bind to form the chain. The nicked polymer is called a concatemer because it contains multiple repeating units.

To detect the growing concatemer in real-time, turn-on fluorescence is ideal because fluorophores produce high intensity signals and can be repeatedly excited for fluorescence emission. One strategy to confer fluorescence of the formed concatemer is to directly conjugate fluorophores onto the hairpins and adsorb the hairpins onto a nanomaterial with the ability for fluorescence quenching[1]. When the hairpin is opened in the reaction, the fluorophore and the quencher are separated. When the concatemer is formed, dissociation of the hairpins restores the fluorescence. Another strategy is to conjugate a fluorophore and dark quencher pair within the same hairpin species, such that the fluorescence is quenched in the hairpin but restored in the concatemer. Lastly, FRET pairs can be conjugated onto separate hairpins. In this case, FRET is detected once the donor and acceptor are in close proximity such as within the concatemer[2,3].

However, these strategies require the fluorophore, quencher, and/or FRET pairs to be conjugated within the sequence of the hairpins as labels. The use of labeled hairpins can increase oligo synthesis and purification costs and is therefore impractical when developing the system due to frequent redesigning of the DNA sequences. One way to avoid direct labeling of the hairpins is to use hybridization probes. However, the use of hybridization probes requires an additional procedural step, increasing the time and labour for the protocol. Removal of unreacted probes is also required. Lastly, hybridization probes are unable to facilitate real-time sensing.

Strand displacement beacons can be used to produce fluorescence signals in response to the formation of dynamic DNA assemblies[4,5]. A strand displacement beacon consists of two strands of DNA hybridized together where one strand is conjugated to a fluorophore and the other is conjugated to a quenching molecule. When hybridized together, the proximity of the fluorophore to the quencher results in quenched fluorescence. Displacement of the strand conjugated to the quencher strand results in increased distance between the fluorophore and the quencher, restoring the fluorescence. To circumvent the requirement for labeling the hairpins in HCR, strand displacement beacons I proposed that strand displacement beacons could be used instead to produce turn-on fluorescence. Strand displacement beacons are advantageous to use when developing HCR because they allow for the optimization of hairpin sequences independent of the strand displacement beacon sequences. Additionally, the modularity of DNA domains allows easy adaptation of the hairpins to accommodate the usage of strand displacement beacons for fluorescence signal output. Lastly, removing unreacted strand displacement beacons is not necessary because no background fluorescence would be produced.

Careful design of HCR is required to accommodate the use of strand displacement beacons. To image the concatemer using strand displacement beacons, the hairpins must be

designed to displace the quencher strand of the strand displacement beacon only when arranged in the concatemer. To enable localized detection signals, the fluorophore strand of the strand displacement beacon must be retained on the concatemer. Therefore, I designed the concatemer to bind to the fluorophore strand of the strand displacement beacon and displace the quencher strand. I split the complement to the fluorophore strand into two domains and placed these domains on separate hairpin species. When the hairpins were arranged adjacently to each other in the concatemer, the domains were brought together to form the full complement strand. The full complement would then bind to the fluorophore strand of the strand displacement beacon and displace the quencher strand, restoring the fluorescence. The fluorophore strand of the strand displacement beacon therefore contained a single stranded toehold region that could bind to one of the complement domains on the concatemer to facilitate the strand displacement mechanism for binding to the second complement domain.

HCR conventionally uses two hairpins which may contribute to background when using strand displacement beacons. Spatially, in HCR using two hairpin species, only one species of hairpin is located on the same side of the concatemer (Figure 3.1). In a two hairpin HCR using a strand displacement beacon for concatemer detection, the two split complementary domains for the fluorophore strand of the strand displacement beacon would both be located on the same hairpin species. Figure 3.2 shows an example hairpin with both complementary domains to the fluorophore strand of the strand displacement beacon on the 5' and 3' ends. The close proximity of the toehold complement of the fluorophore strand could introduce the problem of co-localizing the strand displacement beacon which would result in the displacement of the quencher strand in the absence of concatemers. This could further result in the sequestering of this hairpin species by fluorophore strands. This sequestering would slow the overall rate of

reaction and also increase the baseline fluorescence contributing to background since the

displaced quencher strand would no longer quench the fluorescence. Both of these outcomes

would negatively affect the limit of detection and sensitivity of the HCR system.
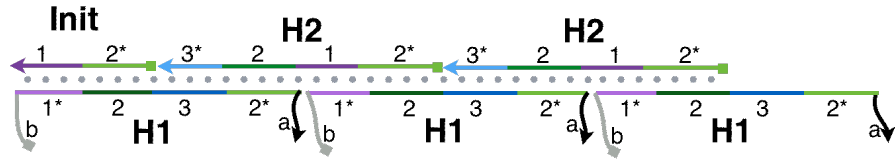
Figure 3.1 Incorporation of **SDB** in a two hairpin HCR requires both complementary domains for the **F** strand to be co-located within the concatemer. Co-localization of the toeholds within the chain requires both toeholds to be on one hairpin species, **H1**.
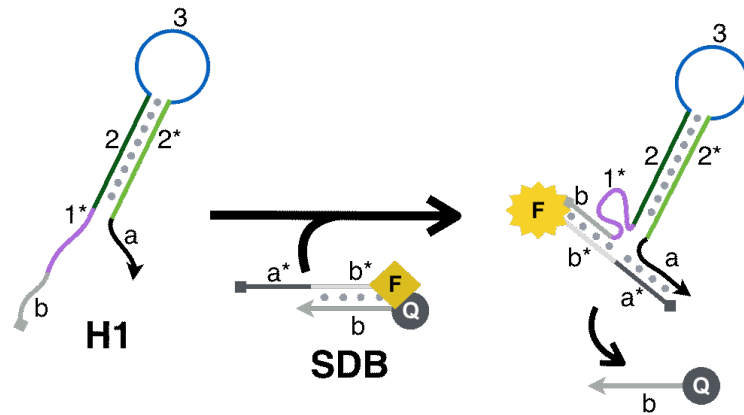
Figure 3.2 One hairpin species (**H1**) with both fluorophore strand complementary domains. This hairpin design may result in single hairpins displacing the quencher strand in the absence of the concatemer.

My strategy to overcome the above challenge of introducing a strand displacement beacon into HCR for turn-on fluorescence using label-free hairpins was to design a four hairpin HCR (Figure 3.3). For ease of design and discussion, I named each functional domain using numbers or lower-case letters and indicated the complementary domains with an asterisk (e.g., **1** is complementary to **1***). The small square on the ends of the DNA indicates the 5' end and the small arrow indicates the 3' end. My HCR design consisted of one initiating strand, **init**, four

hairpins, **H1-H4**, and two strand displacement beacons, **SDB 1** and **SDB 2**. Each hairpin consisted of ssDNA loop (**3**, **4**, **5**, **1**) and corresponding toehold (**1***, **3***, **4***, **5***) domains, and dsDNA stem domains (**2/2***). **SDB 1** and **SDB 2** consisted of fluorophore strands, **F1** (**a***, **b***) and **F2** (**d***, **c***) and quencher strands, **Q1** (**b**) and **Q2** (**c**), conjugated to a fluorophore (FAM) and dark quencher pair (IaBkFQ), respectively. Toeholds could not bind to their loop complements in the hairpins because the stems were relatively more stable. **F1** and **F2** of **SDB 1** and **SDB 2**, respectively, were not displaced because the complementary domains of **F1** were split on **H1** (**a**) and **H3** (**b**) and the complementary domains of **F2** were split on **H2** (**c**) and **H4** (**d**).
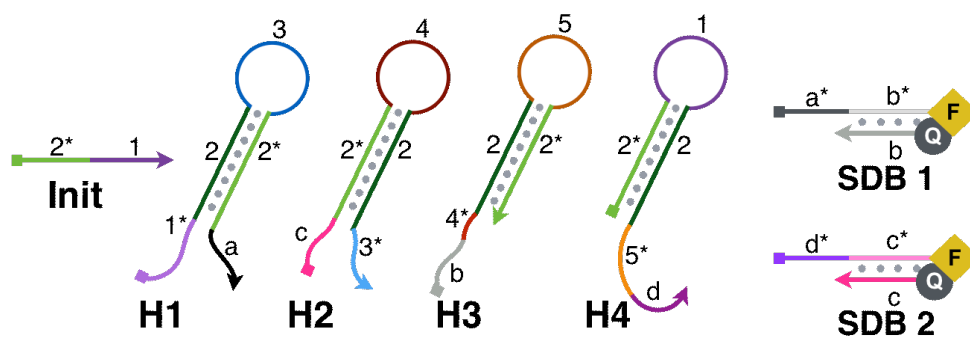
Figure 3.3 Components of the developed four hairpin HCR using two strand displacement beacons. Oligos included an initiator strand, **init**, four hairpins, **H1-H4**, and two strand displacement beacons, **SDB 1** and **SDB 2**. Toehold domains included **1*** of **H1**, **3*** of **H2**, **4*** of **H4**, and **5*** of **H4**. Domains **a** of **H1** and **b** of **H3** were complementary to **F1** of **SDB 1**. Domains **c** of **H2** and **d** of **H4** were complementary to **F2** of **SDB 2**. Loop domains included **3** of **H1**, **4** of **H2**, **5** of **H3** and **1** of **H4**. Stem domains included **2** and **2*** of all four hairpins.

3.2 Experimental

3.2.1 Materials and reagents

The buffer used for all reactions, HCR buffer, contained 10 mM TrisHCl (pH 7.4) and 12 mM

Mg^{2+} made from $MgCl_2 \cdot 6H_2O$, both from Sigma-Aldrich (Oakville, ON, Canada), and 0.05%

Tween-20 from Fisher Scientific (Ottawa, ON, Canada). The buffer was made using water

purified by an ultrapure Milli-Q water system.

DNA sequences were purchased from Integrated DNA Technologies (Coralville, IA,

USA). Prior to analysis, hairpins were annealed in separate solutions containing 5 µL of 100 µM

hairpins and 95 µL of HCR buffer with 250 mM $MgCl_2$. Annealing of hairpins were performed

by slow cooling solutions in a benchtop thermocycler purchased from Bio-Rad (Mississauga,

ON, Canada) from 95°C to 20°C in 1 h. Annealed hairpins were stored at 4°C for up to two

weeks.

3.2.2 Gel electrophoresis

Agarose gels was made up by dissolving agarose powder in 1x TBE buffer and 5 µL of 1%

ethidium bromide. Gels were run using the same 1x TBE buffer. Agarose powder was purchased

from Fisher Scientific (Nepean, ON, Canada) and TBE buffer were purchased from Sigma

Aldrich (Milwaukee, WI, USA). Ethidium bromide was purchased from Fisher Scientific

(Nepean, ON, Canada). The high molecular weight DNA ladder was purchased from New

England Biolabs (Whitby, ON, Canada). DNA Gel Loading Dye was purchased from Fisher

Scientific (Nepean, ON, Canada).

The reaction components were mixed in a total volume of 100 µL. Each hairpin (1 µM)

was mixed with various concentrations of **init** in HCR buffer and left at room temperature for 24

h, 3 h, 2 h, 30 min, or 0 h. After the incubation, 15 µL of the solution was mixed with 5 µL of

loading dye and 12 µL of this solution was added to each well. A volume of 3 µL of 1 kB plus

DNA ladder was added to at least one well. Gels were run at 80 V for about 90 min.

3.2.3 Reaction parameters and analysis

Each species of hairpin was annealed in separate solutions in concentrations of 20 µM in a total

of 100 µL HCR buffer. Strand displacement beacons were annealed by mixing the strand

conjugated to the dark quencher (**Q1** or **Q2**) with the respective strand conjugated to the

fluorophore (**F1** or **F2**) in a 1:0.8 ratio for a final concentration of 20 µM in 100 µL. Annealing

was performed by heating solutions to 90°C and cooling to room temperature over 1 h. The

components and concentrations of a typical reaction is shown in Table 3.1. After mixing, the

real-time florescence was monitored in a multimode fluorescence microplate reader (FilterMax

F5, Molecular Devices, Silicon Valley, CA, USA) for every 2 min at 23°C.

Table 3.1 HCR mastermix components with their final concentrations and volumes per reaction.

Component	Final concentration	Volume per reaction
H1	50 nM	5 µL
H2	50 nM	5 µL
H3	50 nM	5 µL
H4	50 nM	5 µL
SDB 1	50 nM	5 µL
SDB 2	50 nM	5 µL
Target (**init**)	various	10 µL
HCR buffer	10 mM Tris, 12 mM Mg^{2+}, 0.05% Tween-20	60 µL
Final volume		**100 µL**

3.2.4 Calculation of fold change

Fold change (*Eqn. 1*) was calculated by dividing the change in fluorescence intensity from 0 min to 30 min, 60 min, or 120 min of reaction time in minutes (x) of the target by that of the blank within the same experiment. Fold change demonstrates the fold increase of amplification of signal at each specific time relative to the starting value of the target over that of the blank (*Eqn. 1*).

(Eqn. 1)

$$Fold\ change = \frac{\left((FI_{x\ min}) - (FI_{0\ min})\right)_{target}}{\left((FI_{x\ min}) - (FI_{0\ min})\right)_{blank}}$$

Error bars were calculated using the variance (v) (*Eqn.2*) of each term in the fold change equation (*Eqn.3*), where the mean ($\bar{x}$) and standard deviation (σ) (*Eqn. 4*) were calculated at each time point in triplicates within the same run.

(Eqn. 2)

$$v = \sigma^2$$

(Eqn. 3)

$$\pm Error = \sqrt{(v_{target\ 0\ min} + v_{target\ x\ min} + v_{blank\ 0\ min} + v_{blank\ t\ min})}$$

(Eqn. 4)

$$\sigma = \sqrt{\left(\frac{\sum(x - \bar{x})^2}{N - 1}\right)}$$

3.2.5 Sequences of oligos

Strand displacement beacon sequences are shown in Table 3.2. Hairpin sequences using 16 bp stems and 7 nt toeholds are shown in Table 3.3. For the determination of stem length effects (section 3.3.4), hairpin sequences using 12 bp stems and 7 nt toeholds are shown in Table 3.4A and hairpin sequences using 14 bp stems and 7 nt toeholds are shown in Table 3.4B. For the determination of toehold length effects (section 3.3.5), hairpin sequences using 16 bp stems and 7 nt toeholds (Table 3.5A) were compared with 16 bp stems and 6 nt toeholds (Table 3.5B) and used only one strand displacement beacon. For the determination of the effects of **F1** and **F2** complement spacers (section 3.3.7), hairpin sequences using 16 bp stems and 7 nt toeholds with spacers inserted between the concatemer-forming domains and the **F1** and **F2** complement domains are shown in Table 3.7.

Table 3.2 Sequences of **SDB 1** and **SDB 2**. Fl indicates the linkage of a fluorescein molecule (FAM fluorescein) and Qu indicates the linkage to a compatible dark quencher (IaBkFQ Iowa Black® FQ Dark Quencher).

Oligo	Sequence
F1 (**SDB 1**)	TGT GAG AAT CTC TAA AGC TGC TCT - Fl
Q1 (**SDB 1**)	Qu - AGA GCA GCT TTA GAG
F2 (**SDB 1**)	CTT ACG TAG GAT ATG TTC GAG TTA- Fl
Q2 (**SDB 2**)	Qu - TAA CTC GAA CAT ATC

Table 3.3 Sequences of hairpins with 16 bp stems and 7 nt toeholds.

Oligo	Sequence
Init	CAA CCA CTA CCT CAT CTA TAC TG
H1	CAG TAT AGA TGA GGT AGT GGT TGT TTC CAT CAA CCA CTA CCT CAT CAT TCT CAC A
H2	TAA CTC GAA CAT ATC CAA CCA CTA CCT CAT CTA AAC GTG ATG AGG TAG TGG TTG ATG GAA A
H3	AGA GCA GCT TTA GAG ACG TTT AGA TGA GGT AGT GGT TGC AAT CAA CAA CCA CTA CCT CAT C
H4	CAA CCA CTA CCT CAT CTA TAC TGG ATG AGG TAG TGG TTG TTG ATT GTC ACG TAA G

Table 3.4A Sequences of hairpins with 12 bp stems and 7 nt toeholds.

Oligo	Sequence
Init	CAA CCA CTC ATC TAT ACT G
H1	CAG TAT AGA TGA GTG GTT GTT TCC ATC AAC CAC TCA TCA TTC TCA CA
H2	TAA CTC GAA CAT ATC CAA CCA CTC ATC TAA ACG TGA TGA GTG GTT GAT GGA AA
H3	AGA GCA GCT TTA GAG ACG TTT AGA TGA GTG GTT GCA ATC AAC AAC CAC TCA TC
H4	CAA CCA CTC ATC TAT ACT GGA TGA GTG GTT GTT GAT TGC TAC GTA AG

Table 3.4B Sequences of hairpins with 14 bp stems and 7 nt toeholds.

Oligo	Sequence
Init	CAA CCA CTC TCA TCT ATA CTG
H1	CAG TAT AGA TGA GAG TGG TTG TTT CCA TCA ACC ACT CTC ATC ATT CTC ACA
H2	TAA CTC GAA CAT ATC CAA CCA CTC TCA TCT AAA CGT GAT GAG AGT GGT TGA TGG AAA
H3	AGA GCA GCT TTA GAG ACG TTT AGA TGA GAG TGG TTG CAA TCA ACA ACC ACT CTC ATC
H4	CAA CCA CTC TCA TCT ATA CTG GAT GAG AGT GGT TGT TGA TTG CTA CGT AAG

Table 3.5A Sequence of hairpins with 16 bp stems with 7 nt toeholds and one strand displacement beacon (**F** and **Q**).

Oligo	Sequence
Init	CAA CCA CTA CCT CAT CCA GAT TA
H1	TAA TCT GGA TGA GGT AGT GGT TGT TAA CGT CAA CCA CTA CCT CAT CAA TTC CTG C
H2	CAA CCA CTA CCT CAT CAA CTG TAG ATG AGG TAG TGG TTG ACG TTA A
H3	AAG GTC GCT TTA GAG TAC AGT TGA TGA GGT AGT GGT TGC AAA ACT CAA CCA CTA CCT CAT C
H4	CAA CCA CTA CCT CAT CCA GAT TAG ATG AGG TAG TGG TTG AGT TTT G
F	GCA GGA ATT CTC TAA AGC GAC CTT - FAM
Q	Qu - AA GGT CGC TTT AGA G

Table 3.5B Sequences of hairpins with 16 bp stems with 6 nt toeholds and one strand displacement beacon (**F** and **Q**).

Oligo	Sequence
Init	CAA CCA CTA CCT CAT CCA GAT A
H1	TA T CTG GAT GAG GTA GTG GTT GTT ACG TCA ACC ACT ACC TCA TCA ATT CCT GC
H2	CAA CCA CTA CCT CAT CAC TGT AGA TGA GGT AGT GGT TGA CGT AA
H3	AAG GTC GCT TTA GAG TAC AGT GAT GAG GTA GTG GTT GCA AAC TCA ACC ACT ACC TCA TC
H4	CAA CCA CTA CCT CAT CCA GAT AGA TGA GGT AGT GGT TGA GTT TG
F	GCA GGA ATT CTC TAA AGC GAC CTT - FAM
Q	Qu - AA GGT CGC TTT AGA G

Table 3.6 Sequences of hairpins with 16 bp stem and 7 nt toehold with the inclusion of **F1** and **F2** complement domain spacers within the hairpins. The spacers are located between the domains involved in the concatemer and the domains binding to **F1** and **F2**. The spacer nucleotides are underlined and bolded.

Oligo	Sequence
Init	CAA CCA C TA CCT CAT CTA TAC TG
H1	CAG TAT AGA TGA GGT AGT GGT TGT TTC CAT CAA CCA CTA CCT CAT C**TA** ATT CTC ACA
H2	TAA CTC GAA CAT ATC **AA**C AAC CAC TAC CTC ATC TAA ACG TGA TGA GGT AGT GGT TGA TGG AAA
H3	AGA GCA GCT TTA GAG **TT**A CGT TTA GAT GAG GTA GTG GTT GCA ATC AAC AAC CAC TAC CTC ATC
H4	CAA CCA CTA CCT CAT CTA TAC TGG ATG AGG TAG TGG TTG TTG ATT G**TT** CTA CGT AAG

88

3.3 Results and discussion

3.3.1 Working principle of the four-hairpin hybridization chain reaction (HCR)

The reaction began when the initiator, **init**, was added to a solution containing the four hairpins (**H1**, **H2**, **H3**, and **H4**) and two strand displacement beacons (**SDB 1** and **SDB 2**). Domain **1** of **init** bound to its toehold, **1***, on **H1**. Through random walk branch migration[6], domain **2*** of **init** subsequently bound to the adjacent and stem domain of **2** on **H1**, making **2*** on **H1** single stranded (Figure 3.4). Because the stem of **H1** was now opened, loop domain, **3**, was accessible to which **H2** could bind using its toehold domain, **3***. The single stranded stem domain of **H1**, **2**, could then bind to **2*** of **H2**, again through random walk branch migration. As a result, the stem domain **2*** of **H2** was now single stranded and loop domain **4** was accessible to which the toehold domain, **4***, of **H3** could bind. Using the same process, **H3** bound to **H2**, making the stem domain of **H3** single stranded and available to which **H4** could bind. This process was chained because domain **1** of the loop of **H4** was complementary to **H1** and so another molecule of **H1** could then be added to this growing concatemer chain by hybridizing to **H4**. The concatemer thus grew in length until at least one hairpin species was exhausted. Because the concatemer grows with specific species of hairpins added sequentially (i.e., **H1** first, **H2** second, and so on), the exhaustion of any one hairpin species would result in the termination of the reaction.

The growing concatemer could be detected in real-time using turn-on fluorescence enabled by the strand displacement beacons, **SDB 1** and **SDB 2**. The concatemer brought the 3' end of **H1** and the 5' end of **H3** together. When domain **a*** of **F1** within **SDB 1** bound to domain **a** in **H1** within the concatemer, domain **b*** of **F** could bind to the nearby **b** domain of **H3** (Figure 3.5). As a result, **Q1** was displaced, and **F1** remained bound to the concatemer. The increased

distance between **Q1** and **F1** restored the fluorescence of the fluorophore of **F1**. The same

occurred for **SDB 2**, where when **H2** and **H4** were co-localized within the concatemer, the

complementary domains bound to **F2** and displaced **Q2** (Figure 3.6). Every **H1-H4** repeat in the

concatemer therefore retained two fluorophores and so increasing fluorescence intensity

indicated the formation and growth of concatemers.
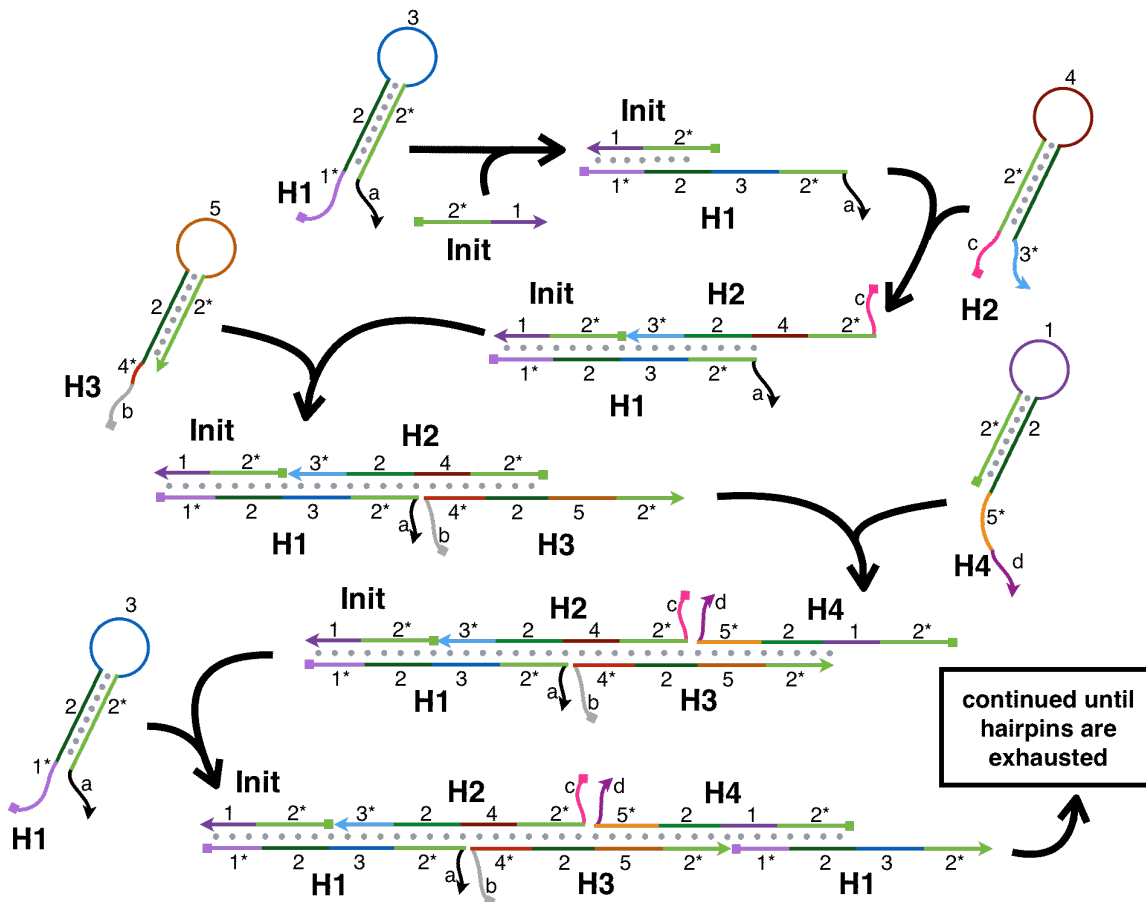
Figure 3.4 Schematic of HCR using four label-free hairpins. **Init** initiated HCR by binding to **H1**. Binding of **H1** to **init** opened **H1** to allow **H2** to bind. **H2** opened to allow **H3** to bind, and **H3** opened to allow **H4** to bind. The reaction was repeated as another molecule of **H1** could bind to **H4**. The reaction continued until at least one hairpin species in solution was exhausted. A long, nicked polymer was formed, called a concatemer.
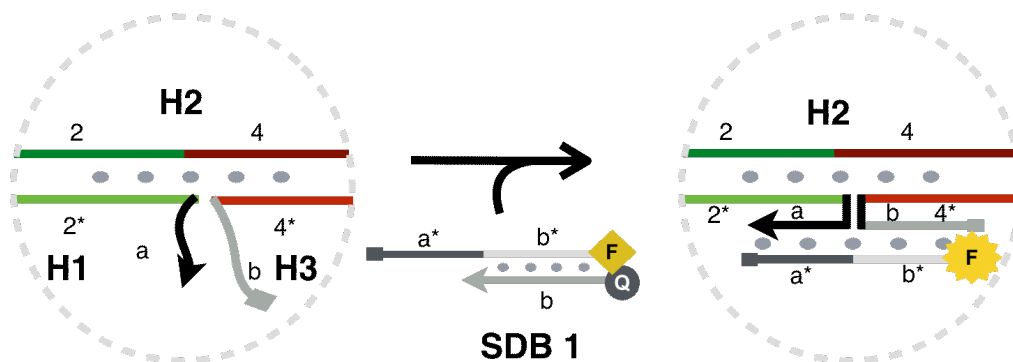
Figure 3.5 Schematic of the binding of **F1** and displacement of **Q1** from **SDB 1** by the concatemer. Toeholds for **SDB 1** (**a** and **b**) were co-localized when **H1** and **H3** were adjacent within the concatemer to facilitate the displacement of **Q1** and binding of **F1**. The increased distance of **F1** from **Q1** after the displacement restored the fluorescence of the fluorophore.
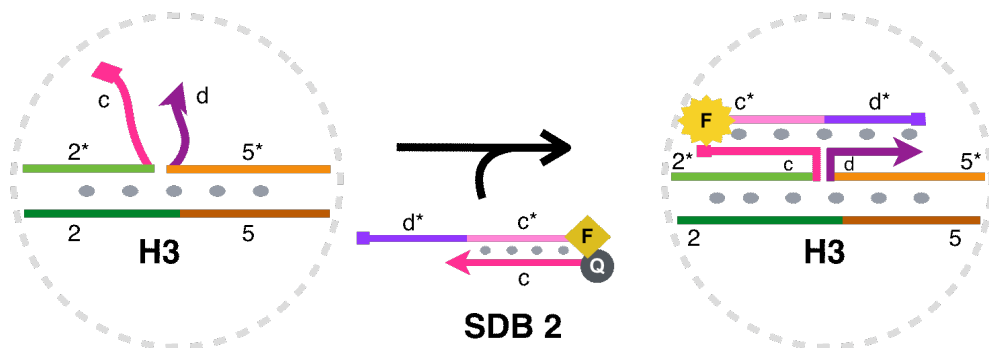
Figure 3.6 Schematic of the binding of **F2** and displacement of **Q2** from **SDB 2** by the concatemer. Similar to the displacement reaction of **SDB 1** in Figure 3.5, for the displacement of **SDB 2**, the concatemer co-localized **H2** and **H4** such that the domains **c** and **d** could bind to **F2**, displacing **Q2**. The increased distance of **F2** to **Q2** after the displacement restored the fluorescence of the fluorophore.

3.3.2 Design considerations

Because HCR relies heavily on the interactions between oligos to function effectively, determining the optimal DNA design and sequence was vital. The main objective in designing sequences was to minimize the time required for the reaction without substantially increasing the background. Reducing the melting temperature of the hairpin stems can increase the rate of the reaction but may also increase the background. Increasing the melting temperature of hairpin stems can reduce the amount of background but may also slow the reaction because longer stems will take a relatively longer time to open. Similarly, if the length of the toehold is long, the reaction may be fast, but if the toehold is too long, it may bind to its complementary domains and initiate the reaction in the absence of **init**. If the toehold is too short, it may not easily bind to its domains and the reaction will be slower as a result. To optimize these parameters, I tested different lengths of hairpin stems and toeholds. Another major consideration in my design for HCR was to minimize the complementarity of domains that were not intended to be complementary. For example, in a concatemer consisting of **init**, **H1**, and **H2**, domains **2*** and **4** of **H2** and **a** of **H1** are single stranded at the growing end, as can be seen in Figure 3.4. These domains should not have any complementarity to each other. If they happen to bind together, the rate of the reaction may be slowed because these bound domains would not be available to either the **SDB 1** or to **H3** to continue growing the concatemer.

Dirks and Pierce used 6 nt toeholds with 18 bp stems and required at least 24 h of incubation at room temperature before detecting the products[7]. To minimize the amount of incubation time required for the formation of the concatemer, I used a longer toehold (7 nt) to increase the speed of hybridization in combination with a shorter hairpin stem (16 bp) to increase

the speed of opening the hairpin. I designed the **a*** domain of **F1** to be 9 nt and the **b*** domain to be 15 nt. Similarly, I designed the **d*** domain of **F2** to be 9 nt and the **c*** domain to be 15 nt.

Furthermore, to reduce the toehold melting temperature, I limited the GC content to at most 2 nt. Ang et al. published a report discussing the effects of GC content within the toeholds of hairpins for HCR[8]. The authors showed that any more than 2 nt of G and/or C within the toehold can substantially increase the melting temperature enough such that the resulting HCR will have increased background. The sequences of the optimized strand displacement beacons, **SDB 1** and **SDB 2**, are shown in Table 3.2 and the sequences of the optimized hairpins using 16 bp stems and 7 nt toeholds are shown in Table 3.3.

3.3.3 Detection of the formation of concatemers

To determine if the designed HCR forms concatemers, I separated the products after various lengths of incubations on a 1% agarose gel stained with ethidium bromide (Figure 3.7). I incubated 1 µM of the hairpins with 40 nM, 200 nM, 400 nM of **init**, or water for blank at room temperature for 24 h, 3 h, 1 h, and 0 h (no prior incubation). A smearing of bands at the highest concentration of **init** at all incubation times and faint bands with no **init** could be observed on the gel. The smearing indicated that there was an abundance of oligos at different lengths, which is characteristic of HCR and indicates the formation of concatemers[7]. The range of smearing indicated the range in the different lengths of concatemers and the density of the bands indicated the quantity of concatemers at that length.

The length of concatemers decreased with decreasing lengths of incubation. This is because concatemers begin with **init** and in solutions with low amounts of **init**, hairpins are used to extend the length of existing concatemers. In solutions with high amounts of **init**, more

concatemers are initiated and the finite number of hairpins are divided amongst them. Therefore, the result of low **init** concentration is a smaller amount of long length concatemers and conversely, the result of high **init** concentration is a larger amount of short length concatemers.

Furthermore, in Figure 3.7, there appears to be slight background with 24 h of prior incubation. However, the bands seen in lanes 9-12 suggest that only a 30 min room temperature incubation was required to form concatemers which indicated the viability of real-time fluorescence monitoring for an experimental time frame of less than 2 h.
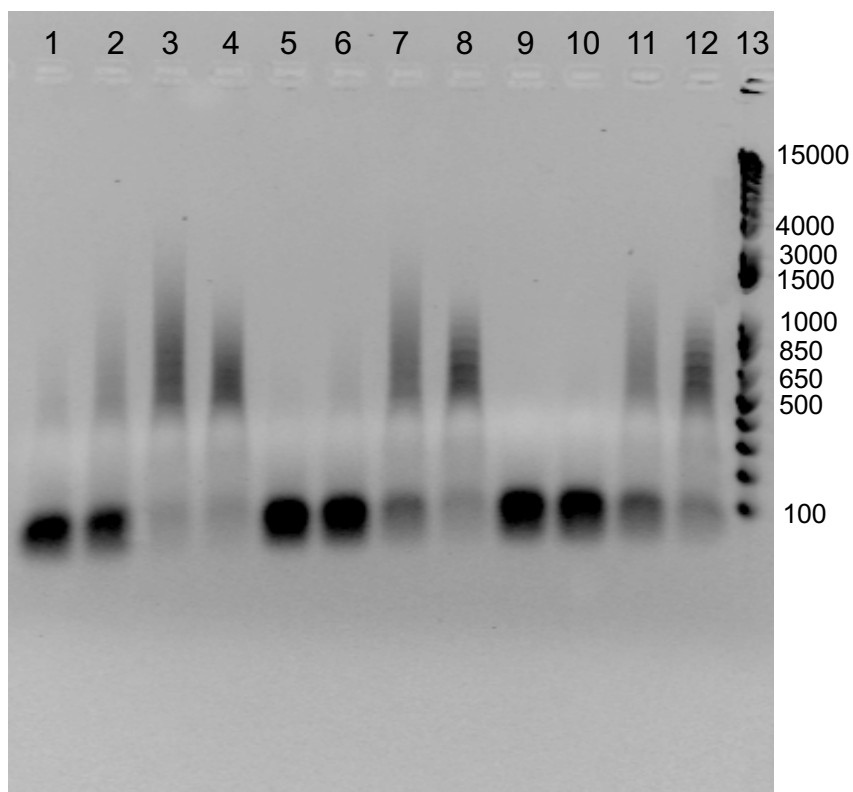
Figure 3.7 Agarose (1%) gel electrophoresis separation of HCR products using 1 µM of hairpins (16 bp stems and 7 nt toeholds). Lanes 1-4 show concatemers separated after 24 h, lanes 5-8 show after 2 h, and lanes 9-12 show after 30 min of incubation at room temperature. **Init** concentrations of 0 nM (blank) in the leftmost wells, followed by 40 nM, 200 nM, and finally 400 nM in the rightmost wells within each length of incubation were used. Lane 13 shows the 1 kb+ DNA ladder. DNA complexes were stained using ethidium bromide.

3.3.4 Effect of stem length

To determine if shorter hairpin stem lengths improved the speed of the reaction, stem lengths of 12 bp and 14 bp were tested in parallel with 16 bp stems (Figures 3.8A-C), each with 7 nt toeholds. The sequences of oligos using 12 bp stems and 14 bp stems are shown in Tables 3.4A and B, respectively. Reducing the stem length was expected to increase the speed of reaction by facilitating faster opening of the hairpins. The speed of the reactions of 14 bp and 12 bp stems were slightly faster than that of the 16 bp stem. However, both 14 bp and 12 bp stems showed an increase in the background signal, seen by the increasing fluorescence intensity of the blank curves. Additionally, the signal of the blank was increased in reactions using 14 bp and 12 bp stems when compared to using 16 bp stems, indicating that there may be some leakage due to the low melting temperature of the shorter stems, contributing to the background signal. Analysis of the amplification fold changes for each of the designs showed that the most optimal amount of signal amplification over the blank fluorescence was provided by 16 bp stems (Figures 3.9).

A)

12 bp stem

B)

14 bp stem

98

C)   16 bp stem
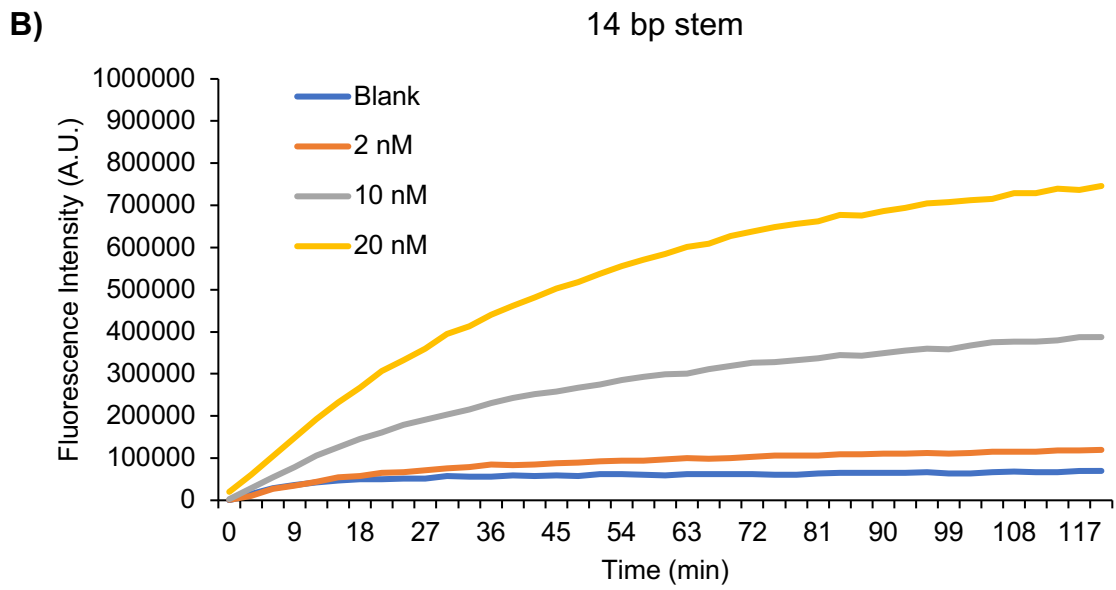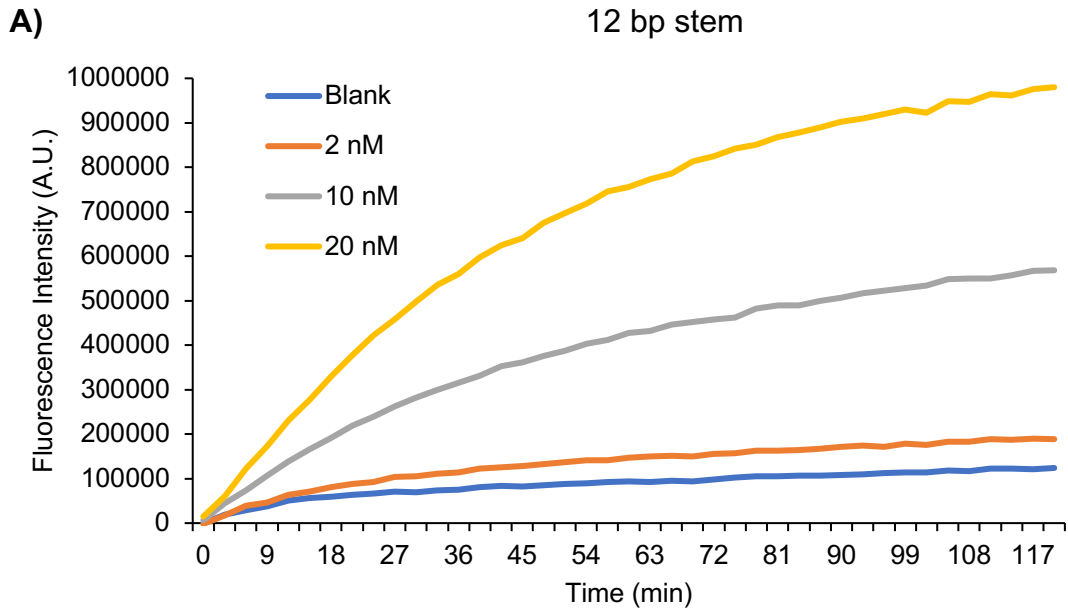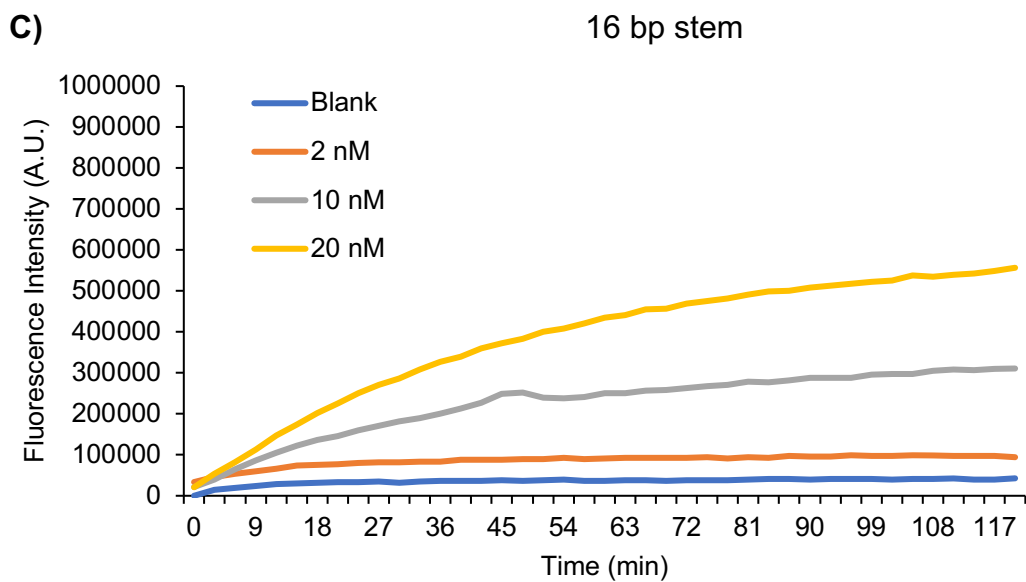
Figures 3.8A-C Real-time fluorescence monitoring of A) 12 bp, B) 14 bp, and C) 16 bp hairpin stems, each with 7 nt toeholds, using various **init** concentrations. Shorter stems of 14 bp and 12 bp yielded faster reactions and increased background. Each curve is an average of triplicate reactions.
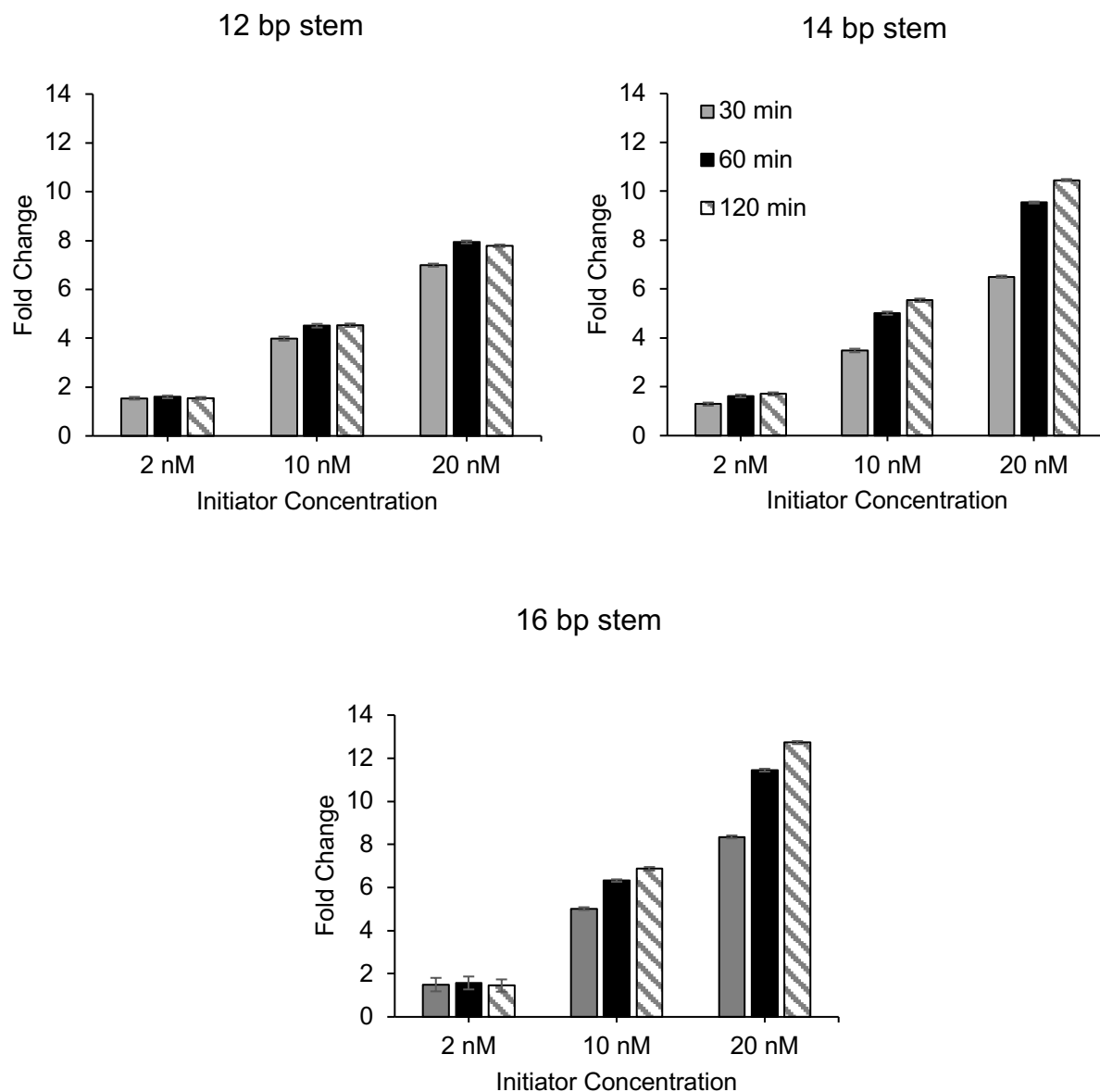
Figure 3.9 Fold changes at 30, 60, and 120 min of reactions using 12, 14, and 16 bp hairpin stems, each with 7 nt toeholds reacted with various **init** concentrations. The error bars represent the standard deviation of triplicate reactions. The reaction using 16 bp stems produced the greatest amplification fold changes across the **init** concentrations and at different reaction time points.

3.3.5 Effect of toehold length

To determine the effect of a shorter hairpin toehold length, I compared reactions using designs toeholds of 7 nt (Figure 3.10A) and toeholds of 6 nt (Figure 3.10B) concurrently to determine the effect of using toeholds lengths of 7 nt or 6 nt. The sequences of the hairpins with 7 nt and 6 nt toeholds, each with 16 bp stems, are shown in Table 3.5A and 3.4B, respectively. **Init** concentrations of 0 (blank), 2, 10, and 20 nM were tested with 50 nM of hairpins for both reactions. The fluorescence intensity of the reaction using design 6 nt toeholds was substantially suppressed. These results indicate that the shorter toehold of 6 nt may not be able to sufficiently bind to hairpins to facilitate hybridization compared to toeholds of 7 nt.
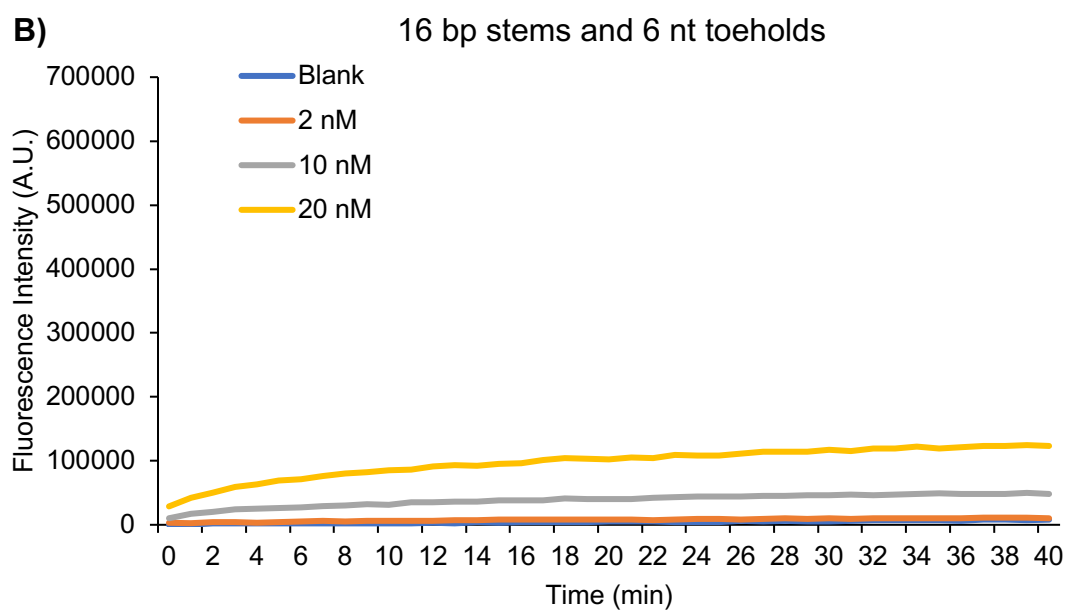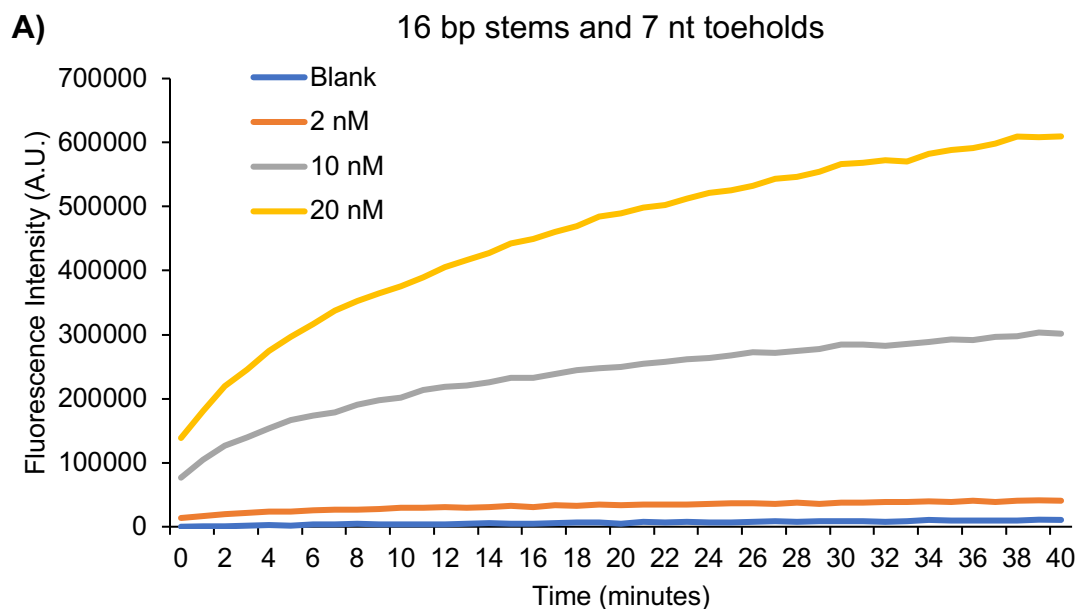
Figures 3.10A, B Real-time fluorescence monitoring of reactions using 7 nt hairpin toeholds (A) and 6 nt toeholds (B) each with 16 bp stems at various **init** concentrations. The background has been reduced as can be seen in the blank signal. Toeholds of 6 nt yielded suppressed fluorescence signals when compared to toeholds of 7 nt. Each curve is an average of triplicate reactions.

3.3.6 Assessment of fluorescence from SDB 1 and SDB 2

To determine the intensity of background fluorescence from the strand displacement beacons,

SDB 1 and **SDB 2** were mixed with **H1** and **H3** or **H2** and **H4**, respectively, or alone. Figure

3.11 shows low fluorescence intensity from **SDB 1** or **SDB 2** alone. **H1** and **H3** did not displace

SDB 1 and similarly **H2** and **H4** did not displace **SDB 2**. Thus, no background fluorescence

arose from the sequence design of **SDB 1** and **SDB 2**.

To determine the amount of fluorescence provided by the strand displacement beacons in

the reaction, the intensity of fluorescence from **SDB 1** was compared with that of **SDB 2** by

reacting either **SDB 1** or **SDB 2** with the hairpins and 20 nM of **init** or water for blank (Figure

3.12). The fluorescence produced by **SDB 1** is substantially faster than that of **SDB 2**. This can

be explained by the principle of the reaction: the assembly of the concatemer begins with **init**

bound to **H1**, followed by **H2**, and then **H3**. Thus, the assembly of the complement of **F1** by the

concatemer precedes the assembly of the complement of **F2**. The difference in fluorescence

intensities between **SDB 1** and **SDB 2** may be further exacerbated by the differing sequences of

the strand displacement beacons, which can cause differences in the rate of displacement. As a

result, the fluorescence resulting from the displacement of **F1** in **SDB 1** increases earlier than

that of **F2** in **SDB 2** when monitoring the reaction in real-time.
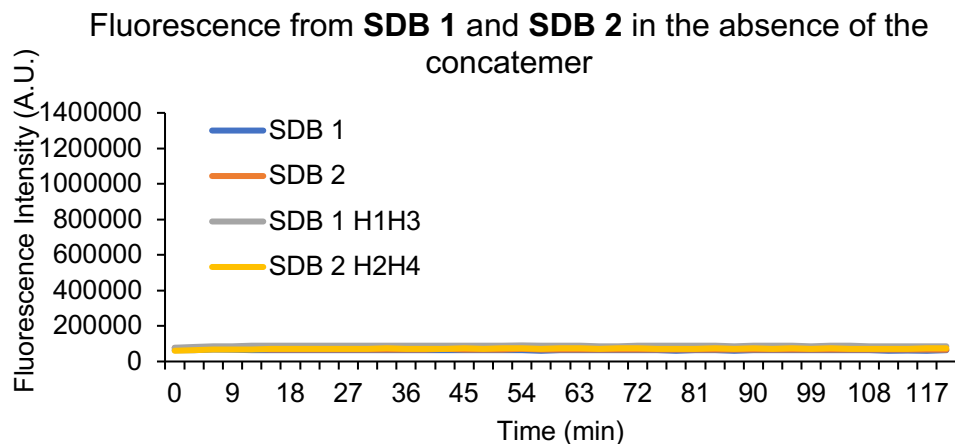
Figure 3.11 Real-time fluorescence monitoring of solutions containing **SDB 1** and **SDB 2** alone (labeled as SDB 1 and SDB 2) or with **H1** and **H3** (labeled as SDB 1 H1H3) or **H2** and **H4** (labeled as SDB 2 H2H4), respectively. No fluorescence is produced in the absence of **init**, indicating that **SDB 1** and **SDB 2** are likely not sources of background.
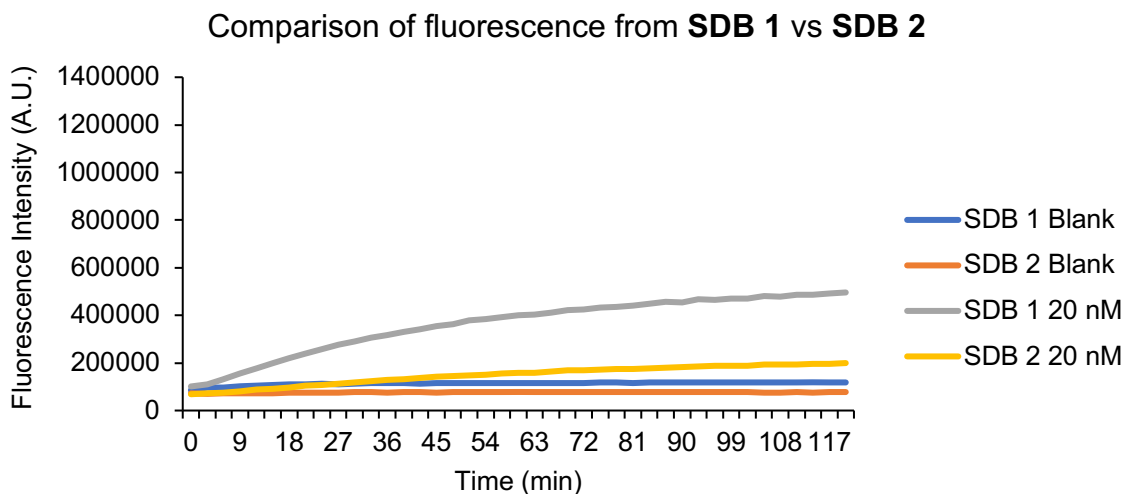
Figure 3.12 Real-time fluorescence monitoring of reactions containing only **SDB 1** or **SDB 2** with 0 (Blank) or 20 nM of **init**. The majority of signal is from **SDB 1** and may be a result of the assembly of the complement of **F1** earlier in the formation of the concatemer than that of **F2**.

3.3.7 Effect of F1 and F2 complement domain spacers

With respect to the hairpins, the junctions between the domains contributing to the concatemer and the domains complementary to **F1** and **F2** were designed to not contain any unpaired bases to act as spacers. The binding of the fluorophore complement domains in the concatemer with the fluorophore strands of the strand displacement beacons creates a four-way junction. Li et al. demonstrated that the three-way DNA junction requires at least a two-nucleobase spacer at the junction of torsion to increase the flexibility of the DNA strands to allow the formation of the binding assembly[9]. Despite that four-way junctions are generally regarded as more flexible than three-way junctions, the use of spacers was tested to determine if the detection signal could be increased[10–12].

I inserted two nucleotide spacers between the concatemer-producing domains and the **F1** and **F2** complement domains on each of the four hairpins. To maintain minimal unintended cross-talk between the hairpins as well as to not change the complementarity of the domains, different nucleobases were used as spacers depending on its location. The bases chosen for the spacers (T or A) were to minimize complementarity with the already existing sequences. A thymine and an adenine residue were inserted immediately upstream of **a** in **H1**, two adenine residues were inserted immediately downstream of **c** in **H2**, two thymine residues were inserted immediately downstream of **b** in **H3**, and two thymine residues were inserted immediately upstream of **d** in **H4**. The sequences of the modified hairpins are shown in Table 3.6. The resulting fluorescence curves are shown in Figure 3.13 with marked reduced fluorescence intensity. The spacers may have caused an increase in the distance between the two **F1** or **F2** complement domains (e.g. distance between domain **a*** and **b*** on **H1** and **H3**, respectively), which may have decreased the local concentration for less favourable binding conditions.

F1 and F2 complement domain spacers
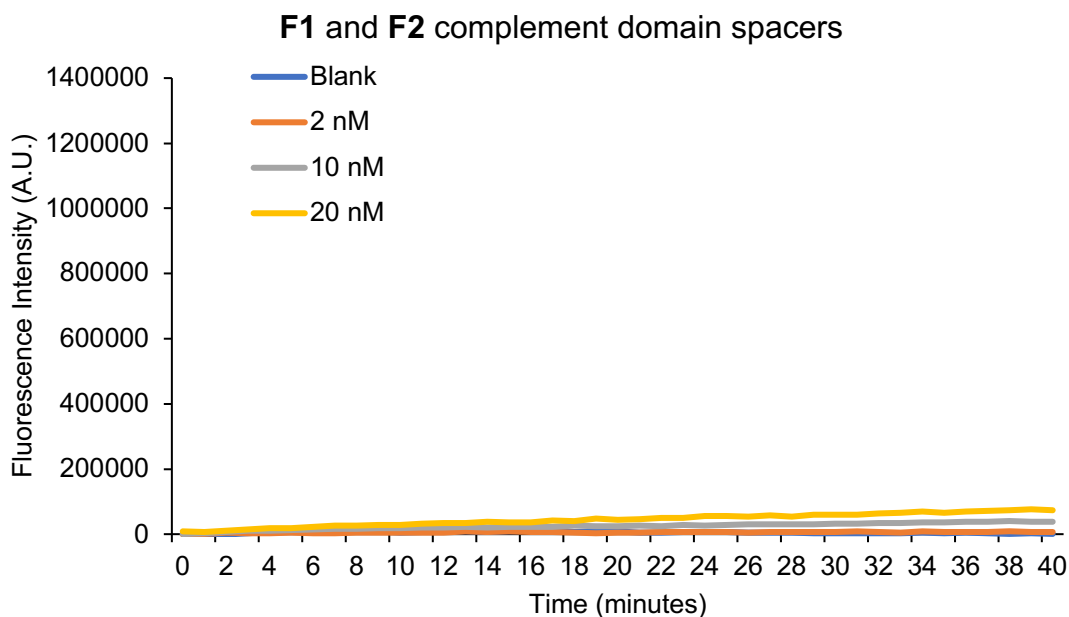
Figure 3.13 Real-time fluorescence monitoring of reactions using **F1** and **F2** complement spacers reacted with various **init** concentrations. The fluorescence in curves resulting from 2 nM, 10 nM, and 20 nM, were all substantially reduced, indicating the ineffectiveness of the spacers. Each curve is the average of triplicate reactions.

3.3.8 Limit of detection

To determine the limit of detecting **init** using design, I generated a calibration curve (Figure 3.14). A detection limit of about 660 pM and a limit of quantitation of 2.2 nM of **init** was achieved after 30 min of reaction monitoring. The fluorescence intensity of concentration corresponding to the limit of detection was calculated using 3 standard deviations above the background ($FI_{blank} + 3\sigma_{blank}$) and solving for the concentration using the formula produced by the calibration. The limit of quantitation was calculated similarly but used 10 standard deviations instead of 3. Because the detection limit of HCR is directly proportional to the concentration of hairpins, Ang et al. suggested that the length of concatemers are terminated by small amounts of

improper DNA synthesis of hairpins and therefore reduce the amount of fluorescence intensity[8].

Thus, an increase in the concentration of hairpin DNA will increase the likelihood of leaks and

spurious concatemer generation in the absence of the initiator (in my design, **init**). The detection

limit of HCR is thus directly proportional to the overall concentration of hairpins and is

described as a tunable limit of detection. The lowest possible detection limit using lower

concentrations of hairpins was not determined.
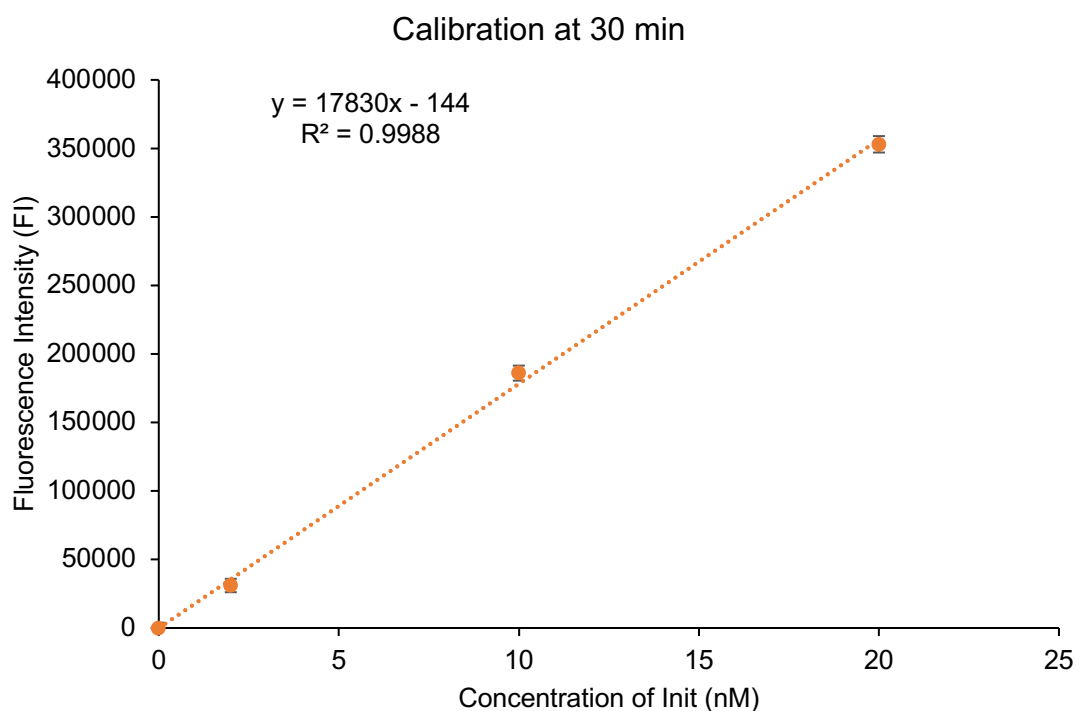
Figure 3.14 Calibration curve of the four hairpin HCR detected using two strand displacement

beacons. A limit of detection of 660 pM and a limit of quantitation of 2.2 nM of **init** was

achieved in 30 min. The error bars represent the standard deviation from triplicates.

3.4 Conclusions

Through rational DNA design, I developed HCR that enabled turn-on fluorescence from label-free hairpins. Features of my developed technique includes the use of four hairpins, using 16 bp stems and 7 nt toeholds, and two strand displacement beacons. Using the optimized sequences and conditions, a detection limit of 660 pM was achieved for **init**, the nucleic acid target, in 30 min. Furthermore, the technical procedure was easy to perform because the technique used a mix-and-read format at room temperature. This developed technique offers a strategy for amplified fluorescence sensing without the use of enzymes. Because the oligos were designed using functional domains, the modularity of the domains allows changing the sequence of **init** to measure clinically significant nucleic acid targets.

3.5 References

(1)   Liao, X.; Li, Z.; Peng, T.; Li, J.; Qin, F.; Huang, Z. Ultra-Sensitive Fluorescent Sensor for Intracellular MiRNA Based on Enzyme-Free Signal Amplification with Carbon Nitride Nanosheet as a Carrier. *Luminescence* **2017**, *32*, 1411–1416.

(2)   Li, J.; Li, D.; Yuan, R.; Xiang, Y. Biodegradable MnO2 Nanosheet-Mediated Signal Amplification in Living Cells Enables Sensitive Detection of Down-Regulated Intracellular MicroRNA. *ACS Appl. Mater. Interfaces* **2017**, *9*, 5717–5724.

(3)   Ou, M.; Huang, J.; Yang, X.; He, X.; Quan, K.; Yang, Y.; Xie, N.; Li, J.; Wang, K. Live-Cell MicroRNA Imaging through MnO2 Nanosheet-Mediated DD-A Hybridization Chain Reaction. *ChemBioChem* **2018**, *19*, 147–152.

(4)   Li, F.; Zhang, H.; Wang, Z.; Li, X.; Li, X. F.; Le, X. C. Dynamic DNA Assemblies Mediated by Binding-Induced DNA Strand Displacement. *J. Am. Chem. Soc.* **2013**, *135*, 2443–2446.

(5)   Paliwoda, R. E.; Li, F.; Reid, M. S.; Lin, Y.; Le, X. C. Sequential Strand Displacement Beacon for Detection of DNA Coverage on Functionalized Gold Nanoparticles. *Anal. Chem.* **2014**, *86*, 6138–6143.

(6)   Srinivas, N.; Ouldridge, T. E.; Šulc, P.; Schaeffer, J. M.; Yurke, B.; Louis, A. A.; Doye, J. P. K.; Winfree, E. On the Biophysics and Kinetics of Toehold-Mediated DNA Strand Displacement. *Nucleic Acids Res.* **2013**, *41*, 10641–10658.

(7)   Dirks, R. M.; Pierce, N. A. Triggered Amplification by Hybridization Chain Reaction. *Proc. Natl. Acad. Sci. U. S. A.* **2004**, *101*, 15275–15278.

(8)   Ang, Y. S.; Yung, L.-Y. L. Rational Design of Hybridization Chain Reaction Monomers for Robust Signal Amplification. *Chem. Commun.* **2016**, *52*, 4219–4222.

(9)   Li, F.; Lin, Y.; Le, X. C. Binding-Induced Formation of DNA Three-Way Junctions and Its Application to Protein Detection and DNA Strand Displacement. *Anal. Chem.* **2013**, *85*, 10835–10841.

(10)   Clegg, R. M.; Zechel, A.; Carlberg, C.; Diekmann, S.; Murchie, A. I. H.; Lilley, D. M. J. Fluorescence Resonance Energy Transfer Analysis of the Structure of the Four-Way DNA Junction. *Biochemistry* **1992**, *31*, 4846–4856.

(11)   Altona, C.; Pikkemaat, J. A.; Overmars, F. J. J. Three-Way and Four-Way Junctions in DNA: A Conformational Viewpoint. *Curr. Opin. Struct. Biol.* **1996**, *6*, 305–316.

(12)   Duckett, D. R.; Lilley, D. M. The Three-Way DNA Junction Is a Y-Shaped Molecule in Which There Is No Helix-Helix Stacking. *EMBO J.* **1990**, *9*, 1659–1664.

Chapter Four: Development of a protein-initiated hybridization chain reaction for localized detection of a cell surface protein

4.1 Introduction

As discussed in Chapter 1, the localized detection of protein targets is routinely performed using immunostaining[1]. The protocol of immunostaining requires multiple incubations, washing steps, and an enzyme for amplified signal generation. Novel techniques based on the isothermal amplification of nucleic acids have been developed for localized protein imaging, such as immuno-RCA[2] or DuoLink® PLA[3]. These techniques require multiple enzymes, which can complicate technical protocols or impose strict storage requirements. Techniques that use enzyme-free nucleic acid signal amplifiers, such as HCR, circumvents these constraints. However, despite the recent developments in localized protein imaging using HCR[4,5], some challenges still remain. These challenges include long incubation times and multiple washing steps, both of which contribute to laborious and time-consuming protocols. Thus, a technique that enables the isothermal and amplified localized detection of proteins without requiring incubations, washing steps, nor enzymes, has not yet been developed.

The use of binding-induced DNA assembly (BINDA) probes for protein detection and subsequent signal transduction has been previously established by the Le research group[6–8]. BINDA requires two probes, consisting of DNA oligos conjugated to affinity ligands against a target. The two DNA oligos are designed to be complementary to each other through a short region but with a low duplex melting temperature. Furthermore, the probes are in low concentration in solution. Combined with the shortness of the complementary region and the low concentration of the probes, the duplex stability of the oligos is poor. Two binding events are required; the affinity ligands of both probes bound to one target molecule (e.g., binding of

two epitopes on one protein unit) allows the stable hybridization of the oligos to each other. Upon binding of both the probes to one target, the local effective concentrations of the oligos are increased. The complex of the two DNA oligos anchored onto one protein confers increased duplex stability analogous to the increased duplex stability in intramolecular interactions (e.g. DNA hairpins) relative to that of intermolecular interactions. The requirement for two probes to bind one target molecule to facilitate the stable hybridization of the two BINDA probes circumvents the need for the separation of unbound probes. In other words, washing steps are unnecessary. For signal transduction, BINDA can be used to convert the detection of protein into a nucleic acid oligo. The new nucleic acid oligo can then be used as a surrogate target and amplified using DNA-based signal amplification strategies. BINDA has achieved ultrasensitive detection to yoctomole and zeptomole concentrations[7,9]. The principle of BINDA has also been coupled with strategies using nanomachines[10,11] and strand displacement amplification[12]. Ultimately, BINDA has the potential for applications in cell-surface imaging by converting the detection of the target to a nucleic acid signal for amplification without introducing any washing steps.

To enable the sensitive, isothermal amplified detection of proteins without the need for enzymes, I aimed to use the strategy of HCR to develop a real-time signal amplifier for the localized detection of proteins. I planned to detect the formation of the HCR concatemer as an indication of the presence of an initiating nucleic acid strand. The initiating nucleic acid strand would be produced by BINDA in response to the detection of a protein target and therefore confers indirect detection of the protein target. In this chapter, I will discuss the development of protein-initiation of my optimized HCR technique by designing probes focused on the principle of BINDA. Through this technique, I would enable the amplified localized detection of proteins

without enzymes or washing steps at isothermal reaction temperatures. I demonstrated this technique's application to the detection of a cell surface protein.

Given that the non-covalent interaction between streptavidin (SA) and biotin can be considered irreversible ($K_d = 10^{-15}$ M)[13], I used the detection of SA in solution as a model system to optimize the reaction conditions of BINDA-HCR for protein detection (Figure 4.1) The SA-biotin system is especially fitting to use to optimize BINDA reactions because SA has multiple biotin binding sites, meaning one molecule of SA is capable of accommodating both BINDA probes. In this chapter, optimizations on BINDA-HCR were performed using 2 nM of SA as the protein target.

I adapted the previously optimized HCR in Chapter 2 for the detection of protein by splitting the **init** strand between its two domains of **2*** and **1**. I intended for the two domains to be brought together only in the presence of the protein target. Thus, I designed two BINDA probes and placed domain **2*** on the 5' end of one probe, **L** probe, and domain **1** on the 3' end of the other BINDA probe, **R** probe. Downstream of **2*** on **L** probe was domain **6***, the complementary domain between the two probes, followed by a poly-T_{20} linker and biotin. Upstream of the **1***, was domain **6**, followed by a poly-T_{20} linker and biotin. Sabir et al. noted that the bases of each strand within a three-way DNA junction are unpaired, even if having full complementarity[15]. Therefore, I added two unbound thymine bases between domains **1*** and **6** and **2*** and **6***. Only when the two BINDA probes bound to the same protein target, the two probes would bind to each other to create **init**. To promote the BINDA probe to bind to **H1**, domain **r**/**r*** was added to increase the degree of complementarity. Two **R** probes were designed with **r** domains of 4 and 2 nt. The modified **H1** with the complementary **r*** domain was denoted as **H1-B**. Table 4.1 shows the sequences of hairpins and Table 4.2 shows the sequences of

BINDA probes used and the modified **H1** strand, **H1-B**, which was created to accommodate the BINDA probes (specifically the **r/r*** domain).
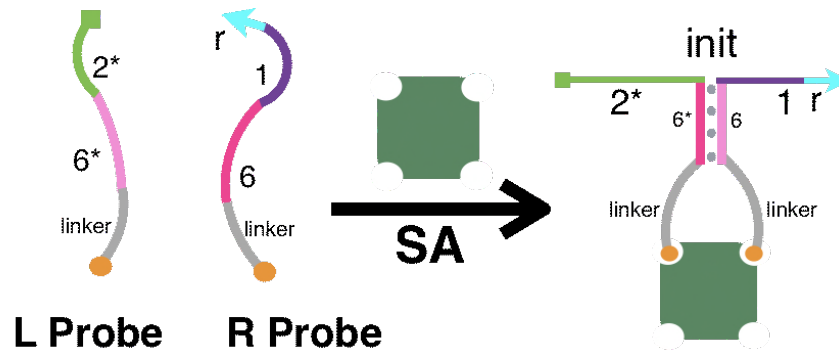
Figure 4.1 Biotinylated BINDA probes binding to the streptavidin (SA) target and forming **init**.

4.2 Experimental

4.2.1 Materials and reagents

SK-BR-3 (HTB-30; American Type Culture Collection (ATCC), Manassas, VA) cell line was

obtained with permission from Dr. Afsaneh Lavasanisfar's laboratory at the University of

Alberta and MDA-MB-231 (HTB-26) cell line was obtained from American Type Culture

Collection (ATCC). Human ErbB2/Her2 Biotinylated Antibody was obtained from R&D

Systems, Inc. (Minneapolis, MN). Streptavidin, biotin, bovine serum albumin (BSA), and fetal

bovine serum (FBS), Canadian origin, and McCoy's 5a modified media were obtained from

Sigma-Aldrich (Oakville, ON). Penicillin-Streptomycin, RPMI 1600 with L-glutamine, 0.25%

Trypsin-EDTA, and Dulbecco's phosphate buffered saline (DPBS) were obtained from Gibco

by Life Technologies (Carlsbad, CA). BioLite cell culture treated T25 flasks and NucBlue

LiveReadyProbes Reagent for DAPI nuclear staining (adenine-thymine region binding dye)

were obtained from Fisher Scientific Company (Ottawa, ON). Chambered cover glasses were

obtained from Cellvis (Mountain View, CA). Fluorescence live cell imaging was enabled by using an Olympus IX-81 motorised microscope base with a Yokogawa CSUx1 spinning disk confocal scan-head and a Hamamatsu EMCCD camera with an x40/1.3 oil objective lens. Pumped diode lasers were used to excite FAM (50mW, 491 nm), Cy5 (45mW, 642 nm) and DAPI (44mW, 405 nM) dyes. Volocity was used for the acquisiton of images and ImageJ was used for the processing and analysis of images.

4.2.2 Sequences of oligos

Sequences of the hairpins, **H2**, **H3**, and **H4**, and of **SDB 1** (**F1** and **Q1**) and **SDB 2** strands (**F2** and **Q2**) are shown in Table 4.1. BINDA probe sequences and **H1-B**, a modified **H1** to accommodate the inclusion of BINDA probes, are shown in Table 4.2.

Table 4.1 Sequences of **H2**, **H3**, **H4**, **F1**, **Q1**, **F2**, and **Q2** from the developed technique in Chapter 3. Qu indicates a dark quencher (IaBkRQ or IaBkFQ), Fl indicates a fluorophore, and (Cy5 cyanine or FAM fluorescein).

Oligo	Sequence of oligo (5'-3')
H2	TAA CTC GAA CAT ATC CAA CCA CTA CCT CAT CTA AAC GTG ATG AGG TAG TGG TTG ATG GAA A
H3	AGA GCA GCT TTA GAG ACG TTT AGA TGA GGT AGT GGT TGC AAT CAA CAA CCA CTA CCT CAT C
H4	CAA CCA CTA CCT CAT CTA TAC TGG ATG AGG TAG TGG TTG TTG ATT GCT ACG TAA G
F1	TGT GAG AAT CTC TAA AGC TGC TCT - Fl
Q1	Qu - AGA GCA GCT TTA GAG
F2	CTT ACG TGA GAT ATG TTC GAG TTA - Fl
Q2	Qu - TAA CTC GAA CAT ATC

Table 4.2 Sequences of BINDA probes and **H1-B**.

Oligo	Sequence of oligo (5'-3')
7.4 **R** probe (7 bp; 4 nt)	Biotin - TT TTT TTT TTT TTT TTT TTT TGA ATC GTT TAT ACT GCT AC
7.2 **R** probe (7 bp; 2 nt)	Biotin - TT TTT TTT TTT TTT TTT TTT TGA ATC GTT TAT ACT GCT
6.4 **R** probe (6 bp; 4 nt)	Biotin - TT TTT TTT TTT TTT TTT TTT TGA TCG TTT ATA CTG CTA C
6.2 **R** probe (6 bp; 2 nt)	Biotin - TT TTT TTT TTT TTT TTT TTT TGA TCG TTT ATA CTG CT
L probe (7 bp)	CAA CCA CTA CCT CAT CTT CGA TTC ATT TTT TTT TTT TTT TTT TTT - Biotin
L probe (6 bp)	CAA CCA CTA CCT CAT CTT CGA TCA TTT TTT TTT TTT TTT TTT TT - Biotin
H1-B	GTA GCA GTA TAG ATG AGG TAG TGG TTG TTT CCA TCA ACC ACT ACC TCA TCA TTC TCA CA

4.2.3 Streptavidin detection protocol in solution

SA (5 mg) was resuspended to 50 µM and aliquoted in 20 µL for storage in -18°C in PBS with

0.1% BSA and 50% glycerol. D-Biotin (500 mg) was resuspended in HCR buffer (10 mM

TrisHCl, 12 mM $MgCl_2$, and 0.05% Tween-20) to 10 M and diluted to 1 M and stored in 100 µL

aliquots at -18°C. SA aliquots were diluted immediately prior to analysis using HCR buffer.

Table 4.3 shows the mastermix components and their concentrations used in SA optimization

experiments.

Table 4.3 BINDA-HCR mastermix components with their final concentrations and volumes per reaction.

Component	Final concentration	Volume per reaction
H1-B	1 µM	5 µL
H2	1 µM	5 µL
H3	1 µM	5 µL
H4	1 µM	5 µL
L probe	100 nM	10 µL
R probe	100 nM	10 µL
SDB 1	1 µM	5 µL
SDB 2	1 µM	5 µL
Target (SA or HER2)	various	5 µL
HCR Buffer	10 nM Tris, 12 mM Mg^{2+}, 0.05% Tween-20	45 µL
Final volume		**100 µL**

4.2.4 Calculation of fold change

The calculations for fold change are discussed in Chapter 3, section 3.2.4 Calculation of fold change.

4.2.5 Time required for BINDA probes to open H1-B

Determining **H1-B** opening time experiments was performed by making two mastermixes, MM1 and MM2. MM1 consisted of **H3**, **H4**, **SDB 1**, **SDB 2**, and **R** and **L** BINDA probes. MM2 consisted of **H1-B** and SA and was kept on ice. For triplicate analysis of the amount of time it takes **H1-B** to be opened by **init**, MM1 was first added to wells of a 96-well plate. MM2 was then also added to each well but at each specified time point in triplicate. Immediately prior to fluorescence detection of the entire plate, **H2** was rapidly added to every well.

4.2.6 Cell culturing conditions

SK-BR-3 cells were cultured in McCoy's 5a modified media with 10% FBS and 100 U/L of streptomycin and penicillin antibiotics at 37°C with 5% CO_2 and 90% humidity. Cells were grown to 70% to 80% confluency before passaging, amounting to once every 3 to 5 days. MDA-MB-231 cells were cultured in RPMI 1640 media with 10% FBS at 37°C with 5% CO_2 and 90% humidity. Cells were grown to 80-90% confluency before passaging, amounting to once every 3 to 5 days.

Both SK-BR-3 and MDA-MB-231 were grown using 50 mL T-25 vented flasks treated for cell culturing. Cells were sub-cultured by aspirating old media, washing with DPBS, and using 0.25% (w/v) trypsin-EDTA to detach adhered cells. Detached cells were centrifuged, resuspended and added into new flasks with fresh, pre-warmed media.

4.2.7 Cell seeding onto chambered glass coverslips

SK-BR-3 and MDA-MB-231 cells were passaged 2 and 1 day(s) prior to seeding onto chambered glass coverslips, respectively. Both cell lines were seeded at a density of 30 000 cells per well. Cells were detached from flasks using 0.25% trypsin-EDTA and centrifuged. Cell pellets were resuspended in the respective cell growth media and counted on a hemocytometer to dilute to a suspension of $15x10^4$ cells/mL. To prepare the chambered glass coverslips, 200 µL of media was added to each well. Various volumes of the the $15x10^4$ cells/mL cell suspension were seeded into each well to achieve 30 000 cells per well, according to the calculation below.

$$\frac{30\ 000\ cells}{well} \ x \frac{well}{0.2\ mL} = \frac{15x10^4 cells}{mL}$$

Seeded chambers were incubated in 37°C with 5% CO_2 and 90% humidity overnight.

4.2.8 BINDA probe preparation

BINDA probes for HER2 protein were assembled using the strong affinity between streptavidin and biotin (K_d of about 10^{-15} M)[13,14]. HER2 biotinylated antibody, goat IgG, (MW=144 000 g/mol) was diluted to 1 µM using PBS with 0.1% BSA and 50% glycerol. Biotinylated oligonucleotides, **R** and **L**, (2 µM) were each mixed in equal parts with SA (2 µM) and incubated for 30 min at room temperature in 10 mM TrisHCl, 12 mM $MgCl_2$, and 0.05% Tween-20 HCR buffer in a volume of 50 µL. One part of anti-HER2 antibody (1 µM) was added to both solutions, for a total volume of 100 µL for each probe, and was incubated for 30 min at 4°C. The **R** and **L** BINDA probes for HER2 were then diluted to 100 nM and stored in 4°C for up to 5 days.

4.2.9 Cell imaging protocol

After cells adhered and grew on chambered flasks, the growth media was aspirated off and cells were gently washed with DPBS once. BINDA-HCR master mix (Table 4.2) omitting **H1-B** and "Target" was added to each well amounting to 90 µL. For each experiment omitting a specific component (e.g., omit **H1-B**, omit **L** or **R** BINDA probes, and **SDB 1** and **SDB 2**), the volume was replaced by an equal volume of HCR buffer. Immediately prior to confocal fluorescence microscopy imaging, one drop of DAPI stain and 5 µL of **H1-B** were added to each well (except for wells omitting **H1-B** to which only DAPI was added). Wells were imaged ranging from 0 to 150 min, where 0 min indicates the time at which DAPI was added. Confocal fluorescence microscopy conditions for test and control imaging were repeated at least three times on three different days.

4.3 Results and discussion

4.3.1 Working principle of the protein-initiated four-hairpin hybridization chain reaction (HCR)

The BINDA-HCR reaction began when the affinity ligands of both probes bound to adjacent epitopes on the same protein target or to individual protein monomers of a dimer and the oligos are brought into close proximity of each other, increasing the local concentration of both probes relative to one another (Figure 4.2). The increase in local concentration allowed the BINDA probes to bind each other through domains **6** and **6***, forming **init (2*, 1, r)**, to which the **R** probe could bind through domains, **1** and **r**. Through random walk branch migration, domain **2*** of **init** subsequently bound to the adjacent stem domain of **2** on **H1-B**, opening the stem of **H1-B**. Because the stem of **H1-B** was now opened, **H1-B** loop domain, **3**, and stem domain, **2***, bound to their respective complementary domains on **H2**, opening the stem of **H2** (Figure 4.3). Similarly, **H2** loop domain, **4**, and stem domain, **2***, bound to their respective complementary domains on **H3**, opening **H3**. **H3** loop domain, **5**, and stem domain, **2***, bound to **H4**, and when **H4** was opened loop domain, **1**, and stem domain, **2***, could bind to another **H1-B** molecule. This cross-opening of hairpins continued until all the hairpins in the solution were exhausted, forming the concatemer, a long, dsDNA nicked polymer. Because the concatemer grew with specific hairpins added sequentially, the exhaustion of any one hairpin species would result in the termination of the reaction. As discussed in Chapter 3, the formation of the concatemer was detected via turn-on fluorescence using strand displacement beacons. Since every **H1-B - H4** repeat within the concatemer could bind one **F1** and one **F2**, every **H1-B** to **H4** cycle in the concatemer could retain two fluorophore molecules.

The usage of BINDA probes introduces new DNA sequences into the system. New sequences can result in spurious hybridization, leading to an increase in background. To

determine the optimal conditions for BINDA-HCR, I tested the optimal concentration of

BINDA probes, sequences of BINDA probes, and the optimal length of the **r** toehold on **H1-B**.
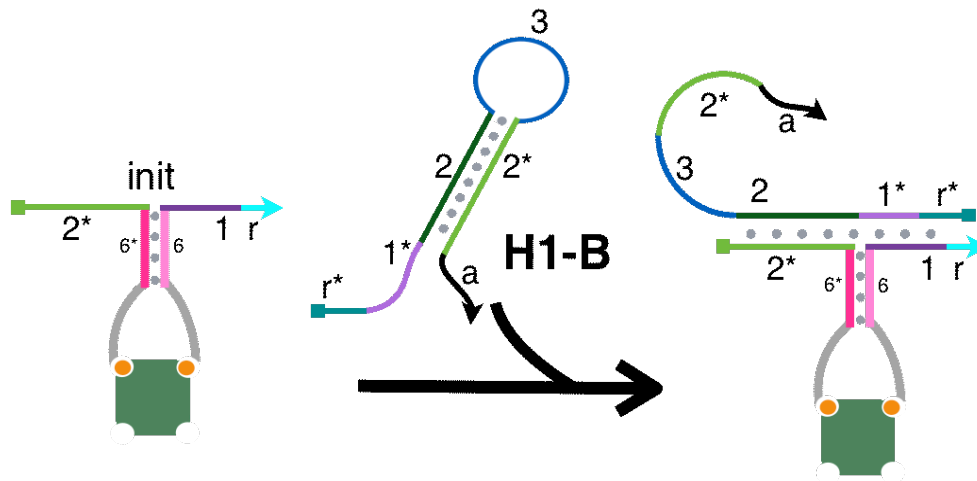
Figure 4.2 Schematic of protein-initiated opening of **H1-B** for SA detection using BINDA probes. The **r*** domain on **H1-B** that was added to accommodate an increased toehold for BINDA probe **R** in an example reaction detecting SA.
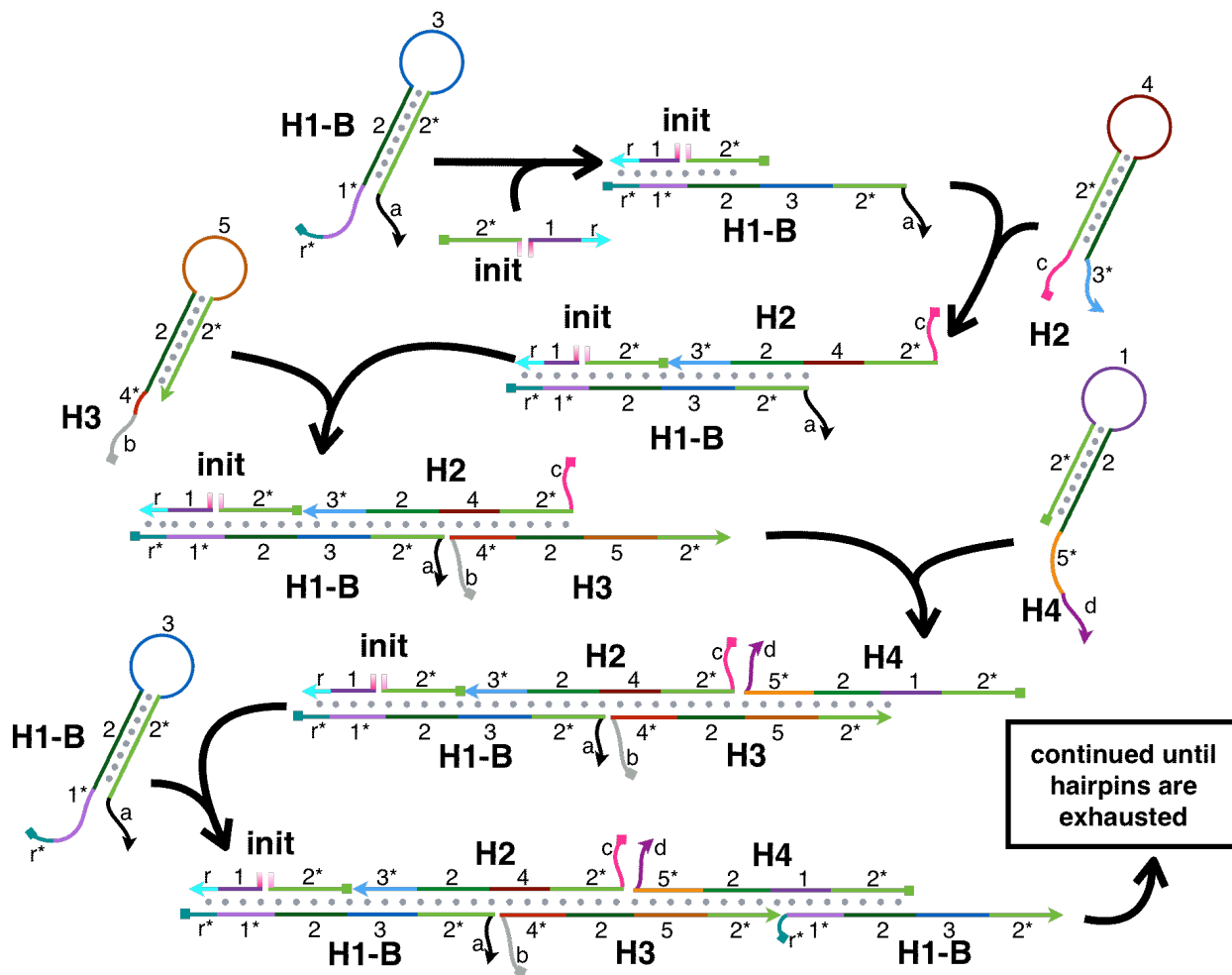
Figure 4.3 Schematic of the four hairpin HCR as a result of the initiation from protein binding, as shown in Figure 4.2.

4.3.2 Concentration of BINDA probes

To determine the optimal concentration of BINDA probes with 50 nM of hairpins, I used

BINDA probes with **6/6*** of 7 nt and **r** of 4 nt in concentrations of 5, 10, and 20 nM to detect 2

nM of SA (Figure 4.4a). Both the signal produced from SA and the blank signal increased with

increasing probe concentrations. Because the differences between the amplification curves

corresponding to each probe concentration were small, it was difficult to determine the most optimal probe concentration. Thus, amplification fold change was used to compare the difference in the change in amplification between time zero and time 30, 60, and 120 min of the reaction between the target and the blank (Figure 4.4). The concentration of probes giving the largest distinction between the target and blank as determined by the greatest fold change was 10 nM.

The source of background may from the BINDA probes binding to each other transiently to initiate the formation of the concatemer. A higher concentration of BINDA probes would increase the likelihood of the probes binding to each other in the absence of SA, contributing to the background. Too low concentration of BINDA probes would produce the lowest amount of background but also would not produce a sufficiently large enough signal for SA sensing. Subsequent experiments use 10 nM of each **L** and **R** probes.
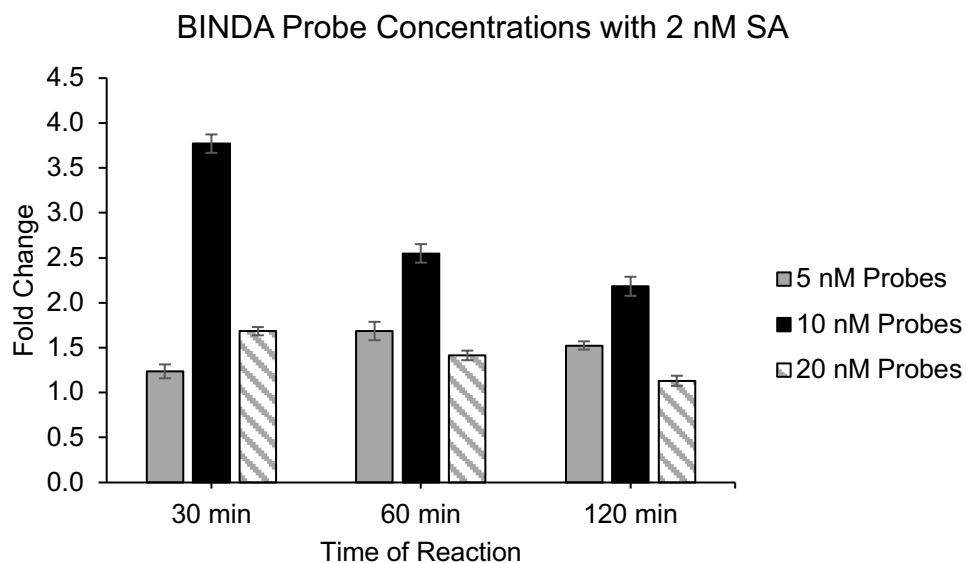
Figure 4.4 Fold changes at 30 min of the detection of 2 nM SA when using 5, 10, or 20 nM of BINDA probes (probe design 7.4) and 50 nM of hairpins.

4.3.3 Length of r domain

Figure 4.5 shows the fold changes for each combination of BINDA probe designs when detecting 2 nM of SA. The differences in fold change in each of the designs were variable, which makes it difficult to determine the optimal design. However, reactions corresponding to domains **6/6*** of 6 nt and **r** of 2 nt (probe design 6.2) yielded the greatest amplification fold change consistently at 30 min, 60 min, and 120 min of reaction time. Therefore, I used this design for subsequent experiments. The fold change in all reactions decreases with increasing reaction time. This is due to the increase in amplification signal from the blank and a plateau of the amplification in the target reaction.
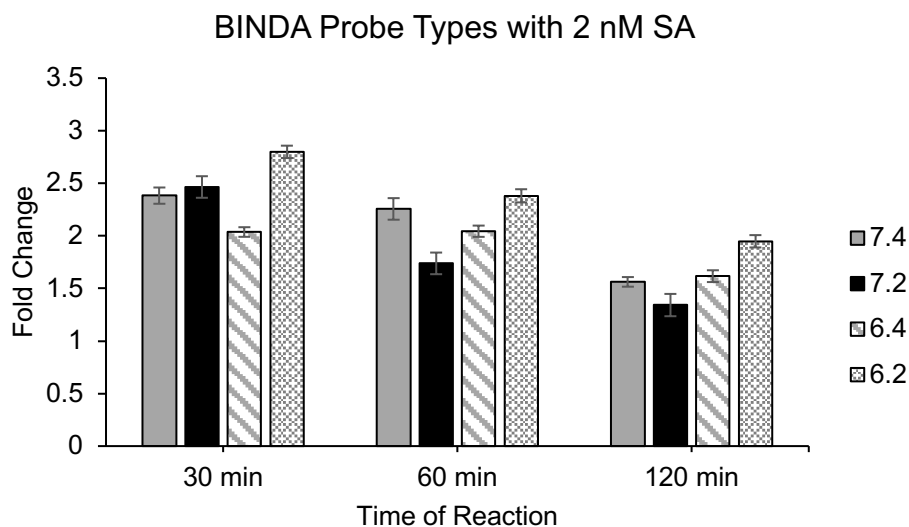
Figure 4.5 Fold changes of 2 nM of SA detected using 6 or 7 bp complementarity probes (**6/6***) with either a 4 or 2 nt **r** domain as indicated by the legend.

4.3.4 Time required for BINDA probes to open H1-B

To determine if the amount of time that is required for the BINDA probes to form **init** and open **H1-B** would substantially impact the HCR reaction, I tested the reaction with a prior incubation period. The protocol is outlined in Section 4.2.5. Briefly, two mastermixes were used, MM1 and MM2. MM1 alone contained the necessary components for the reaction except for **H1-B**, **H2**, and SA. MM2 contained **H1-B** and SA. MM2 containing **H1-B** and SA were added to MM1 and incubated at room temperature for 30 min or 0 min. The addition of MM2 allows both BINDA probes to hybridize to SA to form **init** and to bind to and open **H1-B**. However, when **H1-B** is opened, the reaction does not proceed because **H2** is not present in solution. The rate of polymerization impacted by how fast or how slow **H1-B** is opened by **init** formed through BINDA probes could be observed after **H2** was added immediately prior detecting the fluorescence of each well. Those wells where **H1-B** has been opened would proceed with the

reaction. Wells in which the **init** took longer to open **H1-B** would show a lag in the increase of fluorescence intensity. However, the results shown in Figure 4.6 indicate that there is no difference in the rate of reaction between 30 min of incubation and 0 min of incubation of **H1-B** with the **init** formed by **BINDA** when using 2 nM of SA as the target. These results suggest that time required for the initiation when using the BINDA probes did not substantially impact the speed of the reaction.
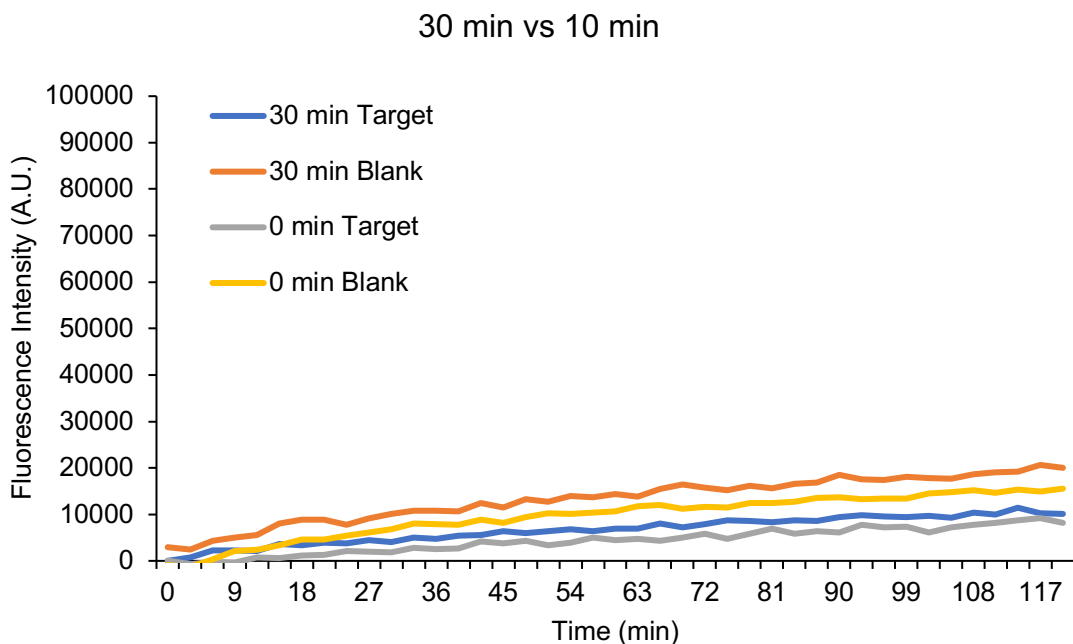
Figures 4.6 Real-time fluorescence monitoring of the amount of time required for the opening of **H1-B** through BINDA probes. The comparison between no incubation (0 min) or 30 min of incubation when detecting 0 (Blank) or 2 nM (Target).

4.3.5 Limit of detection

To determine the limit of detection of SA in solution using BINDA-HCR, I tested various concentrations of SA. Using the optimized BINDA probe pair sequence (probe design 6.2 with 6 bp of complementarity and 2 nt **r** domain) and probe concentrations (10 nM), a dynamic range of SA concentrations was tested in solution (Figure 4.7A). As early as 30 min, a linear calibration was obtained (Figure 4.7B) and was not substantially different than the reaction at 120 min (Figure 4.7C). These results show that BINDA-HCR for the detection of protein in solution was feasible and produced a dose-dependent response in as soon as 30 min. Although Figure 4.7A shows a detection of SA as low as 500 pM was achieved in solution, limits of detection of 1.4 nM and 2.1 nM for 30 min and 120 min reactions, respectively, were calculated using three standard deviations above the background signal ($FI_{blank}+3\sigma_{blank}$) to determine the fluorescence intensity (y) and solving for (x) using the respective equations from calibration curves as shown in Figures 4.8B and C. Since the interaction between SA and biotin is much stronger than that between antibody or aptamer and their ligands, it may be assumed that detecting other proteins using antibodies as affinity ligands would be higher.

Di Gioia et al. have shown that the extracellular domain of HER2 can be shed in serum with median levels of 9.9 ng/mL in healthy females and 11.7 ng/mL and 13.4 ng/mL in females with a +2 or +3 status for HER2+ breast cancer, respectively[16]. However, Petersen et al. reported that elevated levels of serum HER2 greater than 0.015 µg/mL can predict the patients' response to trastuzumab, an anti-HER2 treatment[17]. Using the calculated limit of detection for BINDA-HCR, a concentration of 2.1 nM for proteins translates to about 386 µg/mL of whole HER2; however, this is a rough estimate because the limit of detection was calculated using the detection of SA. A typical enzyme-linked immunosorbent assay (ELISA) for the detection of HER2 in serum is reported to be 14.8 pg/mL and takes 4.5 hours with multiple washing and

incubation steps (R&D systems)[18]. For clinical applications, BINDA-HCR as it is optimized

currently is not ideal for serum HER2 detection. To offer applications in detecting protein serum

targets as an alternative to immunosorbent tests, BINDA-HCR may be optimized in the future

by using lower probe concentrations and/or lower hairpin concentrations. However, because the

intended application was for localized protein detection, I continued onto testing BINDA-HCR

for the detection of protein on cell surfaces (Section 4.3.7).

A)

Streptavidin Detection with BINDA-HCR

B)

Calibration at 30 min

$$y = 3.4651x - 727$$
$$R^2 = 0.9576$$

Fluorescence Intensity vs Concentration (pM)

C)

Calibration at 120 min

$$y = 4.8575x - 1022$$
$$R^2 = 0.9864$$

Fluorescence Intensity vs Concentration (pM)
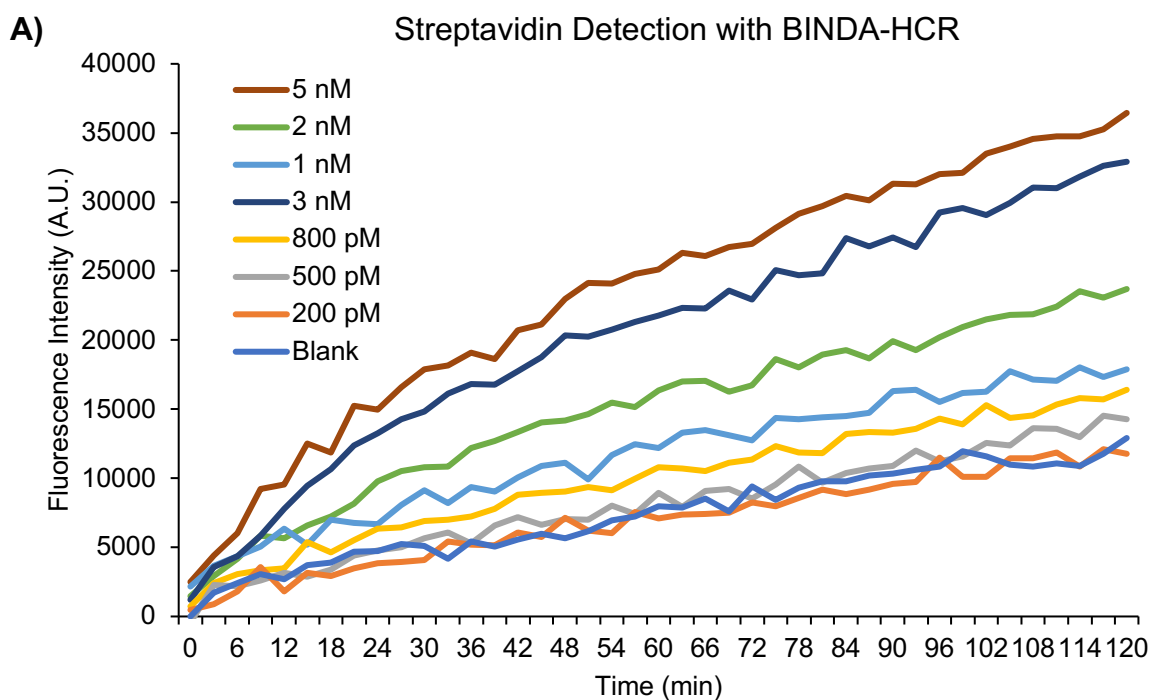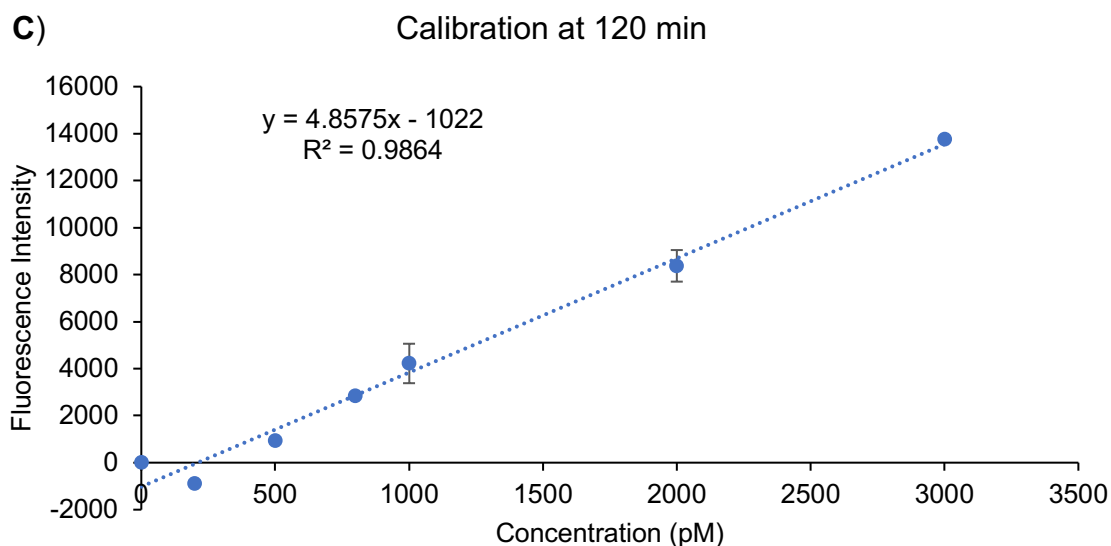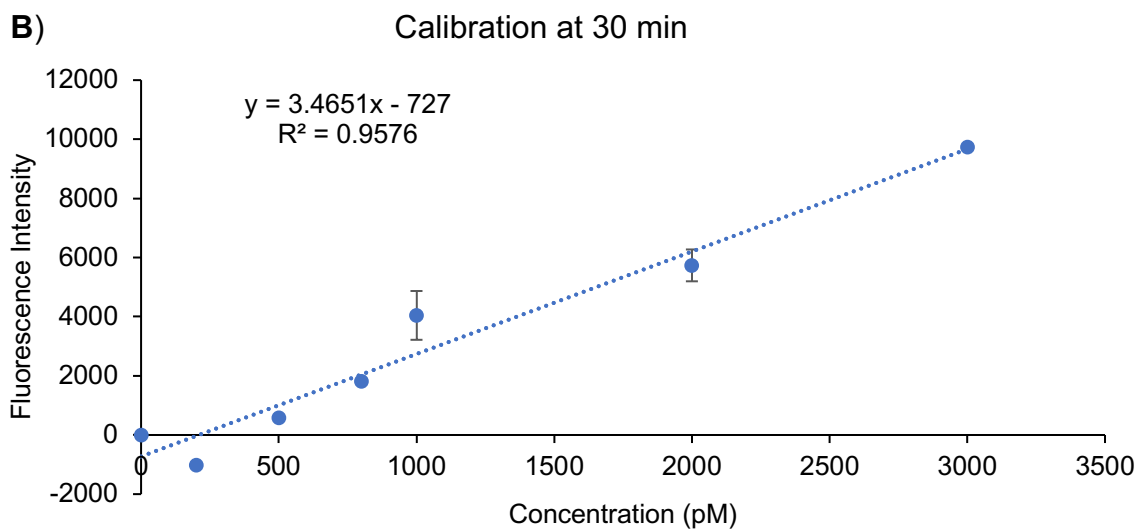
Figures 4.7 A) - C) Real-time fluorescence monitoring of reactions of the optimized BINDA-HCR technique detecting various concentrations of SA (A). Each curve is an average of triplicate reactions. Calibration curves of the fluorescence intensity at 30 min (B) and 120 (C) were made. Error bars represent the standard deviation from triplicate reactions.

4.3.6 Tolerance of increased reaction temperature

To determine if an increased reaction temperature inhibited the detection of SA using BINDA-HCR, an increased reaction temperature was tested using various concentrations of SA. Figure 4.8 shows an increase in overall fluorescent intensities in addition to the blank signal when the reaction temperature was 30°C. The increase in temperature may have increased the speed of the reaction by accelerating hairpin stem opening. Additionally, the increase in background may be due to an increased rate in base breathing of the hairpins. Base breathing could allow the invasion of other hairpins, leading to spurious initiation of the reaction in the absence of the protein target. Despite the increase in background, the overall reaction trend was similar to the reaction at 23°C in that the reaction maintained a dose dependent increase in response to SA. Because the lowest concentration of 200 pM was still discernible from the blank, these results suggest that the reaction could thus tolerate an increase in temperature from 23°C to 30°C.
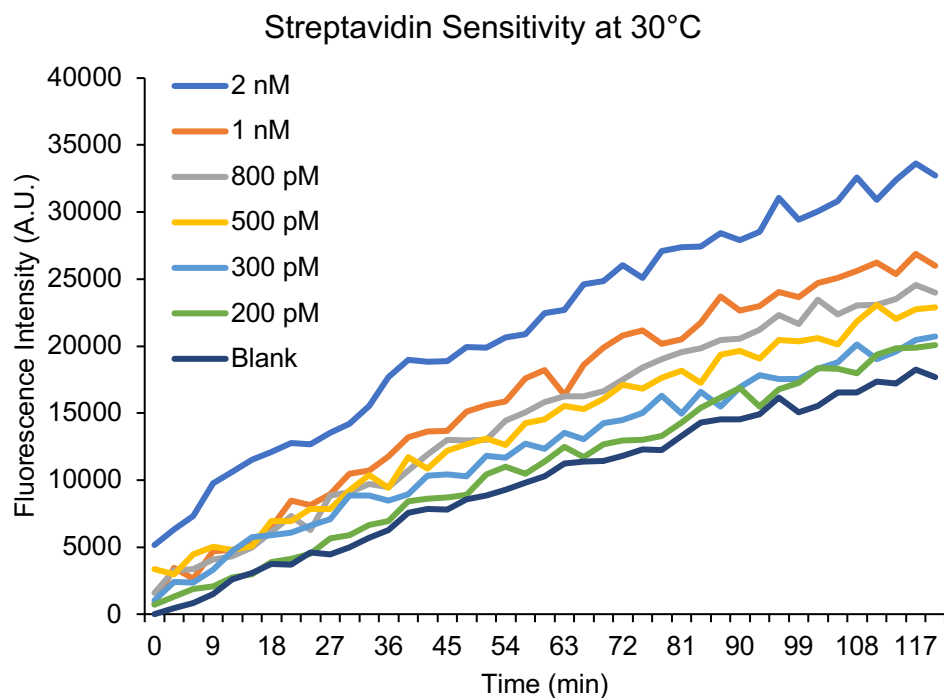
Figure 4.8 Real-time fluorescence monitoring of reactions of the optimized BINDA-HCR system detecting various concentrations of SA at a reaction temperature of 30°C instead of 23°C. Each curve is an average of triplicate reactions.

4.3.7 Detection of HER2 on cells

To demonstrate the applicability of the BINDA-HCR technique, I applied BINDA-HCR to the detection of HER2 on cell surfaces by conjugating biotinylated anti-HER2 antibody to the BINDA probes. When the BINDA probes bound to one or adjacent HER2 proteins on cell surfaces, **init** was formed (Figure 4.9). The formation of **init** initiated the HCR reaction and the concatemer was detected using strand displacement beacons. The fluorescence produced from the reaction was localized to the cell surface because the concatemer that formed was anchored onto the cell surface through the initiation by BINDA probes (Figure 4.10). Because the two strand displacement beacons used different DNA sequences, the sensitivity of the reaction could be increased by conjugating both **F1** and **F2** to the same type of fluorescent dye (e.g., both FAM fluorescein dyes), or the specificity of the reaction could be increased by conjugating **F1** and **F2** to two different types (e.g. Cy5 cyanine dye and FAM fluorescein dye).

The cell lines used, SK-BR-3 (HER2+) and MDA-MB-231 (triple negative), are both adherent epithelial cell lines from breast cancer patients. For the detection of the HER2 protein, about 30 000 cells were seeded into each well of chambered glass slides and allowed to grow for at least one doubling time for each cell line. Estimating that one doubling time elapsed at the time of analysis for both cell lines and not accounting for cell death, there were about 60 000 cells in each well at the time of detection. The morphology of both cell lines was also important to note when detecting transmembrane proteins such as HER2. If the BINDA-HCR technique is working effectively, fluorescence signal should be localized to the membrane while retaining the cell's membrane shape. The morphology of SK-BR-3 was round and cuboidal and the morphology of MDA-MB-231 was elongated and spindle-like.
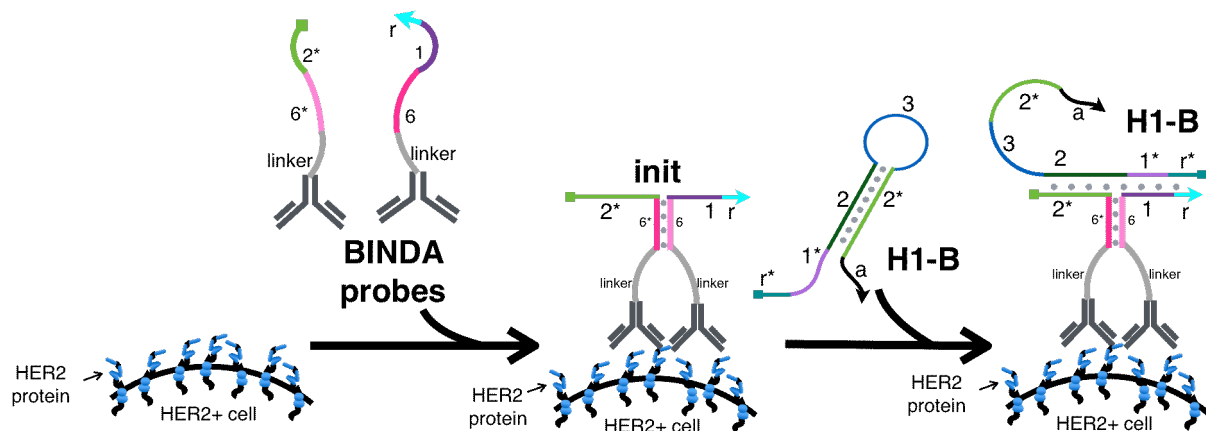
Figure 4.9 Schematic of the BINDA probes forming **init** and opening **H1-B**. BINDA probes could only hybridize together when co-localized by binding to a single or two adjacent HER2 molecule(s). Hybridization of the two probes together via the domains **6-6*** created the strand, **init**, consisting of **1** and **2***. **H1-B** could hybridize to **init**, initiating HCR. Antibodies were linked to DNA oligos using biotin-SA linker (not shown).
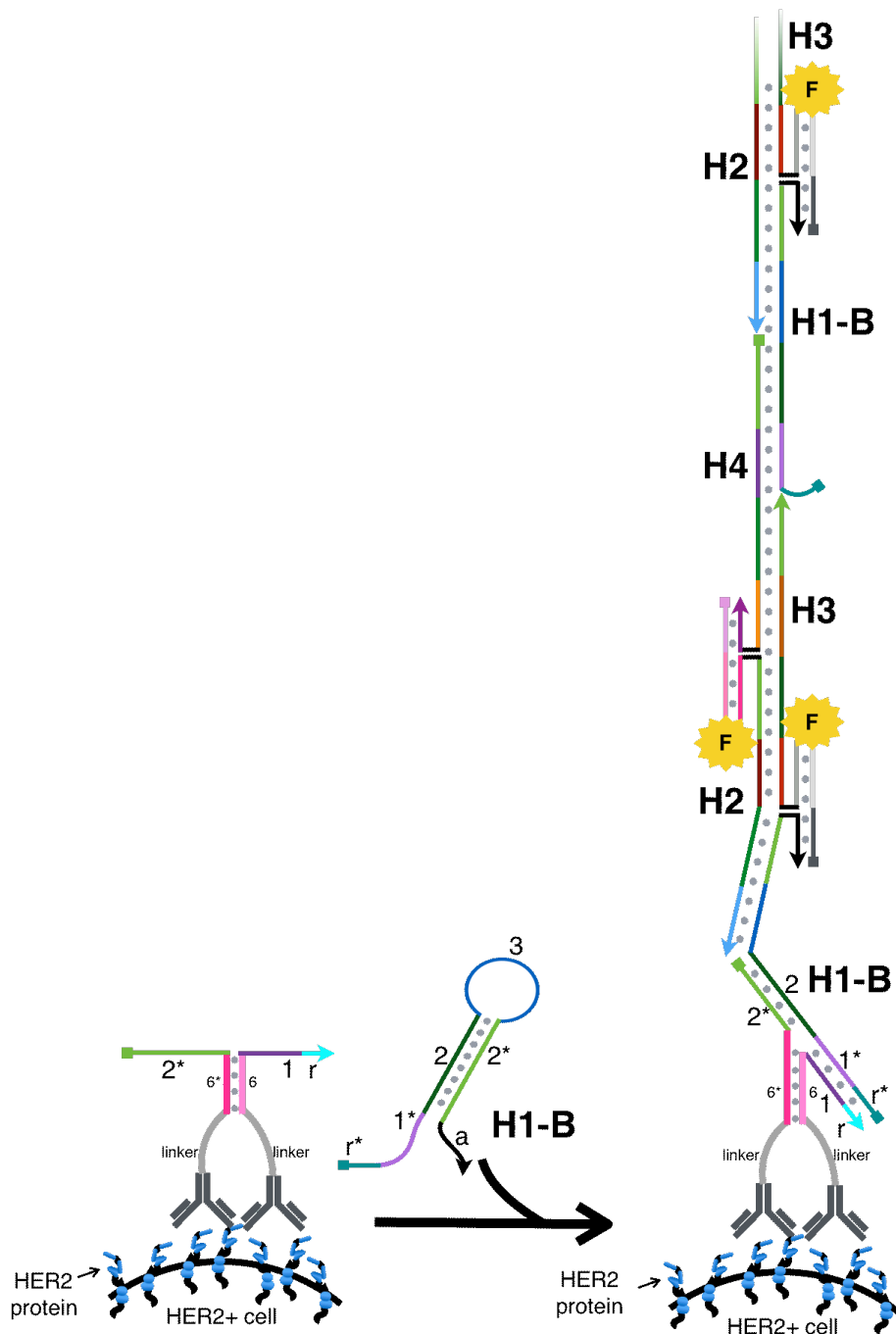
Figure 4.10 Schematic of BINDA-HCR for the detection of HER2 protein on HER2+ cells. HCR concatemers are anchored onto the HER2+ cell surface through the BINDA. Fluorophores retained on the concatemer provide amplified, localized fluorescence. The **r** domain on **H1-B** molecules that were not bound to the BINDA probes but contributed in growing the concatemer remained unbound and single stranded within the concatemer.

4.3.7.1 Fluorescence production using one fluorophore dye

BINDA-HCR was applied to the detection of HER2 protein on HER2+ cell line, SK-BR-3 for

end point fluorescence detection at room temperature. One hour after adding BINDA-HCR and

DAPI nuclear stain to the cells, the cells were imaged on a confocal fluorescence microscope

using Differential Interference Contrast (DIC) and fluorescence channels. Both **F1** and **F2** of

SDB 1 and **SDB 2**, respectively, were conjugated to Cy5 cyanine dye and imaged, shown in

Figure 4.11A or to FAM fluorescein dye and imaged, shown in Figure 4.12B. In both Figures

4.11A and 4.11B, the red Cy5 or green FAM fluorescence produced from the concatemer was

distinct and clearly could be observed on the cell membranes. Cell membranes were visible

using Differential Interference Contrast (DIC). The fluorescence images were taken at a 0.5 μm

slice in a Z-stack at the height of 12 μm and thus all not all cell membranes may be visible in the

field.
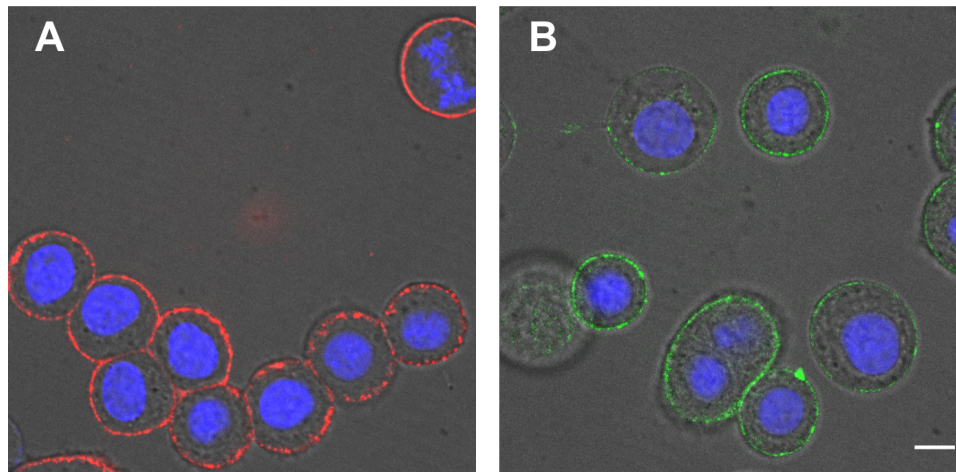
Figure 4.11 Fluorescence imaging of red Cy5 membrane fluorescence (A) and green FAM
membrane fluorescence (B) as a result of BINDA-HCR concatemers on SK-BR-3 cells. The
scale bar is 10 μm.

4.3.7.2 Fluorescence production using two fluorophore dyes

An advantage to BINDA-HCR is the use of two strand displacement beacons for the real-time detection of the concatemer. Two strand displacement beacons allowed the combination of two of the same type or two different types of fluorophores. When both **F1** of **SDB 1** and **F2** of **SDB 2** were conjugated to one type of fluorophore as opposed to two different fluorophores (Section 4.3.7.1), the fluorescence intensity would be increased and therefore the sensitivity of the detection method may be relatively improved. However, when **F1** and **F2** were conjugated to two different types of fluorophores, insight into the specificity of the fluorescence signal could be inferred because the fluorescence of both types of fluorophores would be required to indicate the presence of the concatemer. Figure 4.12 shows end point fluorescence after incubating BINDA-HCR with SK-BR-3 cells at room temperature for one hour using both Cy5 and FAM fluorophores. Row A of Figure 4.12 shows the resulting image of a reaction where **F1** of **SDB 1** was conjugated to Cy5 (red) and **F2** of **SDB 2** was conjugated to FAM (green). Row B shows the resulting image of a reaction where **F1** of **SDB 1** was conjugated to FAM (green) and **F2** of **SDB 2** was conjugated to Cy5 (red). Each column shows the fluorescence channels for FAM in the first, Cy5 in the second, and both FAM and Cy5 channels merged together in the last. Both FAM and Cy5 fluorescence could be seen when using the respective channels with no observable differences when either fluorophore was conjugated to **F1** or **F2**. These results indicate the specificity of BINDA-HCR because the same cluster of cells were imaged using both Cy5 and FAM fluorophore channels separately first, showing that the fluorescence of both fluorophores were localized to cell membranes. This is further evidenced by merging both fluorescence channels where the yellow colour indicates that both Cy5 and FAM fluorophores were in the same locations (i.e., both located on the same concatemers).
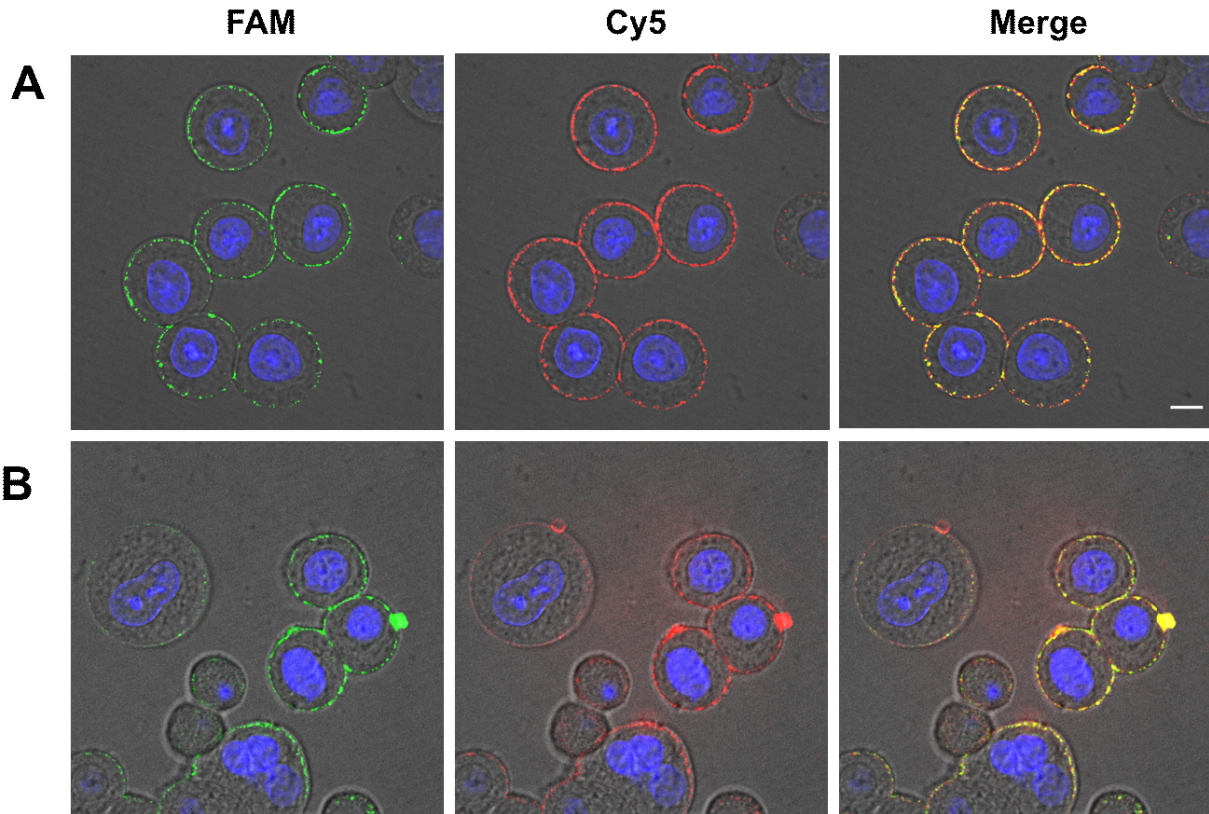
Figure 4.12 Cell imaging using DIC and DAPI channels of HER2 on two groups of SK-BR-3 cells, shown in rows A and B. Row A used **F1** conjugated to FAM and **F2** conjugated to Cy5. Row B used **F1** conjugated to Cy5 and **F2** conjugated to FAM. Fluorescence detection was split into channels in the columns as labeled. In addition to the DIC and DAPI channels, the first column shows group A and B cells with FAM, the second column with Cy5, and the last column with merged FAM and Cy5 channels. The scale bar is 10 µm.

4.3.7.3 Real-time fluorescence detection

To demonstrate real-time detection of growing concatemers on cell membranes I imaged SK-BR-3 cells from the point of applying BINDA-HCR and DAPI nuclear stain at 0 min and at various time intervals up to 60 min (Figure 4.13). Each row shows images at the specific time points and each column shows the DIC, DAPI, Cy5, and merged channels. Both **F1** and **F2** were conjugated to Cy5. The increasing intensity of the blue DAPI nuclear stain demonstrate the passage of time as the stain was entering the nucleus of the cells. Red fluorescence due to Cy5 could faintly be seen on cell membranes in as soon as 5 min, with obvious membrane fluorescence at about 45 to 60 min. The increase in Cy5 fluorescence intensity on the cell membranes over time indicates that the concatemers were growing, displacing the strand displacement beacons, and retaining the fluorophores for localized detection.
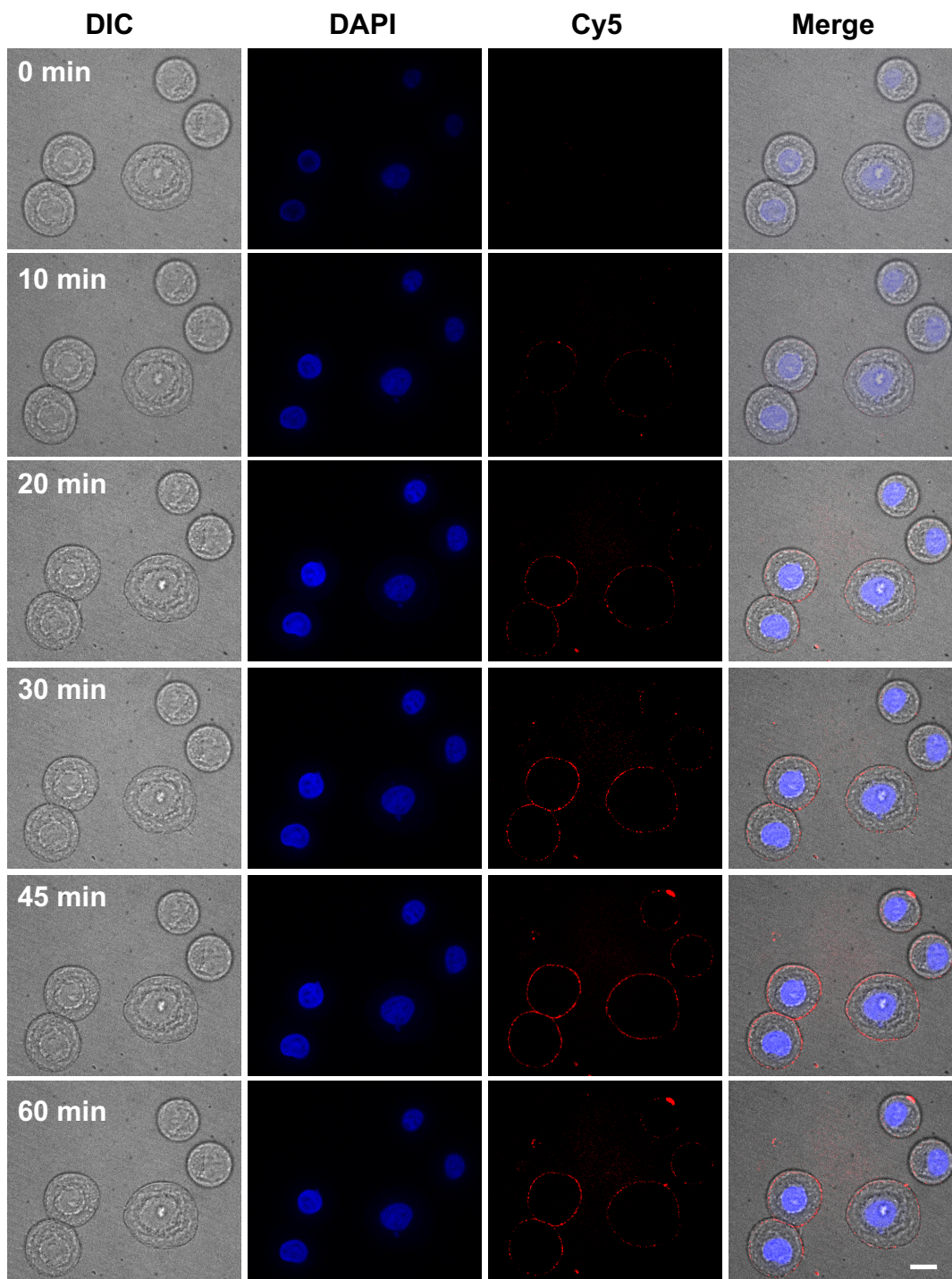
Figure 4.13 Timed fluorescence monitoring of BINDA-HCR on SK-BR-3 cells where each row shows snapshots at time 0 min to 60 min from the point of mastermix addition and columns show each imaging channel separated (labeled as DIC for the channel only showing differential

interference contrast microscopy, DAPI for the channel only showing DAPI nuclear stain fluorescence, Cy5 for the channel only showing Cy5 fluorescence, and Merge showing DIC, DAPI, and Cy5 channels combined and overlaid. The scale bar is 10 μm.

4.3.7.4 Negative controls and clinical specificity

To demonstrate the requirement of all the components in the BINDA-HCR technique for the formation of the concatemer, I tested various negative controls on SK-BR-3. Figures 4.14A-D show the lack of fluorescence from omitting one or more components from the technique. Figure 4.14A shows the omittance of BINDA probe **L**, 4.14B shows the omittance of BINDA probe **R**, 4.14C shows the omittance of **H1-B**, and 4.14D shows the omittance of both **SDB 1** and **SDB 2**. DIC, DAPI, Cy5 and FAM fluorescence channels were all imaged in the panels of Figure 4.14; however, no membrane fluorescence was observed. These results show that all components of BINDA-HCR were necessary for the generation of membrane fluorescence. The concatemer cannot be produced in the absence of either BINDA probe, indicating that the binding of HER2 protein on cell surfaces initiated the reaction. The absence of **H1-B** inhibited the formation of the concatemer demonstrating that the concatemer was required for the displacement of **SDB 1** and **SDB 2** to produce fluorescence. Lastly, the absence of both strand displacement beacons produced no fluorescence, indicating that the fluorescence observed on cell membranes did not arise from the sample itself. In summary, these results show that BINDA-HCR was responsible for the production of fluorescence on cell surfaces in response to an overexpression of the HER2 protein on cell surfaces.
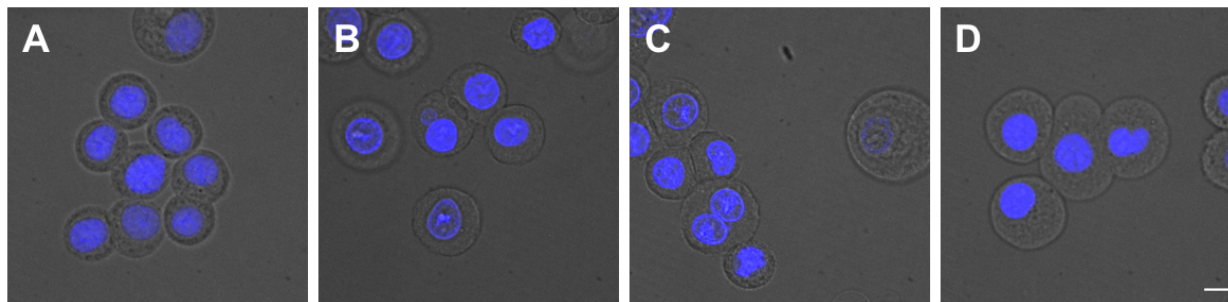
Figure 4.14 Confocal imaging of SK-BR-3 cells using BINDA-HCR with different experimental conditions where in (A) **L** probe was omitted, (B) **R** probe was omitted, (C) **H1-B** omitted, and (D) **SDB 1** and **SDB 2** were omitted. The scale bar is 10 µm.

To test the clinical specificity of the BINDA-HCR technique, triple negative breast cancer cell line, MDA-MB-231 was used. Using the same protocol that was used for the application to SK-BR-3 cells, I applied BINDA-HCR to live MDA-MB-231 cells to determine and imaged the cells at 60 min and 120 min. Figure 4.15 shows the resulting images 120 min after applying BINDA-HCR to the cells. In Figure 4.15, A) shows **F1** and **F2** conjugated to FAM, B) shows **F1** conjugated to FAM and **F2** conjugated to Cy5, C) shows **F1** conjugated to Cy5 and **F2** conjugated to FAM, and D) shows both **F1** and **F2** conjugated to Cy5. With any combination of fluorophores, no membrane fluorescence could be observed. These results suggest that BINDA-HCR could distinguish between HER2+ and HER2- cells and therefore has the potential for clinical use.
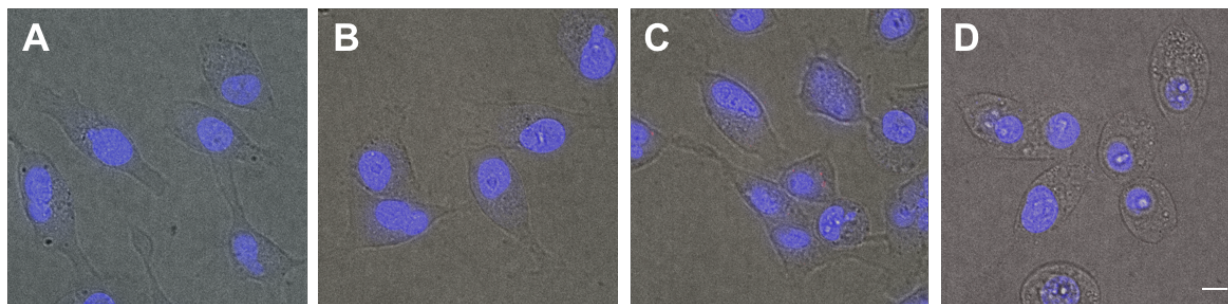
Figure 4.15 Confocal imaging of MDA-MB-231 cells using BINDA-HCR with different experimental conditions where in A) both **F1** and **F2** were conjugated to FAM, B) **F1** was conjugated to FAM and **F2** was conjugated to Cy5, C) **F1** was conjugated to Cy5 and **F2** was conjugated to FAM, and D) both **F1** and **F2** were conjugated to Cy5. The scale bar is 10 μm.

4.3.7.5 Discussion

Both SK-BR-3 and MDA-MB-231 cell lines have HER2 transmembrane protein expression. SK-BR-3 has an increased expression of the HER2 gene product. According to Mclarty et al., the number of HER2 protein molecules on SK-BR-3 is about 1.3 million and the amount on MDA-MB-231 is about 54 000[19]. Although both SK-BR-3 and MDA-MB-231 cell lines express HER2 on cell surfaces, only results from SK-BR-3 cells showed membrane fluorescence in response to the application of BINDA-HCR. These results could indicate two possible events: 1) the fluorescence intensity on MDA-MB-231 was not sufficient to be observed; or 2) the two BINDA probes bind to different, adjacent HER2 molecules (e.g., HER2 protein dimers) on the cell surface as opposed to both BINDA probes binding the same HER2 molecule. If both BINDA probes bound to the same HER2 molecule to form **init**, there could be some fluorescence on MDA-MB-231 cells; however, this was not observed. These results could be explained by the small size of one molecule of extracellular HER2 protein domain (~96.8 kDa)

which may be unable to accommodate two molecules of biotinylated IgG anti-HER2 antibody (~154 kDa) due to steric hindrance. Additionally, the antibody is polyclonal and so the populations of antibody that can bind different epitopes on the HER2 protein could be distributed unevenly. In other words, it may be possible that the population of anti-HER2 antibody used was biased towards one specific epitope on the HER2 protein; which would not easily facilitate one molecule of HER2 accommodating both of the required BINDA probes.

These results are consistent with results from Hildenbrand et al.[20], who showed that HER2 is present in clusters on SK-BR-3 cell membranes. Therefore, it is likely that the BINDA probes were more frequently binding to two adjacent HER2 molecules within these clusters to form **init**, or to HER2 homodimers instead of to two epitopes on a single HER2 molecule.

There are discordant results in the literature on whether HER2 antibodies are internalized when bound to HER2 proteins on cell surfaces. Ram et al.[21] reported that although the number of HER2 protein on the surface of cells decreases when exposed to anti-HER2 antibodies due to cell internalization, the degree to which HER2 is internalized is less on high expressing cells than on low expressing cells. Thus, cells with high levels of HER2 could retain a large amount of HER2 antibody on their surfaces in contrast to low expressing HER2 cell lines. It may be possible that because MDA-MB-231 expresses low amounts of HER2, any antibody bound to HER2 proteins on this low HER2 expressing cell line are internalized and subsequently degraded, inhibiting the formation of **init** and preventing the formation of the concatemer.

4.4 Conclusions

In this chapter, I developed a protein-initiated HCR for localized detection of a cell surface protein. I designed BINDA probes to convert the detection of the protein target into a nucleic acid which initiated HCR for the formation of the concatemer. By using two strand displacement

beacons, the growth of the concatemer was detected using real-time fluorescence and the direct fluorophore labeling of the hairpins was circumvented. I demonstrated the application of the developed BINDA-HCR technique by detecting the upregulation of HER2 protein on live cells. SK-BR-3, HER2+ cells, were successfully detected with membrane-localized fluorescence. MDA-MB-231, triple negative cells, did not yield fluorescence which suggests that this technique has the potential for practical applications.

To further progress this technique toward practical applications, future work may include testing on mid to low expressed HER2 cell lines, testing on fixed cells and tissues, using other affinity ligands such as aptamers, and adapting this technique to the detection of other cell surface proteins. Detecting cells with varying degrees of HER2 expression may better indicate the clinical specificity of the technique and the extent to which a discernible signal can be detected.

BINDA-HCR can also be used for protein-protein interactions. For example, the heterodimerization of HER receptors may be detected using BINDA-HCR because it requires two binding events to produce an anchored, amplified fluorescence signal. In this case, the affinity ligands would be changed to bind to the respective monomers of the heterodimer to be detected and BINDA probe linkers may be adjusted to restrict the detection to only dimerized proteins.

Because this technique relied on antibodies, it may be subject to some of the same difficulties as other methods using antibodies on fixed samples. For example, testing on fixed cells or tissues may require additional steps for adequate detection, such as epitope retrieval, because the fixation can mask antigenic sites.

In conclusion, BINDA-HCR could detect a cell surface protein in less than 60 min at room temperature and achieved isothermal signal amplification. Furthermore, this technique was

technically easy to perform because it did not require the use of enzymes or washing steps and

was performed in a mix-and-read format.

4.4 References

(1)   Fredriksson, S.; Gullberg, M.; Jarvius, J. Protein Detection Using Proximity-Dependent DNA Ligation Assays. *Nat. Biotechnol.* **2002**, *20*, 473–477.

(2)   Schweitzer, B.; Wiltshire, S.; Lambert, J.; O'Malley, S.; Kukanskis, K.; Zhu, Z.; Kingsmore, S. F.; Lizardi, P.; Ward, D. C. Immunoassays with Rolling Circle DNA Amplification: A Versatile Platform for Ultrasensitive Antigen Detection. *Proc. Natl. Acad. Sci.* **2000**, *97*, 10113–10119.

(3)   Duolink® PLA Fluorescence Protocol | Sigma-Aldrich https://www.sigmaaldrich.com/technical-documents/protocols/biology/duolink-fluorescence-user-manual.html#fluorescence (accessed Oct 3, 2019).

(4)   Koos, B.; Cane, G.; Grannas, K.; Löf, L.; Arngården, L.; Heldin, J.; Clausson, C.-M.; Klaesson, A.; Hirvonen, M. K.; de Oliveira, F. M. S.; *et al.* Proximity-Dependent Initiation of Hybridization Chain Reaction. *Nat. Commun.* **2015**, *6*, 7294.

(5)   Choi, J.; Routenberg Love, K.; Gong, Y.; Gierahn, T. M.; Love, J. C. Immuno-Hybridization Chain Reaction for Enhancing Detection of Individual Cytokine-Secreting Human Peripheral Mononuclear Cells. *Anal. Chem.* **2011**, *83*, 6890–6895.

(6)   Zhang, H.; Li, F.; Li, X.-F.; Le, X. C. Yoctomole Detection of Proteins Using Solid Phase Binding-Induced DNA Assembly. *Methods* **2013**, *64*, 322–330.

(7)   Zhang, H.; Li, X.-F.; Le, X. C. Binding-Induced DNA Assembly and Its Application to Yoctomole Detection of Proteins. *Anal. Chem.* **2012**, *84*, 877–884.

(8)   Zhang, H.; Li, F.; Dever, B.; Li, X.-F.; Le, X. C. DNA-Mediated Homogeneous Binding Assays for Nucleic Acids and Proteins. *Chem. Rev.* **2013**, *113*, 2812–2841.

(9)   Zhang, H.; Li, F.; Dever, B.; Wang, C.; Li, X.-F.; Le, X. C. Assembling DNA through Affinity Binding to Achieve Ultrasensitive Protein Detection. *Angew. Chem. Int. Ed.*

Engl. **2013**, *52*, 10698–10705.

(10)   Zhang, H.; Lai, M.; Zuehlke, A.; Peng, H.; Li, X. F.; Le, X. C. Binding-Induced DNA

Nanomachines Triggered by Proteins and Nucleic Acids. *Angew. Chem. Int. Ed. Engl.*

2015, *54*, 14326–14330.

(11)   Peng, H.; Li, X.-F.; Zhang, H.; Le, X. C. A MicroRNA-Initiated DNAzyme Motor

Operating in Living Cells. *Nat. Commun.* **2017**, *8*, 14378.

(12)   Li, F.; Zhang, H.; Wang, Z.; Li, X.; Li, X. F.; Le, X. C. Dynamic DNA Assemblies

Mediated by Binding-Induced DNA Strand Displacement. *J. Am. Chem. Soc.* **2013**, *135*,

2443–2446.

(13)   Green, N. M. Avidin. In *Advances in Protein Chemistry*; Academic Press, 1975; Vol. 29,

pp. 85–133.

(14)   Buckland, R. M. Strong Signals from Streptavidin-Biotin. *Nature* **1986**, *320*, 557–558.

(15)   Sabir, T.; Toulmin, A.; Ma, L.; Jones, A. C.; McGlynn, P.; Schröder, G. F.; Magennis, S.

W. Branchpoint Expansion in a Fully Complementary Three-Way DNA Junction. *J. Am.*

Chem. Soc. **2012**, *134*, 6280–6285.

(16)   Di Gioia, D.; Dresse, M.; Mayr, D.; Nagel, D.; Heinemann, V.; Kahlert, S.; Stieber, P.

Serum HER2 Supports HER2-Testing in Tissue at the Time of Primary Diagnosis of

Breast Cancer. *Clin. Chim. Acta.* **2014**, *430*, 86–91.

(17)   Petersen, E. R. B.; Sørensen, P. D.; Jakobsen, E. H.; Madsen, J. S.; Brandslund, I. Serum

HER-2 Predicts Response and Resistance to Trastuzumab Treatment in Breast Cancer.

Clin. Chem. Lab. Med. **2013**, *51*, 1483–1492.

(18)   Human ErbB2/Her2 Quantikine ELISA Kit DHER20: R&D Systems

https://www.rndsystems.com/products/human-erbb2-her2-quantikine-elisa-kit_dher20

(accessed Oct 31, 2019).

(19)   Mclarty, K.; Cornelissen, B.; Scollard, D. A.; Done, S. J.; Chun, K.; Reilly, R. M. Associations between the Uptake of 111 In-DTPA-Trastuzumab , HER2 Density and Response to Trastuzumab (Herceptin) in Athymic Mice Bearing Subcutaneous Human Tumour Xenografts. *Eur. J. Nucl. Med. Mol. Imaging* **2009**, *36*, 81–93.

(20)   Hildenbrand, G.; Cremer, C.; Müller, P.; Kaufmann, R.; Hausmann, M. Analysis of Her2/Neu Membrane Protein Clusters in Different Types of Breast Cancer Cells Using Localization Microscopy. *J. Microsc.* **2010**, *242*, 46–54.

(21)   Ram, S.; Kim, D.; Ober, R. J.; Ward, E. S. The Level of HER2 Expression Is a Predictor of Antibody-HER2 Trafficking Behavior in Cancer Cells. *mAbs* **2014**, *6*, 1211–1219.

Chapter Five: Conclusions

The introduction and development of novel analytical techniques are vital for continuous improvements in laboratory medicine and can contribute to maintaining best practice of healthcare[1–3]. Recent developments in the use of nucleic acid amplification for analytical techniques have expanded the range of applications and simplified existing applications[4–9].

ASSURED criteria, established by the World Health Organization, are a set of recommendations for emerging diagnostic tests[10,11]. ASSURED is an acronym for affordable, sensitive, specific, user-friendly, robust and rapid, equipment-free, and deliverable to end users. Novel strategies using DNA to enable isothermal amplification of signals for the detection of biomarkers frequently fulfill some or all of the ASSURED criteria. These strategies use the rational design of DNA to facilitate amplified detection of biomolecules. The use of DNA to build these assays can confer improved reagent stability and potentially reduce cost because DNA is relatively inexpensive to synthesize[5,12,13]. Other features of isothermal DNA amplification strategies are also compatible for the development of assays in alignment with the ASSURED criteria. First, signal amplification can maintain or improve the sensitivity of biomarker detection. Second, isothermal reaction conditions enable the reaction to be run at a single temperature, which reduces the requirements for instrumentation and can simplify technical protocols. Third, the small volumes (microlitre) used in these emerging strategies are suitable for applications using microfluidic devices. The use of microfluidic devices would simplify the delivery to users and therefore is an asset in point-of-care assays or testing in resource-limited settings[14,15]. The novel assays that I have developed use low reaction volumes, isothermal conditions, and the rational design of DNA for signal amplification. My developed

techniques offer novel strategies that are a step towards fulfilling the ASSURED criteria for the improvement of clinical testing.

In Chapter 2, I focused on the development of an isothermal and exponential amplification technique, **BEAR**, using only a single enzyme and primer for the detection of a nucleic acid target. **BEAR** achieved a limit of detection of 10 fM and a recovery of ~91% in cell lysate for a 21-nt sequence of a mitochondrial DNA mutation corresponding to MERRF. The strategy of **BEAR** may be particularly useful for applications in detecting short length targets. Examples of short-length nucleic acid targets includes various types of miRNA. The emergence of miRNA targets as a cancer biomarker available in multiple clinical sample types further necessitates the production of novel detection strategies capable of detecting short length targets[16–20] and may be a potential future application for **BEAR**.

In Chapter 3, I focused on the development of an HCR technique using label-free hairpins to generate real-time turn-on fluorescence for the detection of a nucleic acid target. The use of strand displacement beacons can circumvent the direct labeling of the hairpins, reducing synthesis costs. Conventional HCR uses two hairpins which when using strand displacement beacons, could introduce high background fluorescence. To accommodate the use of strand displacement beacons to detect the production and growth of HCR concatemers, I designed a four hairpin HCR. When using 50 nM hairpins, the developed technique achieved a limit of detection of 660 pM in solution for a nucleic acid target in 30 min at room temperature. This technique offers an enzyme-free strategy for amplified turn-on fluorescence without using labeled hairpins and can be coupled to other techniques or adapted for the detection of other targets.

Lastly, in Chapter 4, I focused on the development of an HCR initiated by protein detection using BINDA probes for localized and amplified detection of proteins. In order to use the detection of the protein target to initiate HCR, I split the sequence of an initiating nucleic acid onto two BINDA probes where binding of both the probes to a protein target produced the complete nucleic acid sequence. The completed nucleic acid sequence initiated the four-hairpin HCR, detected using turn-on fluorescence. I detected HER2 protein on cell membranes by adapting the affinity ligand on the BINDA probes to anti-HER2 antibodies. I applied the technique onto adherent breast cancer epithelial cell lines, SK-BR-3 (HER2+) and MDA-MB-231 (triple negative) and membrane fluorescence signals were produced at room temperature in as soon as 5 min with strong signals at 45 min on HER2+ cells. The use of BINDA probes and kinetically trapped hairpins that can only assemble in the presence of the target circumvents the use of washing steps and enzymes for amplified detection signals. Furthermore, the growth of the concatemers on cell surfaces produce localized fluorescent signals. This developed technique uses an easy-to-perform and fast protocol for localized protein imaging and is a potential alternative to immunostaining. Future work can include the adaptation of the affinity ligands from antibody to aptamer to further reduce cost because DNA is inexpensive to synthesize relative to that of antibodies. Furthermore, changing the affinity ligand can provide localized imaging to surface proteins other than HER2.

Features common to all three of my developed techniques include isothermal conditions, low reaction volumes, and modular DNA designs. Isothermal conditions, the reduction of the number of enzymes required, and low reaction volumes simplify technical protocols. The modularity of my DNA designs allows the adaptation to detecting other targets. Although my overall aim was to improve laboratory processes for clinical settings, research laboratories or the

food industry[21] can also benefit from these novel amplification detection strategies for the detection of targets other than biomarkers.

Limitations to my techniques and other emerging technologies include background signal generation and dependence on the availability of strongly binding affinity ligands. Exponential amplification techniques, including **BEAR**, are susceptible to generating exponentially amplified background. Chapter 2 discussed the sources of background for **BEAR** specifically and steps taken to minimize its effect on the sensitivity of the technique. Although linear amplification techniques, including the developed four-hairpin HCR, do not require any enzymes, they are limited in slower rates of amplification relative to exponential amplification strategies. DNA amplification techniques that aim to detect proteins, including BINDA-HCR, require affinity ligands and are therefore subject to the limitations of those affinity ligands. For example, the detection of HER2, discussed in Chapter 4, relied on the availability, affinity, and specificity of anti-HER2 antibodies. The emergence of aptamers expanded the availability of affinity ligands; however, ongoing research is required to further discover aptamers for more targets[22]. Despite these challenges, exciting new advancements in the development of isothermal DNA amplification techniques[23] offer researchers, laboratorians, and clinicians a wider toolbox for detection strategies that can contribute to the continuous improvement of clinical laboratory medicine.

References

(1)   Sturgeon, C.; Hill, R.; Hortin, G. L.; Thompson, D. Taking a New Biomarker into Routine Use - A Perspective from the Routine Clinical Biochemistry Laboratory. *Proteomics Clin. Appl.* **2010**, *4*, 892–903.

(2)   Bossuyt, X.; Verweire, K.; Blanckaert, N. Laboratory Medicine: Challenges and Opportunities. *Clin. Chem.* **2007**, *53*, 1730–1733.

(3)   Rifai, N.; Diamandis, E. P.; Lo, Y. M. D.; Kricka, L. J.; Wilding, P.; Ladenson, J. H.; Wittwer, C. T. Advancing Laboratory Medicine through Innovation: A Tale of Six Inventors. *Clin. Chem.* **2012**, *58*, 502–510.

(4)   Lee, S. H.; Park, S. min; Kim, B. N.; Kwon, O. S.; Rho, W. Y.; Jun, B. H. Emerging Ultrafast Nucleic Acid Amplification Technologies for Next-Generation Molecular Diagnostics. *Biosens. Bioelectron.* **2019**, *141*, 111448.

(5)   Jung, C.; Ellington, A. D. Diagnostic Applications of Nucleic Acid Circuits. *Acc. Chem. Res.* **2014**, *47*, 1825–1835.

(6)   Li, J.; Lin, L.; Yu, J.; Zhai, S.; Liu, G.; Tian, L. Fabrication and Biomedical Applications of "Polymer-like" Nucleic Acids Enzymatically Produced by Rolling Circle Amplification. *ACS Appl. Bio Mater.* **2019**, *2*, 4106–4120.

(7)   Qi, H.; Yue, S.; Bi, S.; Ding, C.; Song, W. Isothermal Exponential Amplification Techniques: From Basic Principles to Applications in Electrochemical Biosensors. *Biosens. Bioelectron.* **2018**, *110*, 207–217.

(8)   Yan, L.; Zhou, J.; Zheng, Y.; Gamson, A. S.; Roembke, B. T.; Nakayama, S.; Sintim, H. O. Isothermal Amplified Detection of DNA and RNA. *Mol. Biosyst.* **2014**, *10*, 970–1003.

(9)   Zhang, D. Y.; Seelig, G. Dynamic DNA Nanotechnology Using Strand-Displacement

Reactions. *Nat. Chem.* **2011**, *3*, 103–113.

(10)   Peeling, R. W.; Holmes, K. K.; Mabey, D.; Ronald, A. Rapid Tests for Sexually

Transmitted Infections (STIs): The Way Forward. *Sex. Transm. Infect.* **2006**, *82*, v1–v6.

(11)   Mashamba-Thompson, T.; Jama, N.; Sartorius, B.; Drain, P.; Thompson, R.

Implementation of Point-of-Care Diagnostics in Rural Primary Healthcare Clinics in

South Africa: Perspectives of Key Stakeholders. *Diagnostics* **2017**, *7*, 3.

(12)   Van Ness, J.; Van Ness, L. K.; Galas, D. J. Isothermal Reactions for the Amplification of

Oligonucleotides. *Proc. Natl. Acad. Sci. U. S. A.* **2003**, *100*, 4504–4509.

(13)   Zhang, D. Y.; Winfree, E. Robustness and Modularity Properties of a Non-Covalent DNA

Catalytic Reaction. *Nucleic Acids Res.* **2010**, *38*, 4182–4197.

(14)   Zanoli, L. M.; Spoto, G. Isothermal Amplification Methods for the Detection of Nucleic

Acids in Microfluidic Devices. *Biosensors* **2013**, *3*, 18–43.

(15)   Zhao, Y.; Chen, F.; Li, Q.; Wang, L.; Fan, C. Isothermal Amplification of Nucleic Acids.

Chem. Rev. **2015**, *115*, 12491–12545.

(16)   Dong, H.; Lei, J.; Ding, L.; Wen, Y.; Ju, H.; Zhang, X. MicroRNA: Function, Detection,

and Bioanalysis. *Chem. Rev.* **2013**, *113*, 6207–6233.

(17)   Shen, J.; Stass, S. A.; Jiang, F. MicroRNAs as Potential Biomarkers in Human Solid

Tumors. *Cancer Lett.* **2013**, *329*, 125–136.

(18)   Deng, R.; Zhang, K.; Li, J. Isothermal Amplification for MicroRNA Detection: From the

Test Tube to the Cell. *Acc. Chem. Res.* **2017**, *50*, 1059–1068.

(19)   Kosaka, N.; Iguchi, H.; Ochiya, T. Circulating MicroRNA in Body Fluid: A New

Potential Biomarker for Cancer Diagnosis and Prognosis. *Cancer Sci.* **2010**, *101*, 2087–

2092.

(20)   Wang, G.-K.; Zhu, J.-Q.; Zhang, J.-T.; Li, Q.; Li, Y.; He, J.; Qin, Y.-W.; Jing, Q. Circulating MicroRNA: A Novel Potential Biomarker for Early Diagnosis of Acute Myocardial Infarction in Humans. *Eur. Heart J.* **2010**, *31*, 659–666.

(21)   Böhme, K.; Calo-Mata, P.; Barros-Velázquez, J.; Ortea, I. Review of Recent DNA-Based Methods for Main Food-Authentication Topics. *J. Agric. Food Chem.* **2019**, *67*, 3854– 3864.

(22)   Li, F.; Zhang, H.; Wang, Z.; Newbigging, A. M.; Reid, M. S.; Li, X. F.; Le, X. C. Aptamers Facilitating Amplified Detection of Biomolecules. *Anal. Chem.* **2015**, *87*, 274– 292.

(23)   Gines, G.; Menezes, R.; Xiao, W.; Rondelez, Y.; Taly, V. Emerging Isothermal Amplification Technologies for MicroRNA Biosensing: Applications to Liquid Biopsies. *Mol. Aspects Med.* **2019**, pre-print.

Bibliography

Ali, M Monsur, Feng Li, Zhiqing Zhang, Kaixiang Zhang, Dong-Ku Kang, James Ankrum, X.
Chris Le, and Weian Zhao. 2014b. "Rolling Circle Amplification: A Versatile Tool for
Chemical Biology, Materials Science and Medicine." *Chemical Society Reviews* 43 (10):
3324–41. https://doi.org/10.1039/c3cs60439j.

Altona, Cornelis, Jeroen A. Pikkemaat, and Franc J.J. Overmars. 1996. "Three-Way and Four-
Way Junctions in DNA: A Conformational Viewpoint." *Current Opinion in Structural
Biology* 6 (3): 305–16. https://doi.org/10.1016/S0959-440X(96)80048-0.

Ang, Yan Shan, and Lin-Yue Lanry Yung. 2016. "Rational Design of Hybridization Chain
Reaction Monomers for Robust Signal Amplification." *Chemical Communications* 52 (22):
4219–22. https://doi.org/10.1039/C5CC08907G.

Bi, Sai, Shuzhen Yue, and Shusheng Zhang. 2017. "Hybridization Chain Reaction: A Versatile
Molecular Tool for Biosensing, Bioimaging, and Biomedicine." *Chemical Society Reviews*
46 (14): 4281–98. https://doi.org/10.1039/C7CS00055C.

Böhme, Karola, Pilar Calo-Mata, Jorge Barros-Velázquez, and Ignacio Ortea. 2019. "Review of
Recent DNA-Based Methods for Main Food-Authentication Topics." *Journal of
Agricultural and Food Chemistry* 67 (14): 3854–64.
https://doi.org/10.1021/acs.jafc.8b07016.

Bossuyt, Xavier, Kurt Verweire, and Norbert Blanckaert. 2007. "Laboratory Medicine:
Challenges and Opportunities." *Clinical Chemistry* 53 (10): 1730–33.
https://doi.org/10.1373/clinchem.2007.093989.

Buckland, R. M. 1986. "Strong Signals from Streptavidin-Biotin." *Nature* 320 (6062): 557–58.
https://doi.org/10.1038/320557a0.

Chang, Chia Chen, Chie Pein Chen, Chen Yu Chen, and Chii Wann Lin. 2016. "DNA Base-

Stacking Assay Utilizing Catalytic Hairpin Assembly-Induced Gold Nanoparticle
Aggregation for Colorimetric Protein Sensing." *Chemical Communications* 52 (22): 4167–
70. https://doi.org/10.1039/c6cc01238h.

Chen, Ying-Xu, Ke-Jing Huang, Liu-Lu He, Yi-Han Wang. 2018. "Tetrahedral DNA probe
coupling with hybridization chain reaction for competitive thrombin aptasensor."
Biosensors and Bioelectronics 100: 274-81.
https://doi.org/10.1016/j.bios.2017.09.022

Choi, Harry M.T., Victor A. Beck, and Niles A. Pierce. 2014. "Next-Generation in Situ
Hybridization Chain Reaction: Higher Gain, Lower Cost, Greater Durability." *ACS Nano* 8
(5): 4284–94. https://doi.org/10.1021/nn405717p.

Choi, Harry M.T., Colby R. Calvert, Naeem Husain, David Huss, Julius C. Barsi, Benjamin E.
Deverman, Ryan C. Hunter, et al. 2016. "Mapping a Multiplexed Zoo of MRNA
Expression." *Development* 143 (19): 3632–37. https://doi.org/10.1242/dev.140137.

Choi, Harry M.T., Joann Y. Chang, Le A. Trinh, Jennifer E. Padilla, Scott E. Fraser, and Niles
A. Pierce. 2010. "Programmable in Situ Amplification for Multiplexed Imaging of MRNA
Expression." *Nature Biotechnology* 28 (11): 1208–12. https://doi.org/10.1038/nbt.1692.

Choi, Harry M.T., Maayan Schwarzkopf, Mark E. Fornace, Aneesh Acharya, Georgios
Artavanis, Johannes Stegmaier, Alexandre Cunha, and Niles A. Pierce. 2018. "Third-
Generation in Situ Hybridization Chain Reaction: Multiplexed, Quantitative, Sensitive,
Versatile, Robust." *Development (Cambridge)* 145 (12): 1–10.
https://doi.org/10.1242/dev.165753.

Choi, Jonghoon, Kerry Routenberg Love, Yuan Gong, Todd M. Gierahn, and J. Christopher
Love. 2011. "Immuno-Hybridization Chain Reaction for Enhancing Detection of Individual
Cytokine-Secreting Human Peripheral Mononuclear Cells." *Analytical Chemistry* 83 (17):

6890–95. https://doi.org/10.1021/ac2013916.

Clegg, Robert M., Annelies Zechel, Carsten Carlberg, Stephan Diekmann, Alastair I.H.
Murchie, and David M.J. Lilley. 1992. "Fluorescence Resonance Energy Transfer Analysis
of the Structure of the Four-Way DNA Junction." *Biochemistry* 31 (20): 4846–56.
https://doi.org/10.1021/bi00135a016.

Compton, J. 1991. "Nucleic Acid Sequence-Based Amplification." *Nature* 350: 273–91.
https://doi.org/10.1385/1-59259-870-6:273.

Connolly, Ashley R., and Matt Trau. 2010. "Isothermal Detection of DNA by Beacon-Assisted
Detection Amplification." *Angewandte Chemie - International Edition* 49 (15): 2720–23.
https://doi.org/10.1002/anie.200906992.

Dai, Shuang, Qingwang Xue, Jing Zhu, Yongshun Ding, Wei Jiang, and Lei Wang. 2014. "An
Ultrasensitive Fluorescence Assay for Protein Detection by Hybridization Chain Reaction-
Based DNA Nanotags." *Biosensors and Bioelectronics* 51: 421–25.
https://doi.org/10.1016/j.bios.2013.07.068.

Deng, Ruijie, Kaixiang Zhang, and Jinghong Li. 2017. "Isothermal Amplification for
MicroRNA Detection: From the Test Tube to the Cell." *Accounts of Chemical Research* 50
(4): 1059–68. https://doi.org/10.1021/acs.accounts.7b00040.

Dirks, Robert M., and Niles A. Pierce. 2004. "Triggered Amplification by Hybridization Chain
Reaction." *Proceedings of the National Academy of Sciences of the United States of
America* 101 (43): 15275–78. https://doi.org/10.1073/pnas.0407024101.

Dong, Haifeng, Jianping Lei, Lin Ding, Yongqiang Wen, Huangxian Ju, and Xueji Zhang. 2013.
"MicroRNA: Function, Detection, and Bioanalysis." *Chemical Reviews* 113 (8): 6207–33.
https://doi.org/10.1021/cr300362f.

Dong, Jing, Qinfeng Xu, Chen Chen Li, and Chun Yang Zhang. 2019. "Single-Color

Multiplexing by the Integration of High-Resolution Melting Pattern Recognition with

    Loop-Mediated Isothermal Amplification." *Chemical Communications* 55 (17): 2457–60.

    https://doi.org/10.1039/c8cc09741k.

Duckett, D.R., and D.M. Lilley. 1990. "The Three-Way DNA Junction Is a Y-Shaped Molecule

    in Which There Is No Helix-Helix Stacking." *The EMBO Journal* 9 (5): 1659–64.

    https://doi.org/10.1002/j.1460-2075.1990.tb08286.x.

"Duolink® PLA Fluorescence Protocol | Sigma-Aldrich." Accessed October 3, 2019.

    https://www.sigmaaldrich.com/technical-documents/protocols/biology/duolink-

    fluorescence-user-manual.html#fluorescence.

Etzoni, Ruth, Nicole Urban, Scott Ramsey, Martin McIntosh, Stephen Schwartz, Brian Reid,

    Jerald Radich, Garnet Anderson, and Leland Hartwell. 2003. "The Case for Early

    Detection." *Nature Reviews Cancer* 3 (4): 243–52. https://doi.org/10.1038/nrc1041.

Finsterer, J., H. F. Harbo, J. Baets, C. Van Broeckhoven, S. Di Donato, B. Fontaine, P. De

    Jonghe, et al. 2009. "EFNS Guidelines on the Molecular Diagnosis of Mitochondrial

    Disorders." *European Journal of Neurology* 16 (12): 1255–64.

    https://doi.org/10.1111/j.1468-1331.2009.02811.x.

Fredriksson, S, M Gullberg, and J Jarvius. 2002. "Protein Detection Using Proximity-Dependent

    DNA Ligation Assays." *Nature Biotechnology* 20: 473–77. https://doi.org/

    10.1038/nbt0502-473.

Gines, Guillaume, Roberta Menezes, Wenjin Xiao, Yannick Rondelez, and Valerie Taly. 2019.

    "Emerging Isothermal Amplification Technologies for MicroRNA Biosensing:

    Applications to Liquid Biopsies." *Molecular Aspects of Medicine* (pre-print).

    https://doi.org/10.1016/j.mam.2019.11.002.

Gioia, Dorit Di, Marie Dresse, Doris Mayr, Dorothea Nagel, Volker Heinemann, Steffen

Kahlert, and Petra Stieber. 2014. "Serum HER2 Supports HER2-Testing in Tissue at the Time of Primary Diagnosis of Breast Cancer." *Clinica Chimica Acta; International Journal of Clinical Chemistry* 430: 86–91. https://doi.org/10.1016/j.cca.2013.12.036.

Gootenberg, Jonathan S., Omar O. Abudayyeh, Max J. Kellner, Julia Joung, James J. Collins, and Feng Zhang. 2018. "Multiplexed and Portable Nucleic Acid Detection Platform with Cas13, Cas12a, and Csm6." *Science* 360 (6387): 439–44. https://doi.org/10.1126/science.aaq0179.

Gootenberg, Jonathan S., Omar O. Abudayyeh, Jeong Wook Lee, Patrick Essletzbichler, Aaron J. Dy, Julia Joung, Vanessa Verdine, et al. 2017. "Nucleic Acid Detection with CRISPR-Cas13a/C2c2." *Science* 356 (6336): 438–42. https://doi.org/10.1126/science.aam9321.

Green, N. Michael. 1975. "Avidin." *Advances in Protein Chemistry*, 29:85–133. Academic Press. https://doi.org/10.1016/S0065-3233(08)60411-8.

Grossmann, Tom N., Lars Röglin, and Oliver Seitz. 2007. "Triplex Molecular Beacons as Modular Probes for DNA Detection." *Angewandte Chemie - International Edition* 46 (27): 5223–25. https://doi.org/10.1002/anie.200700289.

Guatelli, John C, K M Whitfield, D Y Kwoh, K J Barringer, Douglas D Richman, and T R Gingeras. 1990. "Isothermal, in Vitro Amplification of Nucleic Acids by a Multienzyme Reaction Modeled after Retroviral Replication." *Proceedings of the National Academy of Sciences of the United States of America* 87 (5): 1874–78. https://doi.org/10.1073/pnas.87.5.1874.

Hao, Nan, Pan Pan Dai, Tao Yu, Jing Juan Xu, and Hong Yuan Chen. 2015. "A Dual Target-Recycling Amplification Strategy for Sensitive Detection of MicroRNAs Based on Duplex-Specific Nuclease and Catalytic Hairpin Assembly." *Chemical Communications* 51 (70): 13504–7. https://doi.org/10.1039/c5cc05350a.

He, Dinggeng, Xing He, Xue Yang, and Hung-Wing Li. 2017. "A Smart ZnO@polydopamine-Nucleic Acid Nanosystem for Ultrasensitive Live Cell mRNA Imaging by the Target-Triggered Intracellular Self-Assembly of Active DNAzyme Nanostructures." *Chemical Science* 31: 748. https://doi.org/10.1039/C6SC04633A.

Hildenbrand, G., C. Cremer, P. Müller, R. Kaufmann, and M. Hausmann. 2010. "Analysis of Her2/Neu Membrane Protein Clusters in Different Types of Breast Cancer Cells Using Localization Microscopy." *Journal of Microscopy* 242 (1): 46–54. https://doi.org/10.1111/j.1365-2818.2010.03436.x.

Holland, Robert L. 2016. "What Makes a Good Biomarker?" *Advances in Precision Medicine* 1 (1): 66. https://doi.org/10.18063/apm.2016.01.007.

Huang, Jin, Yanrong Wu, Yan Chen, Zhi Zhu, Xiaohai Yang, Chaoyong James Yang, Kemin Wang, and Weihong Tan. 2011. "Pyrene-Excimer Probes Based on the Hybridization Chain Reaction for the Detection of Nucleic Acids in Complex Biological Fluids." *Angewandte Chemie - International Edition* 50 (2): 401–4. https://doi.org/10.1002/anie.201005375.

Huang, Jun Fu, Na Zhao, Han Qing Xu, Han Xia, Kun Wei, Wei Ling Fu, and Qing Huang. 2016. "Sensitive and Specific Detection of MiRNA Using an Isothermal Exponential Amplification Method Using Fluorescence-Labeled LNA/DNA Chimera Primers." *Analytical and Bioanalytical Chemistry* 408 (26): 7437–46. https://doi.org/10.1007/s00216-016-9829-9.

Huang, Mengqi, Xiaoming Zhou, Huiying Wang, and Da Xing. 2018. "Clustered Regularly Interspaced Short Palindromic Repeats/Cas9 Triggered Isothermal Amplification for Site-Specific Nucleic Acid Detection." *Analytical Chemistry* 90 (3): 2193–2200. https://doi.org/10.1021/acs.analchem.7b04542.

"Human ErbB2/Her2 Quantikine ELISA Kit DHER20: R&D Systems." Accessed October 31, 2019. https://www.rndsystems.com/products/human-erbb2-her2-quantikine-elisa-kit_dher20.

Jiang, Hongxin, Yaping Xu, Lihong Dai, Xiaowei Liu, and Deming Kong. 2018. "Ultrasensitive, Label-Free Detection of T4 Ligase and T4 Polynucleotide Kinase Based on Target-Triggered Hyper-Branched Rolling Circle Amplification." *Sensors and Actuators, B: Chemical* 260: 70–77. https://doi.org/10.1016/j.snb.2017.12.203.

Jiang, Yu, Bingling Li, John N. Milligan, Sanchita Bhadra, and Andrew D. Ellington. 2013. "Real-Time Detection of Isothermal Amplification Reactions with Thermostable Catalytic Hairpin Assembly." *Journal of the American Chemical Society* 135 (20): 7430–33. https://doi.org/10.1021/ja4023978.

Jung, Cheulhee, and Andrew D. Ellington. 2014. "Diagnostic Applications of Nucleic Acid Circuits." *Accounts of Chemical Research* 47 (6): 1825–35. https://doi.org/10.1021/ar500059c.

Kim, Joonyul, and Christopher J Easley. 2011. "Isothermal DNA Amplification in Bioanalysis: Strategies and Applications." *Bioanalysis* 3 (2): 227–39. https://doi.org/10.4155/bio.10.172.

Kishi, Jocelyn Y., Thomas E. Schaus, Nikhil Gopalkrishnan, Feng Xuan, and Peng Yin. 2018. "Programmable Autonomous Synthesis of Single-Stranded DNA." *Nature Chemistry* 10 (2): 155–64. https://doi.org/10.1038/nchem.2872.

Koos, Björn, Gaëlle Cane, Karin Grannas, Liza Löf, Linda Arngården, Johan Heldin, Carl-Magnus Clausson, et al. 2015. "Proximity-Dependent Initiation of Hybridization Chain Reaction." *Nature Communications* 6: 7294. https://doi.org/10.1038/ncomms8294.

Kosaka, Nobuyoshi, Haruhisa Iguchi, and Takahiro Ochiya. 2010. "Circulating MicroRNA in

Body Fluid: A New Potential Biomarker for Cancer Diagnosis and Prognosis." *Cancer Science* 101 (10): 2087–92. https://doi.org/10.1111/j.1349-7006.2010.01650.x.

Kubista, Mikael, José Manuel Andrade, Martin Bengtsson, Amin Forootan, Jiri Jonák, Kristina Lind, Radek Sindelka, et al. 2006. "The Real-Time Polymerase Chain Reaction." *Molecular Aspects of Medicine* 27 (2–3): 95–125. https://doi.org/10.1016/j.mam.2005.12.007.

Lee, Sang Hun, Seung min Park, Brian N. Kim, Oh Seok Kwon, Won Yep Rho, and Bong Hyun Jun. 2019. "Emerging Ultrafast Nucleic Acid Amplification Technologies for Next-Generation Molecular Diagnostics." *Biosensors and Bioelectronics* 141: 111448. https://doi.org/10.1016/j.bios.2019.111448.

Lequin, Rudolf M. 2005. "Enzyme Immunoassay (EIA)/Enzyme-Linked Immunosorbent Assay (ELISA)." *Clinical Chemistry* 51 (12): 2415–18. https://doi.org/10.1373/clinchem.2005.051532.

Li, Dandan, Xinmin Li, Bo Shen, Pu Li, Yuanjiao Chen, Shijia Ding, and Weixian Chen. 2019. "Aptamer Recognition and Proximity-Induced Entropy-Driven Circuit for Enzyme-Free and Rapid Amplified Detection of Platelet-Derived Growth Factor-BB." *Analytica Chimica Acta* 1092: 102–7. https://doi.org/10.1016/j.aca.2019.09.046.

Li, Feng, Yanwen Lin, and X Chris Le. 2013. "Binding-Induced Formation of DNA Three-Way Junctions and Its Application to Protein Detection and DNA Strand Displacement." *Analytical Chemistry* 85 (22): 10835–41. https://doi.org/10.1021/ac402179a.

Li, Feng, Hongquan Zhang, Zhixin Wang, Xukun Li, Xing Fang Li, and X. Chris Le. 2013a. "Dynamic DNA Assemblies Mediated by Binding-Induced DNA Strand Displacement." *Journal of the American Chemical Society* 135 (7): 2443–46. https://doi.org/10.1021/ja311990w.

Li, Feng, Hongquan Zhang, Zhixin Wang, Xukun Li, Xing Fang Li, and X Chris Le. 2013b.
"Dynamic DNA Assemblies Mediated by Binding-Induced DNA Strand Displacement."
Journal of the American Chemical Society 135 (7): 2443–46.
https://doi.org/10.1021/ja311990w.

Li, Feng, Hongquan Zhang, Zhixin Wang, Ashley M. Newbigging, Michael S. Reid, Xing Fang
Li, and X. Chris Le. 2015. "Aptamers Facilitating Amplified Detection of Biomolecules."
Analytical Chemistry 87 (1): 274–92. https://doi.org/10.1021/ac5037236.

Li, Jia, and Joanne Macdonald. 2014. "Advances in Isothermal Amplification: Novel Strategies
Inspired by Biological Processes." *Biosensors and Bioelectronics* 64: 196–211.
https://doi.org/10.1016/j.bios.2014.08.069.

Li, Jianbo, Pinhua Lei, Shijia Ding, Ye Zhang, Jianru Yang, Quan Cheng, and Yurong Yan.
2016. "An Enzyme-Free Surface Plasmon Resonance Biosensor for Real-Time Detecting
MicroRNA Based on Allosteric Effect of Mismatched Catalytic Hairpin Assembly."
Biosensors and Bioelectronics 77: 435–41. https://doi.org/10.1016/j.bios.2015.09.069.

Li, Jing, Daxiu Li, Ruo Yuan, and Yun Xiang. 2017. "Biodegradable MnO2 Nanosheet-
Mediated Signal Amplification in Living Cells Enables Sensitive Detection of Down-
Regulated Intracellular MicroRNA." *ACS Applied Materials and Interfaces* 9 (7): 5717–24.
https://doi.org/10.1021/acsami.6b13073.

Li, Jing, Li Lin, Jiantao Yu, Shiyao Zhai, Guoyuan Liu, and Leilei Tian. 2019. "Fabrication and
Biomedical Applications of 'Polymer-like' Nucleic Acids Enzymatically Produced by
Rolling Circle Amplification." *ACS Applied Bio Materials* 2 (10): 4106–20.
https://doi.org/10.1021/acsabm.9b00622.

Li, Jingying, Shuya Liu, Liqin Sun, Wei Li, Su Yun Zhang, Sheng Yang, Juan Li, and Huang
Hao Yang. 2018. "Amplified Visualization of Protein-Specific Glycosylation in Zebrafish

via Proximity-Induced Hybridization Chain Reaction." *Journal of the American Chemical Society* 140 (48): 16589–95. https://doi.org/10.1021/jacs.8b08442.

Liang, Dehai, Jun Zhang, and Benjamin Chu. 2003. "Study of Ethidium Bromide Effect on DsDNA Separation by Capillary Zone Electrophoresis and Laser Light Scattering." *Electrophoresis* 24 (1920): 3348–55. https://doi.org/10.1002/elps.200305604.

Liao, Xianjiu, Zhenzhong Li, Tingting Peng, Jie Li, Fengying Qin, and Zuliang Huang. 2017. "Ultra-Sensitive Fluorescent Sensor for Intracellular MiRNA Based on Enzyme-Free Signal Amplification with Carbon Nitride Nanosheet as a Carrier." *Luminescence* 32 (8): 1411–16. https://doi.org/10.1002/bio.3338.

Lin, Rui, Qiru Feng, Peng Li, Ping Zhou, Ruiyu Wang, Zhe Liu, Zhiqiang Wang, et al. 2018. "A Hybridization-Chain-Reaction-Based Method for Amplifying Immunosignals." *Nature Methods* 15 (4): 275–78. https://doi.org/10.1038/nmeth.4611.

Liu, Lan, Jin Wen Liu, Han Wu, Xiang Nan Wang, Ru Qin Yu, and Jian Hui Jiang. 2018. "Branched Hybridization Chain Reaction Circuit for Ultrasensitive Localizable Imaging of MRNA in Living Cells." *Analytical Chemistry* 90 (3): 1502–5. https://doi.org/10.1021/acs.analchem.7b04848.

Liu, Pei, Xiaohai Yang, Shan Sun, Qing Wang, Kemin Wang, Jin Huang, Jianbo Liu, and Leiliang He. 2013. "Enzyme-Free Colorimetric Detection of DNA by Using Gold Nanoparticles and Hybridization Chain Reaction Amplification." *Analytical Chemistry* 85 (16): 7689–95. https://doi.org/10.1021/ac4001157.

Liu, Shufeng, Chuanbin Cheng, Hongwei Gong, and Li Wang. 2015. "Programmable Mg($^{2+}$)-Dependent DNAzyme Switch by the Catalytic Hairpin DNA Assembly for Dual-Signal Amplification toward Homogeneous Analysis of Protein and DNA." *Chemical Communications* 51 (34): 7364–67. https://doi.org/10.1039/c5cc01649e.

Lizardi, P M, X Huang, Z Zhu, P Bray-Ward, D C Thomas, and D C Ward. 1998. "Mutation

    Detection and Single-Molecule Counting Using Isothermal Rolling-Circle Amplification."

    Nature Genetics 19 (3): 225–32. https://doi.org/10.1038/898.

Ma, Cuiping, Fuxin Wang, Xiudan Wang, Lingzhi Han, Hao Jing, Heng Zhang, and Chao Shi.

    2017. "A Novel Method to Control Carryover Contamination in Isothermal Nucleic Acid

    Amplification." *Chemical Communications* 53 (77): 10696–99.

    https://doi.org/10.1039/c7cc06469a.

Maity, Biswanath, David Sheff, and Rory A. Fisher. 2013. *Immunostaining: Detection of*

    Signaling Protein Location in Tissues, Cells and Subcellular Compartments. Methods in

    Cell Biology. 113:81-105. https://doi.org/10.1016/B978-0-12-407239-8.00005-7.

Martin, Katherine J., Marcia V. Fournier, G. Prem Veer Reddy, and Arthur B. Pardee. 2010. "A

    Need for Basic Research on Fluid-Based Early Detection Biomarkers." *Cancer Research*

    70 (13): 5203–6. https://doi.org/10.1158/0008-5472.CAN-10-0987.

Mashamba-Thompson, Tivani, Ngcwalisa Jama, Benn Sartorius, Paul Drain, and Rowan

    Thompson. 2017. "Implementation of Point-of-Care Diagnostics in Rural Primary

    Healthcare Clinics in South Africa: Perspectives of Key Stakeholders." *Diagnostics* 7 (1):

    3. https://doi.org/10.3390/diagnostics7010003.

Mclarty, Kristin, Bart Cornelissen, Deborah A Scollard, Susan J Done, Kathy Chun, and

    Raymond M Reilly. 2009. "Associations between the Uptake of 111 In-DTPA-

    Trastuzumab , HER2 Density and Response to Trastuzumab (Herceptin) in Athymic Mice

    Bearing Subcutaneous Human Tumour Xenografts." *European Journal of Nuclear*

    Medicine and Molecular Imaging 36: 81–93. https://doi.org/10.1007/s00259-008-0923-x.

Mokany, Elisa, Simon M Bone, Paul E Young, Tram B Doan, and Alison V Todd. 2015.

    "MNAzymes, a Versatile New Class of Nucleic Acid Enzymes That Can Function as

Biosensors and Molecular Switches," *Journal of the American Chemical Society* 132 (3): 1051–59. https://doi.org/10.1021/ja9076777.

Mugasa, Claire M., Thierry Laurent, Gerard J. Schoone, Piet A. Kager, George W. Lubega, and Henk D.F.H. Schallig. 2009. "Nucleic Acid Sequence-Based Amplification with Oligochromatography for Detection of Trypanosoma Brucei in Clinical Samples." *Journal of Clinical Microbiology* 47 (3): 630–35. https://doi.org/10.1128/JCM.01430-08.

Mullis, Kary B., and Fred A. Faloona. 1987. "Specific Synthesis of DNA in Vitro via a Polymerase-Catalyzed Chain Reaction." *Methods in Enzymology* 155 (C): 335–50. https://doi.org/10.1016/0076-6879(87)55023-6.

Newbigging, Ashley Meagan, Hongquan Zhang, and X. Chris Le. 2019. "Beacon-mediated Exponential Amplification Reaction (BEAR) using a single enzyme and primer. " *Chemical Communications* 55:10677-80. https://doi.org/10.1039/C9CC04226A

Ness, Jeffrey Van, Lori K Van Ness, and David J Galas. 2003. "Isothermal Reactions for the Amplification of Oligonucleotides." *Proceedings of the National Academy of Sciences of the United States of America* 100 (8): 4504–9. https://doi.org/10.1073/pnas.0730811100.

Nie, Ji, De Wen Zhang, Fang Ting Zhang, Fang Yuan, Ying Lin Zhou, and Xin Xiang Zhang. 2014. "Reporter-Triggered Isothermal Exponential Amplification Strategy in Ultrasensitive Homogeneous Label-Free Electrochemical Nucleic Acid Biosensing." *Chemical Communications* 50 (47): 6211–13. https://doi.org/10.1039/c4cc00475b.

Notomi, T, H Okayama, H Masubuchi, T Yonekawa, K Watanabe, N Amino, and T Hase. 2000. "Loop-Mediated Isothermal Amplification of DNA." *Nucleic Acids Research* 28 (12): E63. http://www.pubmedcentral.nih.gov/articlerender.fcgi?artid=102748&tool=pmcentrez&rendertype=abstract.

Osborn, L., S. Kunkel, and G. J. Nabel. 2006. "Tumor Necrosis Factor Alpha and Interleukin 1

Stimulate the Human Immunodeficiency Virus Enhancer by Activation of the Nuclear Factor Kappa B." *Proceedings of the National Academy of Sciences* 86 (7): 2336–40. https://doi.org/10.1073/pnas.86.7.2336.

Ou, Min, Jin Huang, Xiaohai Yang, Xiaoxiao He, Ke Quan, Yanjing Yang, Nuli Xie, Jing Li, and Kemin Wang. 2018. "Live-Cell MicroRNA Imaging through MnO2 Nanosheet-Mediated DD-A Hybridization Chain Reaction." *ChemBioChem* 19 (2): 147–52. https://doi.org/10.1002/cbic.201700573.

Paliwoda, Rebecca E., Feng Li, Michael S. Reid, Yanwen Lin, and X. Chris Le. 2014. "Sequential Strand Displacement Beacon for Detection of DNA Coverage on Functionalized Gold Nanoparticles." *Analytical Chemistry* 86 (12): 6138–43. https://doi.org/10.1021/ac501341t.

Peeling, R W, K K Holmes, D Mabey, and A Ronald. 2006. "Rapid Tests for Sexually Transmitted Infections (STIs): The Way Forward." *Sexually Transmitted Infections* 82: v1–6. https://doi.org/10.1136/sti.2006.024265.

Peng, Hanyong, Xing-Fang Li, Hongquan Zhang, and X. Chris Le. 2017. "A MicroRNA-Initiated DNAzyme Motor Operating in Living Cells." *Nature Communications* 8 (May 2016): 14378. https://doi.org/10.1038/ncomms14378.

Peng, Hanyong, Ashley M. Newbigging, Michael S. Reid, Jagdeesh S. Uppal, Jingyang Xu, Hongquan Zhang, and X. Chris Le. 2020. "Signal Amplification in Living Cells: A Review of MicroRNA Detection and Imaging." *Analytical Chemistry* 92 (1): 292–308. https://doi.org/10.1021/acs.analchem.9b04752.

Persing, D. H. 1991. "Polymerase Chain Reaction: Trenches to Benches." *Journal of Clinical Microbiology* 29 (7): 1281–85.

Petersen, Eva Rabing Brix, Patricia Diana Sørensen, Erik Hugger Jakobsen, Jonna Skov

Madsen, and Ivan Brandslund. 2013. "Serum HER-2 Predicts Response and Resistance to Trastuzumab Treatment in Breast Cancer." *Clinical Chemistry and Laboratory Medicine* (7): 1483–92. https://doi.org/10.1515/cclm-2012-0558.

Piepenburg, Olaf, Colin H. Williams, Derek L. Stemple, and Niall A. Armes. 2006. "DNA Detection Using Recombination Proteins." *PLoS Biology* 4 (7): 1115–21. https://doi.org/10.1371/journal.pbio.0040204.

Qi, Hongjie, Shuzhen Yue, Sai Bi, Caifeng Ding, and Weiling Song. 2018. "Isothermal Exponential Amplification Techniques: From Basic Principles to Applications in Electrochemical Biosensors." *Biosensors and Bioelectronics* 110 (March): 207–17. https://doi.org/10.1016/j.bios.2018.03.065.

Qian, Yong, Taotao Fan, Peng Wang, Xing Zhang, Jianjun Luo, Fuyi Zhou, Yao Yao, Xianjiu Liao, Yuanhong Li, and Fenglei Gao. 2017. "A Novel Label-Free Homogeneous Electrochemical Immunosensor Based on Proximity Hybridization-Triggered Isothermal Exponential Amplification Induced G-Quadruplex Formation." *Sensors and Actuators, B: Chemical* 248: 187–94. https://doi.org/10.1016/j.snb.2017.03.152.

Ram, Sripad, Dongyoung Kim, Raimund J. Ober, and E. Sally Ward. 2014. "The Level of HER2 Expression Is a Predictor of Antibody-HER2 Trafficking Behavior in Cancer Cells." *MAbs* 6 (5): 1211–19. https://doi.org/10.4161/mabs.29865.

Reid, Michael S., X. Chris Le, and Hongquan Zhang. 2018. "Exponential Isothermal Amplification of Nucleic Acids and Assays for Proteins, Cells, Small Molecules, and Enzyme Activities: An EXPAR Example." *Angewandte Chemie - International Edition* 57 (37): 11856–66. https://doi.org/10.1002/anie.201712217.

Rifai, Nader, Eleftherios P. Diamandis, Y. M.Dennis Lo, Larry J. Kricka, Peter Wilding, Jack H. Ladenson, and Carl T. Wittwer. 2012. "Advancing Laboratory Medicine through

Innovation: A Tale of Six Inventors." *Clinical Chemistry* 58 (3): 502–10. https://doi.org/10.1373/clinchem.2011.178582.

Sabir, Tara, Anita Toulmin, Long Ma, Anita C. Jones, Peter McGlynn, Gunnar F. Schröder, and Steven W. Magennis. 2012. "Branchpoint Expansion in a Fully Complementary Three-Way DNA Junction." *Journal of the American Chemical Society* 134 (14): 6280–85. https://doi.org/10.1021/ja211802z.

Saiki, R., S Scharf, F Faloona, Kary Mullis, G. Horn, H. Erlich, and N Arnheim. 1985. "Enzymatic Amplification of Beta-Globin Genomic Sequences and Restriction Site Analysis for Diagnosis of Sickle Cell Anemia." *Science* 230 (4732):150-4. https://doi.org/10.1126/science.2999980.

Saka, Sinem K., Yu Wang, Jocelyn Y. Kishi, Allen Zhu, Yitian Zeng, Wenxin Xie, Koray Kirli, et al. 2019. "Immuno-SABER Enables Highly Multiplexed and Amplified Protein Imaging in Tissues." *Nature Biotechnology* 37 (9): 1080–90. https://doi.org/10.1038/s41587-019-0207-y.

Sandhaus, Linda M., Kazimiera J. Gajl-Peczalska, and Richard D. Brunning. 1984. "Immunophenotyping of Leukaemia: An Immunoperoxidase Method Using Air-dried Smears." *British Journal of Haematology* 56 (1): 131–38. https://doi.org/10.1111/j.1365-2141.1984.tb01278.x.

Sano, Takeshi, Cassandra L. Smith, and Charles R. Cantor. 1992. "Immuno-PCR: Very Sensitive Antigen Detection by Means of Specific Antibody-DNA Conjugates." *Science* 258 (5079): 120–22. https://doi.org/10.1126/science.1439758.

Schwarzenbach, Heidi, Dave S.B. Hoon, and Klaus Pantel. 2011. "Cell-Free Nucleic Acids as Biomarkers in Cancer Patients." *Nature Reviews Cancer* 11 (6): 426–37. https://doi.org/10.1038/nrc3066.

Schweitzer, B, S Wiltshire, J Lambert, S O'Malley, K Kukanskis, Z Zhu, Stephen F Kingsmore, PM Lizardi, and D C Ward. 2000. "Immunoassays with Rolling Circle DNA Amplification: A Versatile Platform for Ultrasensitive Antigen Detection." *Proceedings of the National Academy of Sciences* 97 (18): 10113–19. http://www.pnas.org.login.ezproxy.library.ualberta.ca/content/97/18/10113.short.

Shen, Jun, Sanford A. Stass, and Feng Jiang. 2013. "MicroRNAs as Potential Biomarkers in Human Solid Tumors." *Cancer Letters* 329 (2): 125–36. https://doi.org/10.1016/j.canlet.2012.11.001.

Shi, Chao, Qi Liu, Cuiping Ma, and Wenwan Zhong. 2014. "Exponential Strand-Displacement Amplification for Detection of Micrornas." *Analytical Chemistry* 86 (1): 336–39. https://doi.org/10.1021/ac4038043.

Shi, Chao, Qi Liu, Meiling Zhou, Haijie Zhao, Tao Yang, and Cuiping Ma. 2016. "Nicking Endonuclease-Mediated Isothermal Exponential Amplification for Double-Stranded DNA Detection." *Sensors and Actuators, B: Chemical* 222: 221–25. https://doi.org/10.1016/j.snb.2015.08.060.

Špringer, Tomáš, Hana Šípová, Hana Vaisocherová, Josef Štepánek, and Jiří Homola. 2010. "Shielding Effect of Monovalent and Divalent Cations on Solid-Phase DNA Hybridization: Surface Plasmon Resonance Biosensor Study." *Nucleic Acids Research* 38 (20): 7343–51. https://doi.org/10.1093/nar/gkq577.

Srinivas, Niranjan, Thomas E. Ouldridge, Petr Šulc, Joseph M. Schaeffer, Bernard Yurke, Ard A. Louis, Jonathan P K Doye, and Erik Winfree. 2013. "On the Biophysics and Kinetics of Toehold-Mediated DNA Strand Displacement." *Nucleic Acids Research* 41 (22): 10641–58. https://doi.org/10.1093/nar/gkt801.

Stryer, L. 1978. "Fluorescence Energy Transfer as a Spectroscopic Ruler." *Annual Review of*

Biochemistry 47 (1): 819–46. https://doi.org/10.1146/annurev.bi.47.070178.004131.

Sturgeon, Catharine, Robert Hill, Glen L. Hortin, and Douglas Thompson. 2010. "Taking a New
Biomarker into Routine Use - A Perspective from the Routine Clinical Biochemistry
Laboratory." *Proteomics Clinical Applications* 4 (12): 892–903.
https://doi.org/10.1002/prca.201000073.

Sun, Xinya, Li Wang, Mingsha Zhao, Changzhi Zhao, Shufeng Liu, X. X. Zhang, D. Sun, C.
Fan, and F. Xia. 2016. "An Autocatalytic DNA Machine with Autonomous Target
Recycling and Cascade Circular Exponential Amplification for One-Pot, Isothermal and
Ultrasensitive Nucleic Acid Detection." *Chemical Communications* 52 (74): 11108–11.
https://doi.org/10.1039/C6CC06643G.

Swarup, Vishnu, and M. R. Rajeswari. 2007. "Circulating (Cell-Free) Nucleic Acids - A
Promising, Non-Invasive Tool for Early Detection of Several Human Diseases." *FEBS
Letters* 581 (5): 795–99. https://doi.org/10.1016/j.febslet.2007.01.051.

Tan, Eric, Barbara Erwin, Shale Dames, Karl Voelkerding, and Angelika Niemz. 2007.
"Isothermal DNA Amplification with Gold Nanosphere-Based Visual Colorimetric
Readout for Herpes Simplex Virus Detection." *Clinical Chemistry* 53 (11): 2017–20.
https://doi.org/10.1373/clinchem.2007.091116.

Tang, Yanan, Yanwen Lin, Xiaolong Yang, Zhixin Wang, X. Chris Le, and Feng Li. 2015.
"Universal Strategy To Engineer Catalytic DNA Hairpin Assemblies for Protein Analysis."
Analytical Chemistry, 87 (16): 8063-66. https://doi.org/10.1021/acs.analchem.5b02504.

Tian, Leilei, and Yossi Weizmann. 2013. "Real-Time Detection of Telomerase Activity Using
the Exponential Isothermal Amplification of Telomere Repeat Assay." *Journal of the
American Chemical Society* 135 (5): 1661–64. https://doi.org/10.1021/ja309198j.

Toley, Bhushan J., Isabela Covelli, Yevgeniy Belousov, Sujatha Ramachandran, Enos Kline,

Noah Scarr, Nic Vermeulen, Walt Mahoney, Barry R. Lutz, and Paul Yager. 2015. "Isothermal Strand Displacement Amplification (ISDA): A Rapid and Sensitive Method of Nucleic Acid Amplification for Point-of-Care Diagnosis." *Analyst* 140 (22): 7540–49. https://doi.org/10.1039/c5an01632k.

Torres-Chavolla, Edith, and Evangelyn C. Alocilja. 2011. "Nanoparticle Based DNA Biosensor for Tuberculosis Detection Using Thermophilic Helicase-Dependent Isothermal Amplification." *Biosensors and Bioelectronics* 26 (11): 4614–18. https://doi.org/10.1016/j.bios.2011.04.055.

Vincent, Myriam, Yan Xu, and Huimin Kong. 2004a. "Helicase-Dependent Isothermal DNA Amplification." *EMBO Reports* 5 (8): 795–800. https://doi.org/10.1038/sj.embor.7400200.

Walker, G T, M S Fraiser, J L Schram, M C Little, J G Nadeau, and D P Malinowski. 1992. "Strand Displacement Amplification--an Isothermal, in Vitro DNA Amplification Technique." *Nucleic Acids Research* 20 (7): 1691–96. https://doi.org/ 10.1093/nar/20.7.1691

Walker, G T, M C Little, J G Nadeau, and D D Shank. 1992. "Isothermal in Vitro Amplification of DNA by a Restriction Enzyme/DNA Polymerase System." *Proceedings of the National Academy of Sciences of the United States of America* 89 (1): 392–96. https://doi.org/10.1073/pnas.89.1.392.

Wang, Fuan, Johann Elbaz, Ron Orbach, Nimrod Magen, and Itamar Willner. 2011. "Amplified Analysis of DNA by the Autonomous Assembly of Polymers Consisting of DNAzyme Wires." *Journal of the American Chemical Society* 133 (43): 17149–51. https://doi.org/10.1021/ja2076789.

Wang, G.-K., J.-Q. Zhu, J.-T. Zhang, Q. Li, Y. Li, J. He, Y.-W. Qin, and Q. Jing. 2010. "Circulating MicroRNA: A Novel Potential Biomarker for Early Diagnosis of Acute

Myocardial Infarction in Humans." *European Heart Journal* 31 (6): 659–66.

https://doi.org/10.1093/eurheartj/ehq013.

Wang, Qingping, Hanye Zheng, Xiaoyao Gao, Zhenyu Lin, and Guonan Chen. 2013. "A Label-Free Ultrasensitive Electrochemical Aptameric Recognition System for Protein Assay Based on Hyperbranched Rolling Circle Amplification." *Chemical Communications* 49 (97): 11418–20. https://doi.org/10.1039/c3cc46274a.

Wang, Xiangdong, Hui Wang, Chenghui Liu, Honghong Wang, and Zhengping Li. 2017. "A Three-Way Junction Structure-Based Isothermal Exponential Amplification Strategy for Sensitive Detection of 3′-Terminal 2′-O-Methylated Plant MicroRNA." *Chemical Communications* 53 (6): 1124–27. https://doi.org/10.1039/c6cc08726d.

Wang, Yu, Jialei Bai, Bingyang Huo, Shuai Yuan, Man Zhang, Xuan Sun, Yuan Peng, et al. 2018. "Upconversion Fluorescent Aptasensor for Polychlorinated Biphenyls Detection Based on Nicking Endonuclease and Hybridization Chain Reaction Dual-Amplification Strategy." Research-article. *Analytical Chemistry* 90 (16): 9936–42. https://doi.org/10.1021/acs.analchem.8b02159.

Wei, Jie, Xue Gong, Qing Wang, Min Pan, Xiaoqing Liu, Jing Liu, Fan Xia, and Fuan Wang. 2017. "Construction of an Autonomously Concatenated Hybridization Chain Reaction for Signal Amplification and Intracellular Imaging." *Chemical Science* 9 (1): 52–61. https://doi.org/10.1039/c7sc03939e.

Wu, Hao, Kai Zhang, Yaling Liu, Hongyong Wang, Jun Wu, Feifan Zhu, and Pei Zou. 2015. "Binding-Induced and Label-Free Colorimetric Method for Protein Detection Based on Autonomous Assembly of Hemin/G-Quadruplex DNAzyme Amplification Strategy." *Biosensors and Bioelectronics* 64: 572–78. https://doi.org/10.1016/j.bios.2014.09.096.

Wu, Zhan, Gao Qin Liu, Xiao Li Yang, and Jian Hui Jiang. 2015. "Electrostatic Nucleic Acid

Nanoassembly Enables Hybridization Chain Reaction in Living Cells for Ultrasensitive MRNA Imaging." *Journal of the American Chemical Society* 137 (21): 6829–36. https://doi.org/10.1021/jacs.5b01778.

Wu, Zhenkun, Huanhuan Fan, Nitya Sai Reddy Satyavolu, Wen Jing Wang, Ryan Lake, Jian Hui Jiang, and Yi Lu. 2017. "Imaging Endogenous Metal Ions in Living Cells Using a DNAzyme–Catalytic Hairpin Assembly Probe." *Angewandte Chemie - International Edition* 56 (30): 8721–25. https://doi.org/10.1002/anie.201703540.

Wulfkuhle, Julia D., Lance A. Liotta, and Emanuel F. Petricoin. 2003. "Proteomic Applications for the Early Detection of Cancer." *Nature Reviews Cancer* 3 (4): 267–75. https://doi.org/10.1038/nrc1043.

Yan, Lei, Jie Zhou, Yue Zheng, Adam S. Gamson, Benjamin T. Roembke, Shizuka Nakayama, and Herman O. Sintim. 2014a. "Isothermal Amplified Detection of DNA and RNA." *Molecular BioSystems* 10 (5): 970–1003. https://doi.org/10.1039/c3mb70304e.

Yang, Fan, Yaru Cheng, Yu Cao, Haifeng Dong, Huiting Lu, Kai Zhang, Xiangdan Meng, Conghui Liu, and Xueji Zhang. 2019. "Sensitively Distinguishing Intracellular Precursor and Mature MicroRNA Abundance." *Chemical Science* 10 (6): 1709–15. https://doi.org/10.1039/c8sc03305f.

Yang, Xiaolong, Yanan Tang, Sarah M. Traynor, and Feng Li. 2016. "Regulation of DNA Strand Displacement Using an Allosteric DNA Toehold." *Journal of the American Chemical Society* 138 (42): 14076–82. https://doi.org/10.1021/jacs.6b08794.

Yin, Peng, Harry M.T. Choi, Colby R. Calvert, and Niles A. Pierce. 2008. "Programming Biomolecular Self-Assembly Pathways." *Nature* 451 (7176): 318–22. https://doi.org/10.1038/nature06451.

Zang, Yang, Jianping Lei, Pinghua Ling, and Huangxian Ju. 2015. "Catalytic Hairpin

Assembly-Programmed Porphyrin-DNA Complex as Photoelectrochemical Initiator for DNA Biosensing." *Analytical Chemistry* 87 (10): 5430–36. https://doi.org/10.1021/acs.analchem.5b00888.

Zanoli, Laura Maria, and Giuseppe Spoto. 2013. "Isothermal Amplification Methods for the Detection of Nucleic Acids in Microfluidic Devices." *Biosensors* 3 (1): 18–43. https://doi.org/10.3390/bios3010018.

Zhang, Bing, Bingqian Liu, Dianping Tang, Reinhard Niessner, Guonan Chen, and Dietmar Knopp. 2012. "DNA-Based Hybridization Chain Reaction for Amplified Bioelectronic Signal and Ultrasensitive Detection of Proteins." *Analytical Chemistry* 84 (12): 5392–99. https://doi.org/10.1021/ac3009065.

Zhang, David Yu, Sherry Xi Chen, and Peng Yin. 2012. "Optimizing the Specificity of Nucleic Acid Hybridization." *Nature Chemistry* 4 (3): 208–14. https://doi.org/10.1038/nchem.1246.

Zhang, David Yu, and Georg Seelig. 2011. "Dynamic DNA Nanotechnology Using Strand-Displacement Reactions." *Nature Chemistry* 3 (2): 103–13. https://doi.org/10.1038/nchem.957.

Zhang, David Yu, and Erik Winfree. 2010. "Robustness and Modularity Properties of a Non-Covalent DNA Catalytic Reaction." *Nucleic Acids Research* 38 (12): 4182–97. https://doi.org/10.1093/nar/gkq088.

Zhang, Hongquan, Maode Lai, Albert Zuehlke, Hanyong Peng, Xing Fang Li, and X. Chris Le. 2015. "Binding-Induced DNA Nanomachines Triggered by Proteins and Nucleic Acids." *Angewandte Chemie - International Edition* 54 (48): 14326–30. https://doi.org/10.1002/anie.201506312.

Zhang, Hongquan, Feng Li, Brittany Dever, Xing-Fang Li, and X Chris Le. 2013. "DNA-Mediated Homogeneous Binding Assays for Nucleic Acids and Proteins." *Chemical*

Reviews 113 (4): 2812–41. https://doi.org/10.1021/cr300340p.

Zhang, Hongquan, Feng Li, Brittany Dever, Chuan Wang, Xing-Fang Li, and X Chris Le. 2013.
"Assembling DNA through Affinity Binding to Achieve Ultrasensitive Protein Detection."
Angewandte Chemie - International Edition 52 (41): 10698–705.
https://doi.org/10.1002/anie.201210022.

Zhang, Hongquan, Feng Li, Xing-Fang Li, and X. Chris Le. 2013. "Yoctomole Detection of
Proteins Using Solid Phase Binding-Induced DNA Assembly." *Methods* 64 (3): 322–30.
https://doi.org/10.1016/j.ymeth.2013.10.005.

Zhang, Hongquan, Xing-Fang Li, and X Chris Le. 2012. "Binding-Induced DNA Assembly and
Its Application to Yoctomole Detection of Proteins." *Analytical Chemistry* 84 (2): 877–84.
https://doi.org/10.1021/ac203207g.

Zhang, Li Rong, Guichi Zhu, and Chun Yang Zhang. 2014. "Homogeneous and Label-Free
Detection of Micrornas Using Bifunctional Strand Displacement Amplification-Mediated
Hyperbranched Rolling Circle Amplification." *Analytical Chemistry* 86 (13): 6703–9.
https://doi.org/10.1021/ac501645x.

Zhang, Nan, Xiao Mei Shi, Hong Qian Guo, Xiao Zhi Zhao, Wei Wei Zhao, Jing Juan Xu, and
Hong Yuan Chen. 2018. "Gold Nanoparticle Couples with Entropy-Driven Toehold-
Mediated DNA Strand Displacement Reaction on Magnetic Beads: Toward Ultrasensitive
Energy-Transfer-Based Photoelectrochemical Detection of MiRNA-141 in Real Blood
Sample." *Analytical Chemistry* 90 (20): 11892–98.
https://doi.org/10.1021/acs.analchem.8b01966.

Zhang, Yan, and Chun Yang Zhang. 2012. "Sensitive Detection of MicroRNA with Isothermal
Amplification and a Single-Quantum-Dot-Based Nanosensor." *Analytical Chemistry* 84
(1): 224–31. https://doi.org/10.1021/ac202405q.

Zhang, Ye, Yurong Yan, Wenhong Chen, Wei Cheng, Shengqiang Li, Xiaojuan Ding, Dandan
Li, Hong Wang, Huangxian Ju, and Shijia Ding. 2015. "A Simple Electrochemical
Biosensor for Highly Sensitive and Specific Detection of MicroRNA Based on Mismatched
Catalytic Hairpin Assembly." *Biosensors and Bioelectronics* 68: 343–49.
https://doi.org/10.1016/j.bios.2015.01.026.

Zhang, Zhen-zhu, and Chun-yang Zhang. 2012. "Highly Sensitive Detection of Protein with
Aptamer-Based Target-Triggering Two-Stage Amplification." *Analytical Chemistry* 84 (3):
1623–29. https://doi.org/10.1021/ac2029002.

Zhao, Weian, M. Monsur Ali, Michael A. Brook, and Yingfu Li. 2008. "Rolling Circle
Amplification: Applications in Nanotechnology and Biodetection with Functional Nucleic
Acids." *Angewandte Chemie - International Edition* 47 (34): 6330–37.
https://doi.org/10.1002/anie.200705982.

Zhao, Xinyan, Tao Dong, Zhaochu Yang, Nuno Pires, and Nils Høivik. 2012. "Compatible
Immuno-NASBA LOC Device for Quantitative Detection of Waterborne Pathogens:
Design and Validation." *Lab on a Chip* 12 (3): 602–12. https://doi.org/10.1039/c1lc20836e.

Zhao, Yongxi, Feng Chen, Qian Li, Lihua Wang, and Chunhai Fan. 2015. "Isothermal
Amplification of Nucleic Acids." *Chemical Reviews* 115 (22): 12491–545.
https://doi.org/10.1021/acs.chemrev.5b00428.

Zheng, Ai Xian, Jin Ru Wang, Juan Li, Xiao Rong Song, Guo Nan Chen, and Huang Hao Yang.
2012. "Enzyme-Free Fluorescence Aptasensor for Amplification Detection of Human
Thrombin via Target-Catalyzed Hairpin Assembly." *Biosensors and Bioelectronics* 36 (1):
217–21. https://doi.org/10.1016/j.bios.2012.04.019.

Zhou, Guobao, Meihua Lin, Ping Song, Xiaoqing Chen, Jie Chao, Lianhui Wang, Qing Huang,
Wei Huang, Chunhai Fan, and Xiaolei Zuo. 2014. "Multivalent Capture and Detection of

Cancer Cells with DNA Nanostructured Biosensors and Multibranched Hybridization Chain Reaction Amplification." *Analytical Chemistry* 86 (15): 7843–48. https://doi.org/10.1021/ac502276w.

Zhu, Guizhi, Shengfeng Zhang, Erqun Song, Jing Zheng, Rong Hu, Xiaohong Fang, and Weihong Tan. 2013. "Building Fluorescent DNA Nanodevices on Target Living Cell Surfaces." *Angewandte Chemie - International Edition* 52 (21): 5490–96. https://doi.org/10.1002/anie.201301439.

Zhuang, Junyang, Wenqiang Lai, Guonan Chen, and Dianping Tang. 2014. "A Rolling Circle Amplification-Based DNA Machine for MiRNA Screening Coupling Catalytic Hairpin Assembly with DNAzyme Formation." *Chemical Communications* 50 (22): 2935–38. https://doi.org/10.1039/c3cc49873e.

Zong, Yingxia, Fang Liu, Yue Zhang, Tianrong Zhan, Yunhua He, and Xu Hun. 2016. "Signal Amplification Technology Based on Entropy-Driven Molecular Switch for Ultrasensitive Electrochemical Determination of DNA and Salmonella Typhimurium." *Sensors and Actuators, B: Chemical* 225: 420–27. https://doi.org/10.1016/j.snb.2015.11.086.